Quaternary Ammonium Salts and Brønsted Superacids based on Weakly Coordinating $[Al(OTeF_5)_4]^-$ Anion

Inaugural-Dissertation
to obtain the academic degree
Doctor rerum naturalium (Dr. rer. nat.)

by

Sofiya Kotsyuda

Fachbereich Biologie, Chemie, Pharmazie
Institut für Chemie und Biochemie
Freie Universität Berlin

2023

The work for the present dissertation has been conducted between May 2017 and March 2023 under the supervision of Prof. Dr. Sebastian Hasenstab-Riedel at the Institute of Chemistry and Biochemistry (Department of Biology, Chemistry, Pharmacy) of the Freie Universität Berlin.

Statement of Authorship

I, Sofiya Kotsyuda, assure that I of my own volition and by myself, with the assistance of the provided sources and resources, composed the following dissertation. Subsequently, I assure that the following dissertation has not been submitted for review elsewhere.

Selbstständigkeitserklärung

Hiermit versichere ich, Sofiya Kotsyuda, dass ich die vorliegende Dissertation selbständig und lediglich unter Benutzung der angegebenen Quellen und Hilfsmittel verfasst habe. Ich versichere außerdem, dass die vorliegende Dissertation noch nicht einem anderen Prüfungsverfahren zugrunde gelegen hat.

First Referee: Prof. Dr. Sebastian Hasenstab-Riedel

Second Referee: Prof. Dr. Christian Müller

Date of Defense: 10.07.2023

Acknowledgement

In the first place, I would like to thank my supervisor Prof. Dr. Sebastian Hasenstab-Riedel for giving me the opportunity to conduct my doctoral thesis in his group and this interesting topic. Prof. Hasenstab-Riedel deserves my gratitude for his all-embracing support of my PhD thesis. Many thanks for supporting conference participation, group trips, barbeques and running events, as well as for talented and friendly surroundings in the research group.

I am grateful to Prof. Dr. Christian Müller for his time and effort to assess my work as a second reviewer.

I would like to thank Dr. habil. Helmut Beckers for his magnificent support and interest in my topic during the whole time. Many thanks for fruitful discussions and very helpful proofreading of articles and reports. Many thanks for the friendly atmosphere and good scientific advice.

My greatest gratitude to Dr. M. A. Ellwanger for being the biggest support and for bringing the most valuable input into all scientific projects, for proofreading my articles, any helpful advice and discussions. Thanks for teaching me scientific and life lessons, and being a great teacher and mentor. I thank you from the bottom of my heart.

I want to thank Dr. Anja Wiesner for introducing me to the research topic, being always friendly, helpful and supporting. Also, thanks to all members of the teflate-mini-group for their support and helpful fruitful discussions.

Thanks to Dr. Simon Steinhauer and Dr. Julia Bader for valuable scientific contributions to my articles.

Thanks to colleagues that performed crystal measurements: Dr. Anja Wiesner, Dr. Karsten Sonneberg, Dr. Daniel Franz, Dr. Simon Steinhauer and M. Sc. Patrick Voßnacker. Thank you Dr. Carsten Müller for valuable tips and discussions regarding the DFT calculations.

My best thank you to all my lab mates in order of appearance: Dr. Jan Hendrick Nissen for being supportive and always understanding my jokes. Thank you Dr. Sebastian Hämmerling for your valuable tips and helping. Thank you Maite Nößler

for being my lab-soulmate, your support and being there for me when needed. Thank you for making "Schlager-Freitags". Thanks Dr. Daniel Franz for staying with me in the lab and help. Last but not least, thank you Lukas Fischer for being a fancy lab mate and always in the good mood.

Thanks to all the other PhD students that started in the order Dr. Lisa Mann, Dr. Tony Stüker, Dr. Benjamin Schmidt, Dr. Frenio Redeker, Dr. Lin Li, Dr. Patrick Pröhm, Dr. Kurt Hoffmann, Dr. Tyler Gully, Gene Senges, Marlon Winter, Paul Golz, Jonas Schmid, Dr. Alberto Perez-Bitrian, Daniel Wegener, Johanna Schlögl for a great time, always ready to help and nice atmosphere. It was a pleasure to work with you and learn from you. Thanks to all members of AG Riedel for the working atmosphere and support. My warm thanks to my student Ahmet Toraman for his great work and excellent results.

I would like to acknowledge AG Thiele and AG Malischewski and their group leaders for support.

Thanks to Holger Pernice, Thomas Drews and Maximilian Stahnke for being helpful any time needed. Thank you Holger for pushing me to speak more German and for your kindness. Thanks to Dirk Hauenstein and the whole team from the Materialverwaltung, to Dirk Busold, Jesse Holloway, Jürgen-Peter Böttcher and Sven Sasse. Thank you to our secretaries Inge Kanakaris-Wirtl, Ines Stock and Marie Nickel.

I would like to thank my beloved for the continuous support, care and motivation.

I would like to thank all the people I met during my stay in Berlin. Thanks to SAMS WG for being friendly and careful all the time. Thanks to my big Ukrainian family for being the solid foundation to rely on. Especially thanks to mother Olena, my grandparents Volodymyr and Nina for always believing in me, giving me support and love. Thanks to my sister Iva for always being on my side and by my side. Thank you my little sister Anastasiia for being an amazing child. When you grow up, I want you to read these words and be proud of yourself.

Finally, thanks to the universe for organizing challenges and circumstances in my life, I must have learnt from.

Special Acknowledgement

After the 24th of February 2022 my life has changed forever. Afterwards, this part of acknowledgment was written.

In dark times you can clearly see bright people. To those I also want to thank from the bottom of my heart.

I would like to thank all warm-hearted people and folks all over the world who now host Ukrainians at their homes. My honor and gratitude. For the support and guidance during these dark times, I would like to thank Aya and Ksenia Shaposhnikova.

My thanks to the Kössel family, who hosted and helped my family during their stay in Germany. I thank Julia Lubomirska for being a true friend and warm-hearted person, for your kindness, braveness and huge heart, full of love. My warm thanks to the Papke family for their good advice and always welcoming me. I want to thank the Bschorer family for their kindness and support. Warm thanks to the Lamert family for their great support and care.

My gratitude and honor to all Ukrainian men and women who protect Ukraine and gave their lives for our freedom. My honor and love to my uncle Maksym and a great warrior who paid with his life in this horrible war.

This dissertation I dedicate to the bravery of my big Ukrainian family – my folk, which is over 40 million people.

Моєму хороборому Українському Народові

To my brave Ukrainian folk

Abstract

A series of tetraalkylammonium tetrakis(pentafluoroorthotellurato)aluminate salts $[NAlk_4][Al(OTeF_5)_4]$, Alk_4 = $-(CH_3)_4$, $-(C_2H_5)_4$, $-(C_2H_5)_3CH_3$, $-(C_3H_7)_4$, $-(C_4H_9)_4$ were described, characterized and some identified as ionic liquids. The Brønsted superacid $[o\text{-}C_6H_4F_2\text{-}H][Al(OTeF_5)_4]$ was applied for the protonation of very weak bases – halogenated pyridines C_5F_5N, C_5F_4ClN, C_5Cl_5N and $C_5H_2F_2N$ and C_5H_4BrN – to yield the corresponding $[C_5F_5N\text{-}H][Al(OTeF_5)_4]$, $[(C_5F_5N)_2H][Al(OTeF_5)_4]$, $[C_5F_4ClN\text{-}H][Al(OTeF_5)_4]$, $[(C_5Cl_5N)_2H][Al(OTeF_5)_4]$, $[C_5H_4BrN\text{-}H][Al(OTeF_5)_4]$ and $[C_5F_3H_2N\text{-}H][Al(OTeF_5)_4]$ salts. The obtained crystal structures in the solid state of these salts show rare non-covalent interactions like anion-π and σ-hole interactions between pyridinium cations and the $[Al(OTeF_5)_4]^-$ weakly coordinating anion. The reaction of commercial refrigerant HFO-1234yf with arene-based Brønsted superacids lead to selective C(sp^3)-F bond activation and resulted in the typical trifluoroallyl-substituted arenes, which are Friedel-Crafts like products.

Zusammenfassung

Eine Serie von Tetraalkylammonium-tetrakis-(pentafluoroorthotellurato)aluminatsalzen $[NAlk_4][Al(OTeF_5)_4]$, Alk_4 = $-(CH_3)_4$, $-(C_2H_5)_4$, $-(C_2H_5)_3CH_3$, $-(C_3H_7)_4$, $-(C_4H_9)_4$, wurde beschrieben, charakterisiert und einige als ionische Flüssigkeiten identifiziert. Die Brønsted-Supersäure $[o\text{-}C_6H_4F_2\text{-}H][Al(OTeF_5)_4]$ wurde für die Protonierung von schwachen Basen – den halogenierten Pyridinen C_5F_5N, C_5F_4ClN und C_5Cl_5N, $C_5H_2F_2N$ und C_5H_4BrN – verwendet, um die entsprechenden Salze $[C_5F_5N\text{-}H][Al(OTeF_5)_4]$, $[(C_5F_5N)_2H][Al(OTeF_5)_4]$, $[C_5F_4ClN\text{-}H][Al(OTeF_5)_4]$, $[(C_5Cl_5N)_2H][Al(OTeF_5)_4]$, $[C_5H_4BrN\text{-}H][Al(OTeF_5)_4]$ und $[C_5F_3H_2N\text{-}H][Al(OTeF_5)_4]$ zu erhalten. In den erhaltenen Festkörperstrukturen dieser Salze wurden seltene nicht-kovalente Wechselwirkungen wie Anion-π und σ-Loch-Wechselwirkungen zwischen Pyridiniumkationen und dem schwach koordinierenden $[Al(OTeF_5)_4]^-$ Anion gefunden. Die Reaktion des kommerziellen Kältemittels HFO-1234yf mit Brønsted-Supersäuren auf Aren-Basis führte zu einer selektiven Aktivierung der C(sp^3)-F-Bindung und ergab die typischen trifluorallyl-substituierten Arene, welche Friedel-Crafts-ähnliche Produkte sind.

List of Abbreviations

°C	degrees centigrade
a, b, c	unit cell axes
a. u.	atomic units
B3-LYP	Becke three-parameter Lee-Yang-Parr
CCDC	Cambridge Crystallographic Data Centre
d	doublet
D3	Grimme dispersion correction
DFT	density functional theory
eq.	equivalent
ESP	electrostatic potential
FIA	fluoride ion affinity
J	coupling constant
HFO-1234yf	2,3,3,3-Tetrafluoropropene
m	multiplet
NMR	nuclear magnetic resonance
*o*DFB	*ortho*-difluorobenzene
Q_{zz}	quadrupole moment
s	singlet
t	triplet
TZVPP	triple-ζ with two sets of polarization functions
vdW	van der Waals
WCA	weakly coordinating anion
XRD	X-Ray diffraction
Z	amount of formula units in the unit cell
α, β, γ	unit cell angles
γ	activity coefficient
δ	chemical shift
ε_R	relative permittivity
Θ	scattering angle
μ	absorption coefficient

Table of Contents

I Introduction

1.1 Brønsted Superacids

The term of superacids was first published in 1927 by *Conant et. al*. and used for the definition of acids that can protonate ketones and aldehydes in nonaqueous solution.[1] Nowadays, the term "Brønsted superacid" is referred to any acid stronger than anhydrous 100% sulfuric acid.[2] The importance of Brønsted superacids has been shown as *Olah* received the Nobel prize for his work about the use of superacids in formation of carbenium ions in 1994.[3] The acidity can be tremendously increased by the combination of a Brønsted acid with a Lewis superacid under formation of a conjugated Brønsted-Lewis superacid. A famous example from the group of *Olah* is the *magic acid*, a conjugate of fluorosulfonic acid with antimony pentafluoride HSO_3F-SbF_5.[4] It is known to even dissolve ordinary candles under cleavage and isomerization of the long alkyl chain to form *tert*-butyl cations.[5] The strongest *only*-Brønsted superacid was claimed to be the fluorinated carborane acid $H[CHB_{11}F_{11}]$, which is able to protonate alkanes and carbon dioxide.[6] *Olah* classified common Brønsted superacids as:[3]

- Primary Brønsted superacids like $HClO_4$, HSO_3Cl, HSO_3F, HSO_3CF_3;
- Binary Brønsted superacids like HF-HSO_3F, HF-CF_3SO_3F, $HB(SO_4)_4$;
- Fluorinated conjugate Brønsted-Lewis superacids of type HF-EF_5, E = Sb, P, Ta, Nb, Sb;
- Conjugate Brønsted-Lewis superacids of type HX-AlX_3, X = F, Br, Cl, I;
- Conjugate Brønsted-Lewis superacids of type BA-LA, where BA = H_2SO_4, HSO_3F, CF_3SO_3H; LA = SO_3, SbF_5, AsF_5, TaF_5, NbF_5.

For the isolation of metal carbonyl cations, Brønsted superacids, containing weakly coordinating anions, were used to yield $[M(CO)_6][Sb_2F_{11}]$, M = Fe,[7] Ru,[8] Os,[8] Ir,[9] Pd,[10] Pt,[10] Rh,[9] and $[M(CO)_6][BF_4]_2$, M = Fe,[11] Ru,[11] Os,[11] respectively. The acidity of a Brønsted superacid depends on the stability of the corresponding anion after proton abstraction. In order to reach higher acidities, the acid must be able to ionize the solvent medium, thus forming delocalized counterions.[3] In most cases the anion can be considered as adduct of a neutral Lewis acid and a negative charged Lewis base, where the Lewis acidity is one of the crucial factors considering the stability.

The strength of a Brønsted superacid is also judged by the ability to protonate extremely weak bases to access such species like protonated arenes $[C_6H_6\text{-}H]^+$,[12,13] $[C_6H_3(CH_3)_3\text{-}H]^+$,[14] $[H_2C_6(CH_3)_5]^+$,[12,13] and also $[HPX_3]^+$, X = F, Cl, Br;[15] $[C_5F_5NH]^+$;[16] $[P_4H]^+$.[17] For the estimation of the acidity of liquid Brønsted superacids, the Hammett acidity function H_0 is used, where $[BH^+]$ – displays the conjugate acid, B – the base and $\mathrm{p}K_{BH^+}$ – log(K) the dissociation of $[BH^+]$:[3]

$$H_0 = \mathrm{p}K_{BH^+} + \log\frac{[B]}{[BH^+]}$$

For gaseous and solid Brønsted superacids, acidity can be determined by the ^{13}C NMR chemical shift difference ($\Delta\delta$) between the C_α and C_β carbons upon the protonation of mesityl oxide.[18] The higher the $\Delta\delta$ values are, the larger the Brønsted acidity of the examined superacid.

1.2 Lewis Superacids

In 1923, *Lewis* developed a concept that described Lewis bases as electron pair donors and Lewis acids as electron pair acceptors.[19] In 2008, *Krossing* defined Lewis superacids as compounds with a fluoride ion affinity (FIA) higher than the one of SbF_5.[20] Theoretical fluoride ion affinities are calculated as the negative enthalpy difference ($_\Delta H$) of the gas-phase reaction between the corresponding Lewis acid (LA) and the fluoride ion (F^-). Nowadays, FIA is calculated from the isodesmic reactions by using a well-known anchor molecule such as Me_3SiF (Fig. 1.2.1).[20]

$$LA + Me_3SiF \xrightarrow{\Delta H} [LA\text{-}F]^- + [Me_3F]^+$$

$$Me_3SiF \xrightarrow{\Delta H} [Me_3Si]^+ + [F]^-$$

$$LA + F \xrightarrow{FIA} [LA\text{-}F]^-$$

Figure 1.2.1. Isodesmic benchmark reactions used for the calculation of fluoride ion affinity (FIA).

The computational studies showed the tendency that independently from the central atom, very high FIA values are found for Lewis acids bearing pentafluoroorthotellurate $OTeF_5$ groups.[21,22] Lewis acidity increases with an increasing

amount of $OTeF_5$ groups (Table 1.2.1).[21] In addition, there is a correlation between an increased thermodynamic stability of a WCA and a high FIA value of its parent Lewis acid.[23]

Table 1.2.1. Fluoride ion affinities (FIA) of Lewis superacids.[21]

Lewis acid	FIA, kJ/mol
SbF_5	496
$B(OTeF_5)_3$	506
$Al(OTeF_5)_3$	598
$As(OTeF_5)_5$	580
$Sb(OTeF_5)_5$	623

The monomeric $Al(OTeF_5)_3$ was calculated to be a Lewis superacid with a FIA exceeding SbF_5 by a 100 $kJ \cdot mol^{-1}$ (Table 1.2.1). However, the solid state structure of neat $Al(OTeF_5)_3$ is still missing. Recently, the dimeric $[Al(OTeF_5)_3]_2$ Lewis superacid was synthesized from the $Al(C_2H_5)_3$ and three equivalents of teflic acid in *n*-pentane by our working group[13] Later, the synthesis was modified by using two equivalent of $Al(CH_3)_3$ and six equivalents of teflic acid in *n*-pentane with warming up of the reaction mixture to room temperature.[24] Lewis superacids often are complicated to isolate as neat substances, since they tend to coordinate to any present weak base in solution to form Lewis acid-base adducts. For instance, when the equimolar amount of coordinating solvent is present in the solution, this yields to the Lewis acid-bases $CH_3CN \rightarrow Al(OTeF_5)_3$,[13] $Al(OTeF_5)_3 \rightarrow C_7H_8$,[24] $Al(OTeF_5)_3 \rightarrow ((CH_3)_2O)_2$,[24] $Al(OTeF_5)_3 \rightarrow (SO_2ClF)_2$,[24] and $Al(OTeF_5)_3 \rightarrow (C_6H_5F)_2$[24] adducts. Similarly, the $Al(OTeF_5)_3 \rightarrow (RCN)_3$, R = CH_3, C_6H_5 is formed and additionally undergoes self-ionization in solution.[24] Generally, aluminium-based Lewis acids are widely used in organic synthesis as catalysts.[25] Introducing bulky fluorinated moieties to such species can fine-tune their coordination geometry by the steric control and reinforce their reactivity as Lewis and Brønsted superacids. For instance, the Lewis acid-base adduct $Al(OR^F)_3 \rightarrow PhF$, $R^F = C(CF_3)_3$ has been used in the abstraction of fluoride from $[SbF_6]^-$, proving its character as Lewis superacid.[26] Another implementation of fluorinated aluminium-based superacids was found for the preparation of the Lewis superacid

$Al(OC_5F_4N)_3$, its Lewis acid-base $Al(OC_5F_4N)_3 \rightarrow ((CH_3)_2O)_2$ and $Al_2(OC_5F_4N)_6 \rightarrow (CH_3CN)_4$ adducts and the corresponding weakly coordinating $[Al(OC_5F_4N)_4]^-$ anion, which indicates strong acceptor properties this aluminium-based system.[27]

1.3 Weakly Coordinating Anions

The definition of weakly coordinating anions (WCAs) takes its route from the question whether so-called "non-coordinating anions" exist. They were first implemented to describe some complexes with tetrafluoridoborate anion $[BF_4]^-$, perchlorate anion $[ClO_4]^-$ and hexafluorophosphate anion $[PF_6]^-$.[28] Spectroscopic investigations showed that upon the presence of a coordinating solvent or base, these ions easily change their symmetry and, thus, cannot be called non-coordinating.[29] The more accurate term "weakly coordinating anions" is nowadays used for the description of those anions that interact weakly with cations.[30,31] *Strauss* summarized the properties of WCAs[31]:

- WCAs must have a delocalized negative charge over a large surface area.
- WCAs must have a low polarizability, nucleophilicity and basicity.
- WCAs should possess chemical robustness and inertness towards electrophiles and oxidation agents.

The experimental estimation of the weakly coordinating behavior of WCAs is accomplished by the use of NMR-, IR-spectroscopy, and single crystal X-ray diffraction. In the NMR spectroscopy, weak coordination is e.g. estimated by the criterion of the downfield ^{29}Si NMR shift in the silylium cation in its salt with the WCA, i.e. $[Si(\mathit{/}C_3H_7)_3][WCA]$.[32] In case of IR spectroscopy, weakly coordinating properties can be estimated by the increase of N-H stretching vibration frequency in the tri-*n*-octylammonium salt, i.e. $[(n\text{-}C_8H_{17})_3N\text{-}H][WCA]$.[33] The N-H stretching vibration is the higher, the weaker the cation-anion interaction is and, thus, results in stronger N-H bonding. Solid state structures are used for the quantification of interionic distances between cation and weakly coordinating anion, indicated by short contacts being less than their sum of van der Waals radii. Introduction of WCAs to any salt will significantly change its properties, since it lowers their lattice energy of and thus, the electrostatic

cation-anion interactions.[34] In order to reduce the polarizability of WCAs, usually bulky, electron-withdrawing fluorinated ligands are used, which are introduced in order to preserve WCAs from the ligand scrambling and electrophilic attacks. WCA salts are the best soluble in non-polar solvents with low dielectric constants that reduce solvation energies.[31] Due to these properties, WCAs have important cases in fundamental chemistry for the stabilization of highly basic, reactive and oxidizing cations. For these purposes commonly used WCAs are polyfluorinated tetraarylborates BAr^F, polyfluorinated alkoxyaluminates $[Al(OR^F)_4]^-$, perhalogenated carboranes $[R\text{-}CB_{11}X_{12}]^-$ (X = F, Cl, Br) and pentafluoroorthotellurates $[E(OTeF_5)_n]^-$ (E = B, Al, Sb, As, Bi, Nb; n = 4-6). These will be discussed in more detail in the next chapters.

1.3.1 Polyfluorinated Tetraarylborates

Polyfluorinated tetraarylborates WCAs coordinate weaker, if compared to the classical weakly coordinating $[PF_6]^-$ or $[ClO_4]^-$ anions, which are used in crystal engineering, supramolecular chemistry and analytical chemistry as components of ion-selective electrodes. Since in the tetrafluoroborate $[BF_4]^-$ structures the decomposition by fluoride abstraction compete with coordination[35], a need in more stable borate-based WCAs is raised. Exchanging fluorine atoms $[BF_4]^-$ towards alkyl and fluoroalkyl groups improved the chemical properties of such WCAs. For instance, the $[B(CF_3)_4]^-$ anion is resistant towards strong oxidizing and reducing agents, in particular, not affected by the presence of liquid ammonia, dilute mineral acids or anhydrous HF.[36] Moreover, the synthesis of the $[B(CF_3)_4]^-$ anion requires handling of the explosive organolithium intermediate LiC_6F_5, which is a disadvantage of this WCA for practical applications.

In 1984, *Kobayashi et al.* synthesized the first polyfluorinated tetraarylborate, often abbreviated as BAr^F, represented by the [3,5-bis(trifluoromethyl)phenyl]borate anion.[37] The salts of non-fluorinated $[B(C_6H_5)_4]^-$ anions tend to form π-complexes and tight ion pairs,[38] whereas its perfluorinated $[B(C_6F_5)_4]^-$ analogue demonstrates weakly coordinating properties that are used in homogeneous catalysis.[39] Since WCAs are mainly used for the stabilization of reactive counter ions like triphenylsilylium $[(C_6H_5)_3Si]^+$, the salts of the $[B(C_6F_5)_4]^-$ anion tend to form oils and liquid clathrates,

rather than to crystallize. Furthermore, the disadvantage of this anion is that the C-B bond is prone to electrophilic cleavage. $[B(3,5\text{-}(CF_3)_2C_6H_3]^-$ and $[BC_6F_5]^-$ are frequently used due to their weak basicity, kinetic stability and increased solubility. In particular, the fluorinated borane-based WCAs are used for ionic liquids with tunable melting points.[40]

1.3.2 Carboranes

An important role for the WCA chemistry plays the class of *closo*-carborane anions – polyhedral electron-deficient cluster anions. These WCAs possess a closed cage structural arrangement of the carbon and boron atoms that occupy all vertices of an icosahedron. In 1969, *Knoth et. al.* reported the synthesis of the first weakly coordinating 12-vertex *closo*-icosahedral carborane anion – $[HCB_{11}H_{11}]^-$.[41] The carborane WCAs exhibit unusual aromaticity. *C. Reed* compared them to a "3D analogue of benzene" due to the presence of strong delocalized σ-bonding with σ-aromaticity, i.e. HOMO-LUMO gap being larger than in π-aromatic systems.[42]

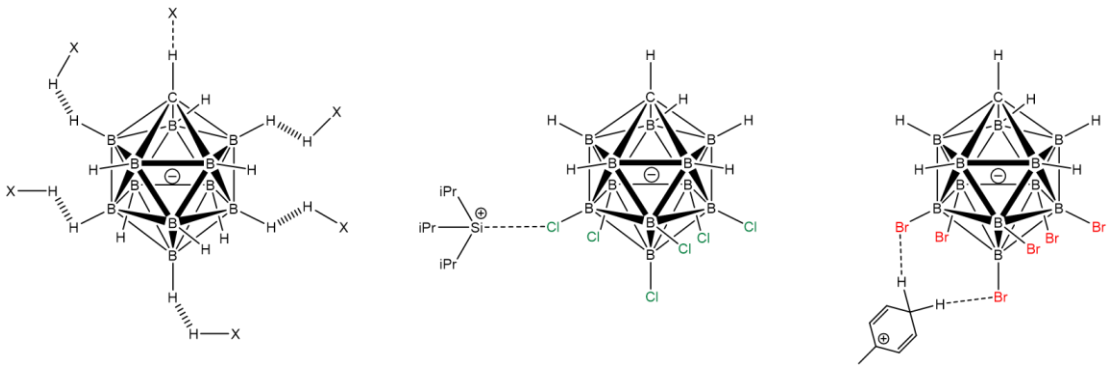

Figure 1.3.2.1. Schematic representation of intramolecular interactions in selected carbaboranes $[HCB_{11}H_{11}]^-$ (left)[43], $[HCB_{11}H_6Cl_6]^-$ (middle)[18], $[HCB_{11}H_6Br_6]^-$ (right)[18].

Because the outer sphere of carboranes usually contains a Brønsted acidic C-H moiety, they can participate in intramolecular interactions and form hydrogen bonds of the type C–H···X (X = O, N, S, F, π-aromatic system, (Fig. 1.3.2.1).[43] The B-H units of carboranes can form dihydrogen interactions of the B-H···H-X type, where X equals the electronegative element or π-system (Fig. 1.3.2.1).[43] The nucleophilic properties of carboranes could be decreased by their halogenation and alkylation on boron

vertices. Halogenation of carboranes improves their weakly coordinating properties and thus, decreases solubility. Polyhalogenated carboranes can be obtained from their parent $[HCB_{11}H_{11}]^-$ anion by the use of F_2, ICl, SO_2Cl_2 or SbF_5.[44][45] The disadvantages of these anions are their small yields (<3%) and complicated and expensive multistep synthesis.[46]

1.3.3 Polyfluorinated Alkoxyaluminates

Another important class of WCAs are fluorinated alkoxyaluminates of the general type $[Al(OR^F)_4]^-$ with fluorinated alkyl and aryl ligands R^F = $C(CF_3)_3$, $C(H)(CF_3)_2$, $C(CH_3)(CF_3)_2$, $C(C_6H_5)(CF_3)_2$.[47] The typical synthesis of alkoxyaluminates is known for decades and includes reaction of fluorinated alcohols with $LiAlH_4$.[47]Among alkoxyaluminates, $[Al(OC(CF_3)_3)_4]^-$ WCA is one of the least coordinating due to its bulkiness and the distribution of the negative charge over 36 fluorines that shields the aluminium center. Moreover, $[Al(OC(CF_3)_3)_4]^-$ derivatives can be synthesized on the multigram scale.[47] Due to high electrochemical stability of perfluorinated alkoxyaluminates, they can stabilize highly redox-active cations that are used for electrochemical applications.[48] The corresponding silver salt $Ag[Al(OR^F)_4]$ can be obtained from the metathesis reaction of the lithium salt with AgF.[47] The single downside for the $[Al(OR^F)_4]^-$ WCAs is the decomposition in the presence of small electrophiles like $[Si(CH_3)_3]^+$[49] or $[PCl_2]^+$[50] and $[SiCl_3]^+$[50], whereas, they can stabilize bulky silylium cations like $[Si(C_6(CH_3)_5)_3]^+$.[51] The $[Al(OC(CF_3)_3)_4]^-$ anion coordinates to small cations like Li^+,[52] $[C_2H_5Zn]^+$[53] or $[PCl_2]^+$[54] through the oxygen atom, which is a disadvantage of this type of WCAs. The increased Lewis acidity could be reached in the Lewis acid-base adduct $Al(OC(CF_3)_3)_3 \rightarrow {}^t(C_4H_9)_3SiF$ and $Al(OC(CF_3)_3)_3 \rightarrow (CH_3)_3SiF$ allowing their application for the synthesis of weakly coordinating $[Al(OC(CF_3)_3)_3F]^-$ and even the fluorine-bridged $[((CF_3)_3CO)_3Al\text{-}F\text{-}Al(OC(CF_3)_3)_3]^-$ anions.[55] These are known for many counter-cations including Li^+, K^+, Ag^+, $[NO]^+$ and $[(C_6H_5)_3C]^+$.[50] This fluorine-bridged representative is used for the stabilization of a pentacoordinated silylium $[(CH_3)_4C_4\text{-}Si(CH_3)_3]^+$ cation.[56] However, this anion undergoes dissociation to the Lewis acid and solvent adduct when dissolved in coordinating solvents like Et_2O.[56]

1.4 Pentafluoroorthotellurates

Due to its high steric demand and distribution of the negative charge over a large area, the pentafluoroorthotellurate or teflate $[OTeF_5]^-$ ligand possesses electron-withdrawing properties comparable to fluorine.[57][58–60]. This is reflected in multiple multinuclear NMR studies, which include investigations of chemical shift differences and/or quadrupolar splitting in ^1H NMR spectra of CH_3X[59,60] and C_2H_5X (X = F, Cl, Br, I, $OTeF_5$);[57,60] ^{31}P NMR spectra of OPF_2X (X = F, Cl, Br, $OTeF_5$);[59] ^{125}Te NMR spectra of TeX_n, (n = 4, 6, X = F, $OTeF_5$);[57] ^{129}Xe NMR and ^{129}Xe Mößbauer spectra of XeX_n (n = 2, 4) and $OXeX_4$ (X = F, $OTeF_5$)[57]. The octahedral arrangement of the pentafluoroorthotellurate $[OTeF_5]^-$ ligand results in AB_4 a spin-spin splitting system, which is used for the detection of pentafluoroorthotellurates in the multinuclear NMR spectra.[58] In addition, pentafluoroorthotellurates exhibit unique characteristic bands in vibrational spectra.[58]

The pentafluoroorthotellurate ligand resembles the chemical properties of fluoride, especially in the ability of fluoride to stabilize high oxidation states.[13] Thus, the electronegative $[OTeF_5]^-$ was used for the synthesis of compounds such as $O{=}Mo(OTeF_5)_4$, $W(OTeF_5)_6$, $Ta(OTeF_5)_5$, $ReO_2(OTeF_5)_3$, $OsO(OTeF_5)_4$, as well as $E(OTeF_5)_6$ (E = Xe, Te, W, U) or $I(OTeF_5)_5$.[58,61]

Typically, for the synthesis of the WCAs based on pentafluoroorthotellurates, $HOTeF_5$, $AgOTeF_5$, $B(OTeF_5)_3$, and $Xe(OTeF_5)_2$ are used as common $OTeF_5$ transfer reagents.[58] The pentafluoroorthotelluric or teflic acid $HOTeF_5$, was initially synthesized in 1964 by Engelbrecht and Sladky from $BaTeO_4$ and HSO_3F with 25% yield.[62] Alternative synthesis of teflic acid includes reaction of HSO_3F and $BaO_2Te(OH)_4$.[63] The biggest yields of teflic acid (40-60%) can be obtained by the reaction of telluric acid $Te(OH)_6$ and fluorosulfonic acid HSO_3F.[64] Teflic acid is also formed as the hydrolization product of TeF_6.[65] Teflic acid has a melting point of 39.1 °C and boiling point of 59.7 °C and is moisture-sensitive and therefore must be handled under inert conditions in order to prevent hydrolysis to hydrofluoric acid HF and telluric acid $Te(OH)_6$.[62]

The alkali pentafluoroorthotellurates are white crystalline solids that are stable above T = 250 °C and obtained from the reaction of corresponding alkali chloride MCl (M = Li, Na, K, Rb, Cs) with an excess of teflic acid $HOTeF_5$.[66] Ammonium and

pyridinium derivatives are synthesized with an equimolar amount of $HOTeF_5$ and NH_3 or C_5H_5N in CCl_4 to give $[NH_4][OTeF_5]$ and $[C_5H_5N\text{-}H][OTeF_5]$, respectively.[66]

In the row of $[Tl(OTeF_5)_3]$, $[Au(OTeF_5)_3]$ and $[Al(OTeF_5)_3]_2$, the enhanced Lewis acidity on metal center is reached due to the presence of electron-withdrawing $OTeF_5$ ligands.[67] Lewis acidic $Au(OTeF_5)_3$ is prepared from AuF_3 and an excess of $B(OTeF_5)_3$, the corresponding dimer $[Au(OTeF_5)_3]_2$.[68]

The homoleptic tetrakis(pentafluoroorthotellurate) anions are known with B, Au, Al central atoms to give $[B(OTeF_5)_4]^-$,[69] $[Al(OTeF_5)_4]^-$,[13] $[Au(OTeF_5)_4]^-$[70] WCAs, respectively (Table 1.4.1.1). Tetrakis(pentafluoroorthotellurato)aluminate $[Al(OTeF_5)_4]^-$ is an only recently reported anion with tetrahedrally coordinated teflic groups over an aluminium center.[13]

The Brønsted superacid $[o\text{-}C_6H_4F_2\text{-}H][Al(OTeF_5)_4]$ synthesis is an ideal starting point for the most salts of the tetrakis(pentafluoroorthotellurato)aluminate.[13] It is prepared by the treatment of one equivalent of triethylaluminium $Al(C_2H_5)_3$ with four equivalents of pentafluoroorthotelluric acid, $HOTeF_5$, in the presence of *ortho*-difluorobenzene as a solvent at −30 °C.[13]

For the synthesis of pentakis(pentafluoroorthotellurato) derivatives of the general formula $M(OTeF_5)_5$ (M = Sb,[71] As[72]), metal chloride or the metal fluoride is reacted with either $B(OTeF_5)_3$, $Xe(OTeF_5)_2$ or $HOTeF_5$.

Hexakis(pentafluoroorthotellurate) anions $[Cat]^+[M(OTeF_5)_6]^-$ M = As, Sb, Bi, Nb; $[Cat]^+ = Cs^+$, Ag^+, $[N(CH_3)_4]^+$, $[N(C_2H_5)_4]^+$, $[SbCl_4]^+$, $[SbBr_4]^+$, are known and described by the literature.[73] Among them, the salts of the $[Sb(OTeF_5)_6]^-$ WCA were reported to be the most stable.[74] The weakly coordinating $[Sb(OTeF_5)_6]^-$ anion is known for the stabilization of $[XeOTeF_5]^+$,[75] the fluorine-bridged $[Cl_3Te\text{-}F\text{-}TeCl_3]^+$,[76] and even oxidizing elemental tellurium to give $[Te_4][Sb(OTeF_5)_6]_2$.[76]

Recently, our working group revealed the novel dianions $[Al(OTeF_5)_5]^{2-}$[24] and $[Ni(OTeF_5)_4]^{2-}$[77]. Pentafluoroorthotellurates often undergo dimerization or/and oxygen bridge formation. In the dimers of pentafluoroorthotellurate derivatives, the main bridging motifs are M-O(TeF_5)-M, where M = Ag,[78,79,80] Al,[24] Au,[68] Ga,[81] Hg,[82] Ti,[83] Tl,[69,84] Zn.[79]

Table 1.4.1.1. An overview of some derivatives stabilized by the tetrakis(pentafluoroorthotellurate).

WCA	$[B(OTeF_5)_4]^-$	$[Al(OTeF_5)_4]^-$	$[Au(OTeF_5)_4]^-$
Cations	$[K]^+$[85], $[Ag]^+$[80], $[Cs]^+$[86], $[Tl]^+$[69,80], $[N(CH_3)_4]^+$,[69] $[N(C_4H_9)_4]^+$[69], $[Ag(CO)]^+$[87], $[Ag(CO)_2]^+$[88], $[C(C_6H_5)_3]^+$[80], $[C_6F_5Xe]^+$[85]	$[Li]^+$[89], $[Na]^+$[89], $[K]^+$[89], $[Ag]^+$[89], $[Rb]^+$[89], $[Cs]^+$[13,89], $[Tl]^+$[69,80], $[(CH_3)_2Cl]^+$, $[NO]^+$, $[P_4H]^+$, $[CH_3P(CF_3)_3]^+$, $[(C_8H_{17})_3NH]^+$, $[Ag(CO)]^+$[87], $[Ag(CO)_2]^+$[88], $[C_6H_7]^+$[13], $[C_9H_{13}]^+$[13], $[o\text{-}C_4F_2H_4\text{-}H]^+$[13], $[C(C_6H_5)_3]^+$[13][80], $[C(C_6F_5)_3]^+$[90], $[P(C_6H_5)_4]^+$[13]	$[Cs]^+$,[70] $[N(CH_3)_4]^+$,[70] $[N(C_2H_5)_3CH_3]^+$ [70]

1.5 Noncovalent Interactions

The class of noncovalent interactions consist of weak electrostatic interactions that do not involve sharing electrons and orbital overlapping between atoms and can be judged from partial charges.[92] The term "noncovalent interactions" is used in supramolecular chemistry as intra- and intermolecular term and is a synonym of noncovalent.[93] Unlike the covalent bonding, noncovalent interactions exhibit lower energy and are less directed. The enthalpy of noncovalent interactions is within the range of 1-100 kJ/mol per contact, which is below the formation of covalent bonds at 400 kJ/mol.[94] Therefore, noncovalent interactions include a wide range of different binding energies like London forces, hydrogen bonding, halogen bonding, steric repulsions, anion- and cation-π interactions, π-π stacking, and dipole-dipole interactions and many more.[95,96] Noncovalent interactions appear hidden as short interatomic contacts between the voids of covalently bound atoms in the solid state structures.[96] They directly influence important physical and biological properties like melting points, boiling points, as well as unfolding proteins, RNA and DNA strands. Noncovalent interactions have found their implementation in the molecular design and are used in crystal engineering,[94] synthesis of molecular building blocks,[97] for designing catalysts[98] and adsorbents[99] and for the investigation of host-guest interactions for the biomedical utilization.[100]

1.5.1 Halogen Bonding

In the 1950s, Nobel Prize Laureate *O. Hassel* did his X-ray diffraction training in Berlin and investigated charge-transfer complexes that laid the fundament of halogen-bonded complexes.[101] In 1954, he reported the first example of halogen bonding in the crystal structure of a halogen bonded complex of a 1 : 1 adduct of 1,4-dioxane and bromine with a short oxygen-bromine distance of 2.71 Å, being below the vdW radii sum (3.37 Å).[102] Nowadays, halogen bonding is described as the net attractive interaction between the electrophilic region in halogen atoms and the nucleophilic region of the same or different molecular entity.[103] The electrophilic region in halogen atoms is called σ-hole – an area of depleted electron density, located on the halogen bond axis. The concept of σ-hole was first published in the literature in 2007 and was developed by *Clark et al*.[104] The σ-hole can be visualized computationally by mapping the electrostatic potential onto the electron density. In general, the σ-hole is associated with a positive electrostatic potential (ESP) region that is used to form attractive noncovalent interactions with negative sites.[105] For the definition of the σ-hole size and position of any molecular entity, the electrostatic potential V(*r*) is calculated from the Coulomb's Law using equation below,

$$V(r) = \sum_A \frac{Z_A}{|R_{A-r}|} + \int \frac{-\rho(r')dr'}{|R_A - r|}$$

where Z_A – charge on nucleus A, located at R_A; ρ(r) – molecule's electronic density. In the electrostatic potential regions where *V*(r) is positive indicate predominantly nuclear contributions and form the σ-holes. Regions of negative *V*(r) indicate predominantly electronic contributions and they are attractive to positive sites. The ESP is measured for a set of atomic nuclei and electrons in atomic units (a.u.) or e/bohr^3. *Bader et al*. suggested a surface with an electron density of 0.001 e/bohr^3, which includes about 96% of the electronic charge of molecule.[106] This density value became standard in calculations of electrostatic potential of neutral molecular species, although other values, such as 0.0015 au and 0.002 e/bohr^3, have remained in use.[107] Often halogen bond species are denoted as R–X···Y, where R – covalently bound species, X – halogen bond donor with σ-hole, i.e. electron electrophilic region, Y – halogen bond acceptor

with electron rich region. A halogen bond is an attractive noncovalent interaction and is a highly directional interaction with general connectivity R–X···Y at a contact angle close to 180°. The σ-hole concept explains why L-shaped structural arrangement of Cl_2 dimers is preferred over the expected T-shape in the solid state structure of Cl_2.[108] The presence of a σ-hole on fluorine is debated and mostly not affecting structural arrangement.[109] The positive character of the σ-hole increases with polarizability of the halogen atom in the row F<Cl<Br<I.[110] The change in hybridization of a carbon atom, i.e. more s-character of the hybrid orbitals that is covalently bound to a halogen atom, increases the electron-withdrawing property of the particular halogen, thus its σ-hole, and follows the trend C(sp)>C(sp^2)>C(sp^3).[111]

1.5.2 Anion-π Interactions

Anion-π interactions are defined as favorable noncovalent interactions involving an anion and an electron-deficient arene.[112] Typically, anion-π interactions are studied in the solid state as short centroid-anion distances and carbon-anion distances between the arene and the corresponding anion. Anion-π interactions are directional and must be located above the centroid ring with the distance shorter than the sum of the vdW radii of the interacting atoms.[113] In order to design strong anion-π interaction, the aromatic molecule should possess a large positive quadrupole moment and large molecular polarizability.[114] Electron-withdrawing substituents on the arene ring cause an increase of the electric quadrupole moment Q_{zz}, thus, leading to a larger positive quadrupole moment. In hexafluorobenzene the $Q_{zz}(C_6F_6)$ equals +9.5 B, in comparison to the negative one in benzene $Q_{zz}(C_6H_6)$ = –8.48 B or pyridine $Q_{zz}(C_5H_5N)$ = –2.6 B (Fig. 1.5.2.1).[115,116]

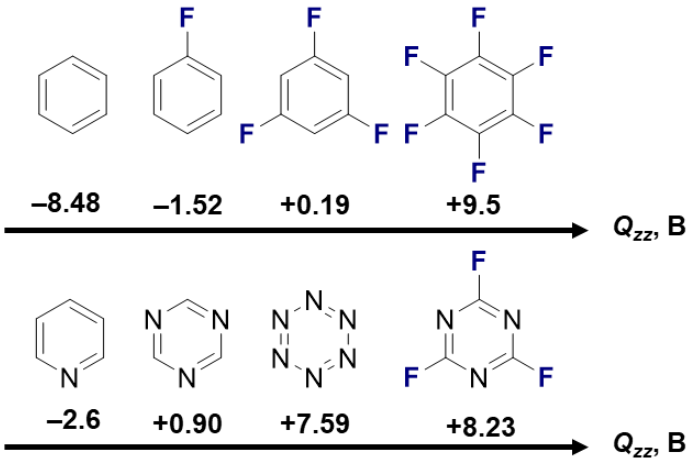

Figure 1.5.2.1. Quadrupole moments (Q_{zz}) of some arenes in Bukinghams (B). The values are taken from the literature.[115]

Unlike the reported covalent Meisenheimer complex in which a fluoride is covalently bound to the hexafluorobenzene (Fig. 1.5.2.2), solid state structures of noncovalent anion-π interactions between fluoride and perfluorinated arenes are still lacking.[117]

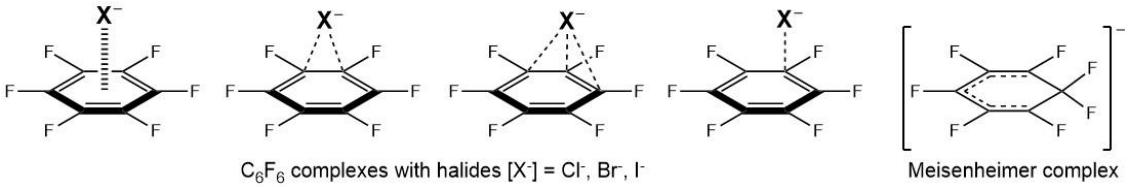

Figure 1.5.2.2. Depiction of plausible anion-π complexes of hexafluorobenzene C_6F_6 with halides Cl^-, Br^-, I^- and covalent Meisenheimer complex of hexafluorobenzene with fluoride F^-.

The anion-arene distance is also dependent on the anion size and nature. Thus, smaller anions are more polarizing, causing shorter anion-π distances, like it was reported for complexes of spherical monoatomic halides Cl^-, Br^-, I^- anions and hexafluorobenzene C_6F_6.[118] Theoretical studies report the reinforcement of anion-π interactions, if the arene is involved as a hydrogen bond acceptor.[119] The degree of fluorination of the anion and its bulkiness play key roles for the minimization of cation-anion interactions. In solid state structures of small fluorinated WCAs like $[BF_4]^-$, $[PF_6]^-$ and $[CF_3SO_3]^-$ the electrostatic effects dominate the anion-π interactions.[120]

II Objectives and Scientific Goals

The Brønsted superacid [*o*-$C_6H_4F_2$-H][$Al(OTeF_5)_4$] discovery by our group has led to the development of the new class of compounds, containing the weakly coordinating $[Al(OTeF_5)_4]^-$ anion. The presence of the weakly coordinating $[Al(OTeF_5)_4]^-$ anion in its compounds significantly impacts the structural and chemical properties.

The purpose of this work is to synthesize and characterize properties of quaternary ammonium salts and Brønsted superacids, based on the weakly coordinating $[Al(OTeF_5)_4]^-$ anion. The Brønsted superacid [*o*-$C_6H_4F_2$-H][$Al(OTeF_5)_4$] was used for synthesis of tetraalkylammonium and halogenated pyridinium salts of the weakly coordinating $[Al(OTeF_5)_4]^-$ anion. These salts demonstrated ionic liquid behavior and rare, previously undiscovered anion-π interactions, respectively. Aiming to find perspective applications, arene-based Brønsted superacids [arene-H][$Al(OTeF_5)_4$], arene = *o*-$C_4H_4F_2$, C_6H_6, C_6H_8 were used for the selective C(sp^3)-F bond activation in the commercial refrigerant HFO-1234yf.

III Outline

This chapter contains a brief outline of the results obtained in this work. Chapter IV contains the complete results by means of two peer-reviewed articles.

3.1 Halogenated Pyridinium Cations

The halogenation of pyridine lowers its basicity, depending on the type, amount and position of the halogens that are introduced to the pyridine ring. Due to its high electronegativity, the largest impact on the pyridine basicity is caused by fluorine, when compared to higher halogen homologues in *para*-position of pyridine, as summarized in Fig. 3.1.1 and 3.1.2.

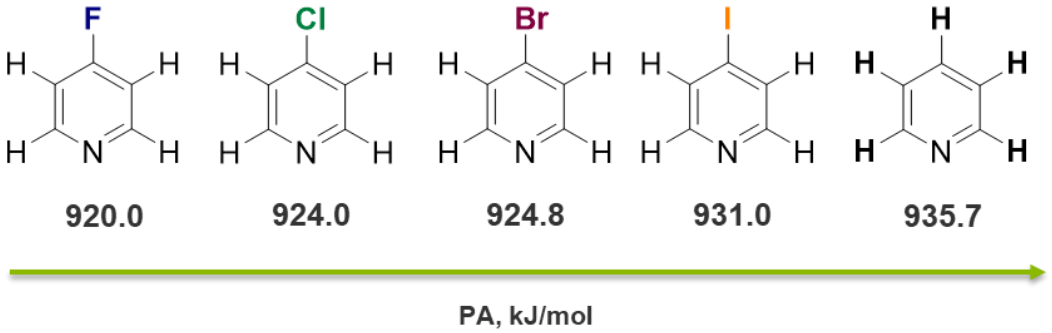

Figure 3.1.1. Proton affinities (PA) of C_5H_4FN, C_5H_4ClN, C_5H_4BrN, and C_5H_4IN, in kJ/mol, calculated on the B3LYP-D3/def2-TZVPP level of theory.

The basicity trend follows the row C_5F_5N<C_5F_4ClN<C_5F_4BrN<C_5F_4IN, indicating the weaker impact of higher halogen homologues on the basicity, when compared to fluorine (Fig. 3.1.2).

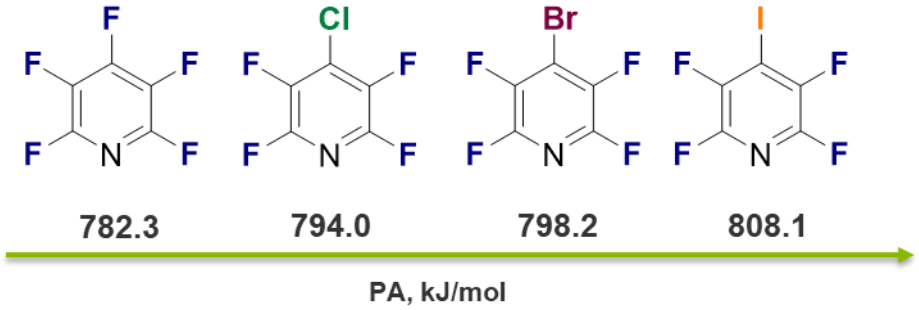

Figure 3.1.2. Proton affinities (PA) of C_5F_5N, C_5F_4ClN, C_5F_4BrN and C_5F_4IN in kJ/mol, calculated on the B3LYP-D3/def2-TZVPP level of theory.

The computed ESP plots of the *para*-halogen-substituted tetrafluoropyridine cations demonstrate differently sized σ-holes for the $[C_5F_5N\text{-}H]^+$, $[C_5F_4ClN\text{-}H]^+$, $[C_5F_4BrN\text{-}H]^+$ and $[C_5F_4IN\text{-}H]^+$ cations (Fig. 3.1.3).

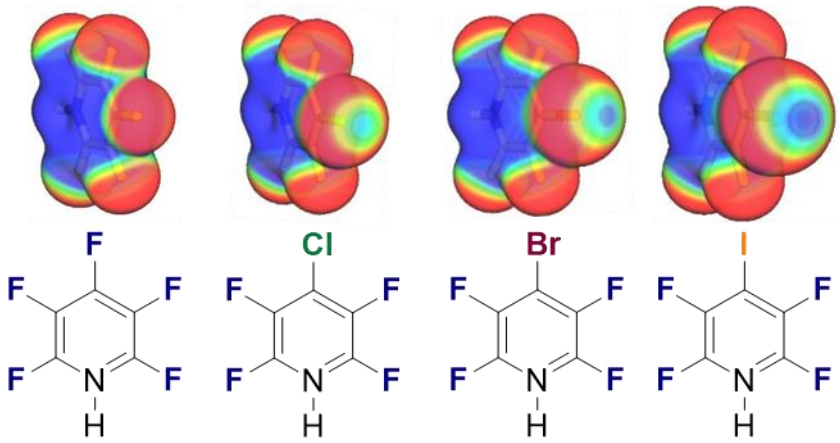

Figure 3.1.3. Electrostatic potentials of *para*-substituted tetrafluoropyridines in the range of 0.15 a.u (red) to 0.20 a.u. (blue) have been mapped onto their electron densities (isosurface value 0.0035 a.u.); calculated on B3LYP/def2-TZVPP level of theory.

Whereas the presence of a σ-hole on fluorine atoms is generally uncommon, the biggest σ-hole is found as expected for the iodine-substituted compound. The σ-hole size in protonated *para*-halogen-substituted tetrafluoropyridines follows the row $[C_5F_5N\text{-}H]^+ < [C_5F_4ClN\text{-}H]^+ < [C_5F_4BrN\text{-}H]^+ < [C_5F_4IN\text{-}H]^+$ (Fig. 3.1.3). Meanwhile, the π-electron density on the aromatic ring of the *para*-halogen-substituted tetrafluoropyridine cations indicates a very weak change in the depletion of electron density. According to the ESP plots (Fig. 3.1.3), the strongest noncovalent interactions are to be expected from the site of the N-H moiety (hydrogen bonding) and on the σ-holes (halogen bonding) in *para*-position of the *para*-halogen-substituted pyridinium cations. In attempts to crystalize and structurally characterize halogen-substituted tetrafluoropyridines, the crystal structures of protonated pyridines, i.e. C_5F_5N, C_5F_4ClN, C_5Cl_5N, with the $[Al(OTeF_5)_4]^-$ WCA were obtained and published in the peer-review article that can be found in chapter 4.2.

3.1.1 $[C_5F_3H_2N\text{-}H][Al(OTeF_5)_4]$

Introduction of fluorine substituents to the pyridine ring drastically decrease its basicity by more than 100 kJ/mol (Fig. 3.1.1.1, A), making it a rather hard base to protonate. The electrostatic potential (ESP) plot of the $[C_5F_3H_2N\text{-}H]^+$ cation shows the depleted π-electron density above the π-bonds in a plane perpendicular to the pyridinium ring (Fig. 3.1.1.1, B). The highest density depletion is observed in 3- and 5-position of the pyridine ring and, thus, is a primary target for potential anion-π interactions.

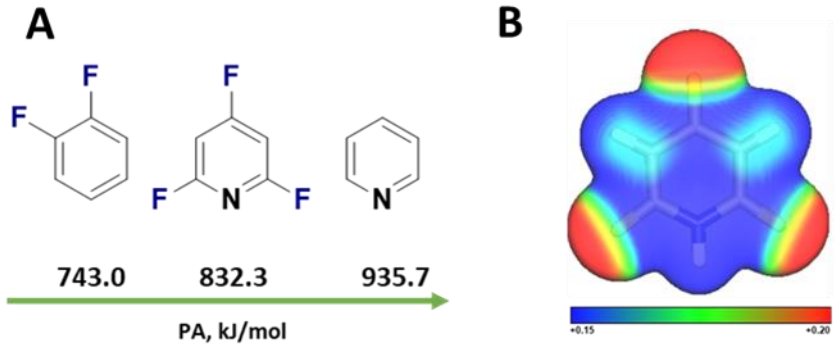

Figure 3.1.1.1. A - Proton affinities (PA) of the *ortho*-difluorobenzene (left), 2,4,6-trifluoropyridine (middle) and pyridine (right); calculated on the B3LYP-D3/def2-TZVPP level of theory. B - Electrostatic potential of $[C_5F_3H_2NH]^+$ in the range of 0.15 a.u (red) to 0.20 a.u. (blue) have been mapped onto its electron density (isosurface value 0.0035 a.u.); calculated on B3LYP/def2-TZVPP level of theory

Whereas the $[C_5H_2F_3N\text{-}H]^+$ cation is literature unknown, the alkylated $[C_5H_2F_3N\text{-}C_2H_5]^+$ cation can be assessed by the reaction of 2,4,6-trifluoropyridine with ethyl triflate.[121] This reaction leads to formation of N-ethyl-2,4,6-trifluoropyridinium triflate, which is used for the synthesis of building block for biomedical applications (Fig. 3.1.1.2).[121]

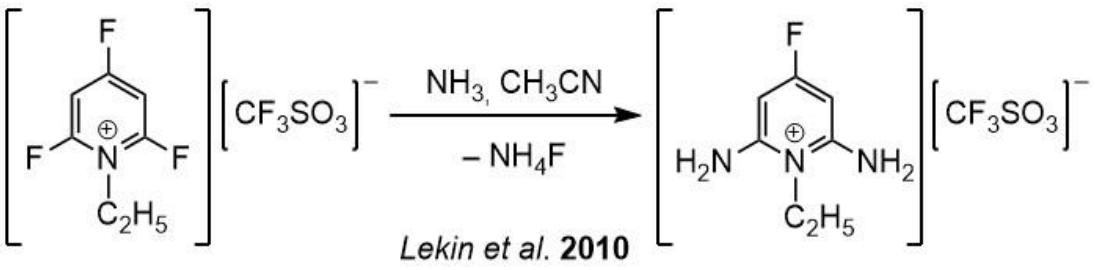

Figure 3.1.1.2. Synthesis of 8-fluoro-4-ethyl-4H-bis[1,2,3]dithiazolo[4,5-b:5′,4′-e]pyridine-3-yl.[121]

For the protonation of the 2,4,6-trifluoropyridine, the Brønsted superacid [*o*-$C_6F_2H_4$-H][Al(OTeF$_5$)$_4$] was used. The procedure was similar to the synthesis of [C_5F_5N-H][Al(OTeF$_5$)$_4$], described in chapter 4.2. Even though, the NMR characterization suggested mainly formation of [$C_5H_2F_3N$-H][Al(OTeF$_5$)$_4$], two different crystal structures were obtained from the reaction solution of [$C_5H_2F_3N$-H][Al(OTeF$_5$)$_4$] in *o*DFB. Crystals of [$C_5H_2F_3N$-H][Al(OTeF$_5$)$_4$] have been obtained by slow cooling of the reaction mixture in *o*DFB to –40°C (Fig. 3.1.1.3). The salt crystallizes in the monoclinic space group P2$_1$/n. The weakly coordinating [Al(OTeF$_5$)$_4$]$^-$ anion shows a slightly disturbed tetrahedron with ∡(O-Al1-O) bond angles of 106.375(3)° and 111.625(3)°, respectively.

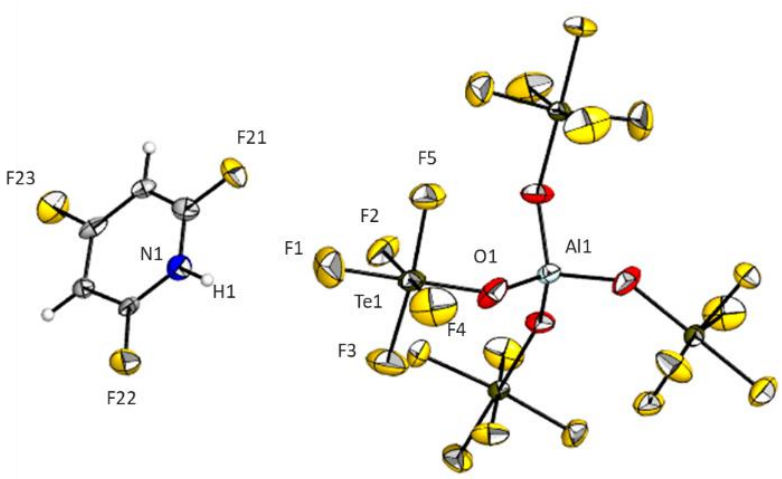

Figure 3.1.1.3. Molecular structure of [$C_5F_3H_2N$-H][Al(OTeF$_5$)$_4$] in the solid state with thermal ellipsoids shown at the 50 % probability level.

The Al-O bond of 174.4(7) pm lays within the range of previously reported aluminates.[13,89,122,123] The [$C_5H_2F_3N$-H]$^+$ cation is caved in a field of weak interactions with the WCA [Al(OTeF$_5$)$_4$]$^-$ (Fig. 3.1.1.4, A). The weak interaction between O4 and F21 from the cation is indicated by its short contact of 283.37(1) pm that is about 14 pm less than the sum of vdW radii (Fig. 3.1.2).[124] In addition to the weak interactions in-plane of the [$C_5F_3H_2N$-H]$^+$ pyridinium cation, anion-π interactions between the [$C_5F_3H_2N$-H]$^+$ cation and the [Al(OTeF$_5$)$_4$]$^-$ anion are found (Fig. 3.1.1.4). These are directed above and below the aromatic ring with short C-F contacts, namely F20-C4, F20-C5, F11-C3 and F14-C5 (Fig. 3.1.1.4).

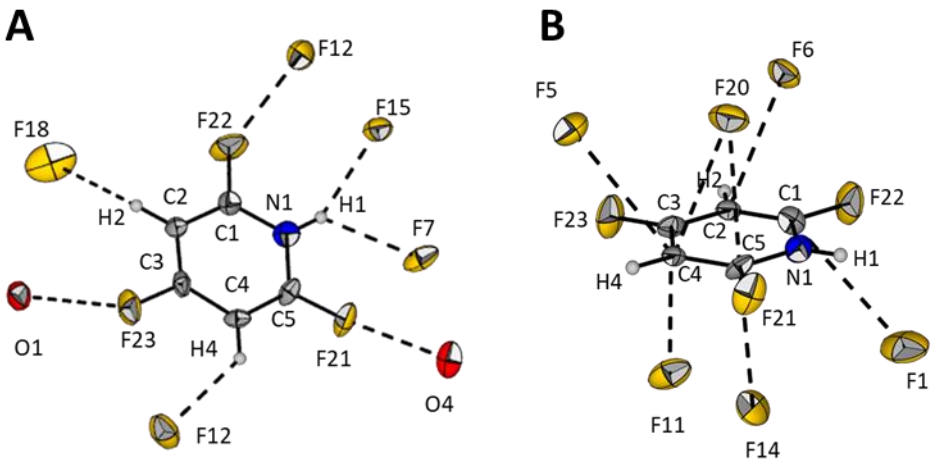

Figure 3.1.1.4. Short contacts within the $[C_5F_3H_2N\text{-}H]^+$ cation in the solid state structure of $[C_5F_3H_2NH][Al(OTeF_5)_4]$ with thermal ellipsoids shown at the 50 % probability level. Anionic moieties are omitted for clarity. A **-** Visualization of in-plane interactions. Selected bond lengths in pm: F23-O1 284.74(1), F18-C2 321.42(1), F22-F12 292.77(1), F15-N1 307.88(1), F7-N1 322.08(1), F21-O4 283.37(1), F12-C4 321.56(1). B **-** Visualization of the anion-π interactions. Selected bond lengths in pm: F6-C2 300.50(1), F20-C4 319.45(1), F20-C5 296.89(1), F5-C4 318.52(1) F11-C3 313.99(1), F14-C5 303.05(1), F1-C1 320.97(1).

The biggest number of short contacts is found between the fluorine atoms of the WCA and the carbon atoms of the cation in 3- and 5-position, which is in agreement with the calculated ESP (Fig. 3.1.1.4, B). Secondary interactions between cation and anion are between F5-C4, F6-C2, F1-C1 with interatomic distances being less or close to the sum of vdW radii (317 pm) of the atoms that lays within experimental error of the method.[124]

The Lewis acid-base adduct $C_5F_3H_2N\rightarrow Al(OTeF_5)_3$ of 2,4,6-trifluoropyridine – $C_5F_3H_2N\rightarrow Al(OTeF_5)_3$ – was also crystallized from the solution of $[C_5H_2F_3N\text{-}H][Al(OTeF_5)_4]$ in *o*DFB (Fig. 3.1.1.5). This is in particular remarkable as substitution of $OTeF_5$ groups from the $[Al(OTeF_5)_4]^-$ anion has not been observed under similar conditions and stabilization of the Lewis acid $Al(OTeF_5)_3$ in *o*DFB still is in question. The Lewis acid-base $C_5F_3H_2N\rightarrow Al(OTeF_5)_3$ crystalizes in the monoclinic space group *Cc* (Fig. 3.1.1.5). The Al-O bond length is 172.6(8) pm and shows about the same bond lengths range as in the related $[C_5H_2F_3N\text{-}H][Al(OTeF_5)_4]$ salt.

In the recorded ^{27}Al NMR spectrum of $[C_5H_2F_3N\text{-}H][Al(OTeF_5)_4]$ solution in *ortho*-difluorobenzene, the major sharp resonance at δ = 50.1 ppm corresponds to the

symmetric homoleptic $[Al(OTeF_5)_4]^-$ anion.[13,17,89,122] This major resonance is accompanied by a broad singlet at δ = 53.5 ppm and is within the typical region of four-coordinate aluminum centers and could be assigned to $C_5F_3H_2N{\rightarrow}Al(OTeF_5)_3$. The formation of $C_5F_3H_2N{\rightarrow}Al(OTeF_5)_3$ can either be attributed to a ligand exchange reaction in *o*DFB, which is aided by the presence of the 2,4,6-trifluropyridine, as nitrogen donor base.

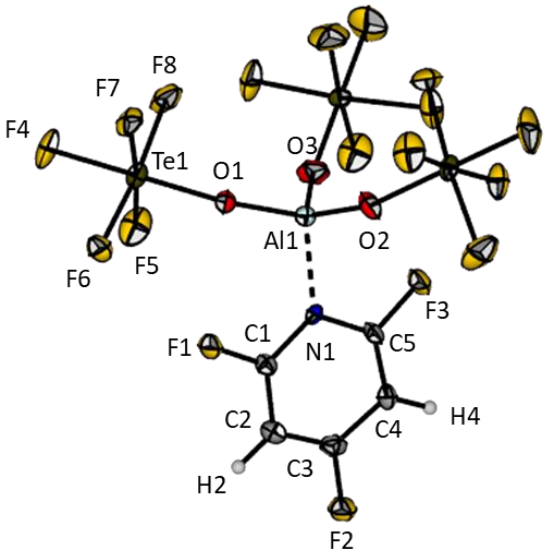

Figure 3.1.1.5. Molecular structure of $C_5F_3H_2N{\rightarrow}Al(OTeF_5)_3$ in the solid state with thermal ellipsoids shown at the 50 % probability level. Selected bond lengths in pm: Al1-N1 196.0(7), Te1-F4 183.5(5), Te1-F5 182.9(6), Te1-F6 181.0(6), Te1-F7 181.8(5), Te1-F8 182.9(6), Te1-O1 181.5(6), Al1–N1 196.0(7). Selected angles in °: O1-Al1-N1 110.3(4), O2-Al1-N1 103.7(4), O3-Al1-N1 102.6(3).

The ^{1}H NMR low-temperature +20-(–70) °C spectra show the resonance of the acidic proton of the $[C_5H_2F_3NH]^+$ cation between 10.6 and 18.5 ppm, depending on the temperature, which can be reverted after warm up (appendix). The ^{19}F NMR low-temperature +20-(–70) °C spectra (appendix) revealed coalescence at higher temperatures of chemically equivalent *ortho*-fluorine atoms in $[C_5H_2F_3N\text{-}H]^+$ cation.

3.1.2 $[C_5H_4BrN\text{-}H][Al(OTeF_5)_4]$

The calculated electrostatic potential plot of the $[C_5H_4BrN\text{-}H]^+$ cation reveals strongest interaction with WCA will be observed via the N-H moiety, which is the most probable site to form hydrogen bonds (Fig. 3.1.2.1). Also, the $[C_5H_4BrN\text{-}H]^+$ cation shows an enhanced σ-hole on bromine, which is a potential site for halogen bonding. The depletion of the density from the aromatic ring is rather weak (Fig. 3.1.2.1), especially when compared to $[C_5F_4BrN\text{-}H]^+$ (Fig. 3.1.3).

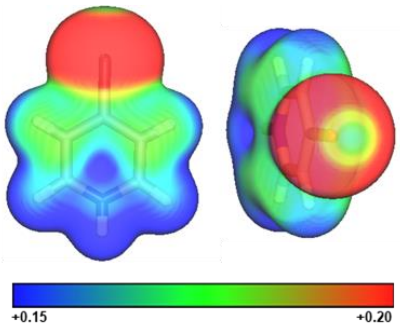

Figure 3.1.2.1. Electrostatic potential of $[C_5H_4BrN\text{-}H]^+$ cation in the range of 0.15 a.u (red) to 0.20 a.u. (blue) have been mapped onto its electron density (isosurface value 0.0035 a.u.); calculated on B3LYP/def2-TZVPP level of theory. Left – top view; right – front view.

In the attempts to fully characterize and crystalize the whole row of commercially available *para*-halogen-substituted pyridinium salts with weakly coordinating $[Al(OTeF_5)_4]^-$ anion, crystals of $[C_5H_4BrN\text{-}H][Al(OTeF_5)_4]$ were obtained (Fig. 3.1.2.2).

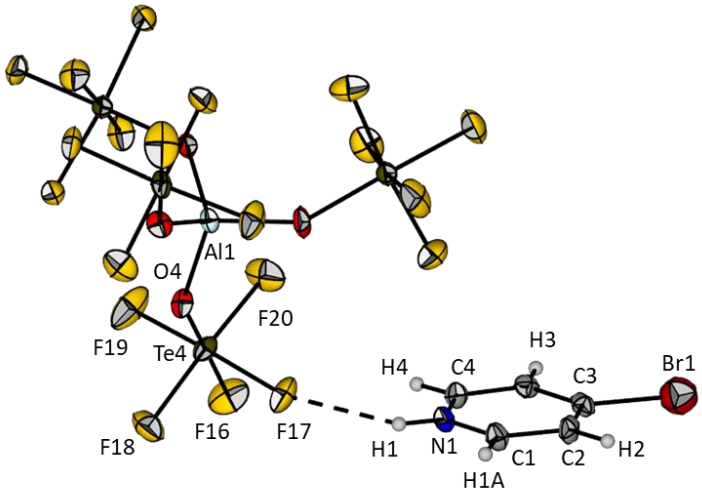

Figure 3.1.2.2. Molecular structure of $[C_5H_4BrN\text{-}H][Al(OTeF_5)_4]$ in the solid state with thermal ellipsoids shown at the 50 % probability level.

The synthesis of $[C_5H_4BrN\text{-}H][Al(OTeF_5)_4]$ was similar to the synthesis of $[C_5F_5N\text{-}H][Al(OTeF_5)_4]$, described in chapter 4.2. The solid-state structure of $[C_5H_4BrN\text{-}H][Al(OTeF_5)_4]$ was obtained by slowly cooling the reaction mixture in *o*DFB to –40 °C. The salt crystallized in the triclinic $P\bar{1}$ space group (Fig. 3.1.3.2). The solid state structure of $[C_5H_4BrN\text{-}H][Al(OTeF_5)_4]$ shows directed short contacts of 358.98(20) pm, via bromine atoms between two cationic $[C_5H_4BrN\text{-}H]^+$ units, being less than the sum of their vdW radii (370 pm).[124] In addition, anion-π interactions can again be found between the $[C_5H_4BrN\text{-}H]^+$ cation and the fluorine atoms of the WCA (Fig. 3.1.2.3).

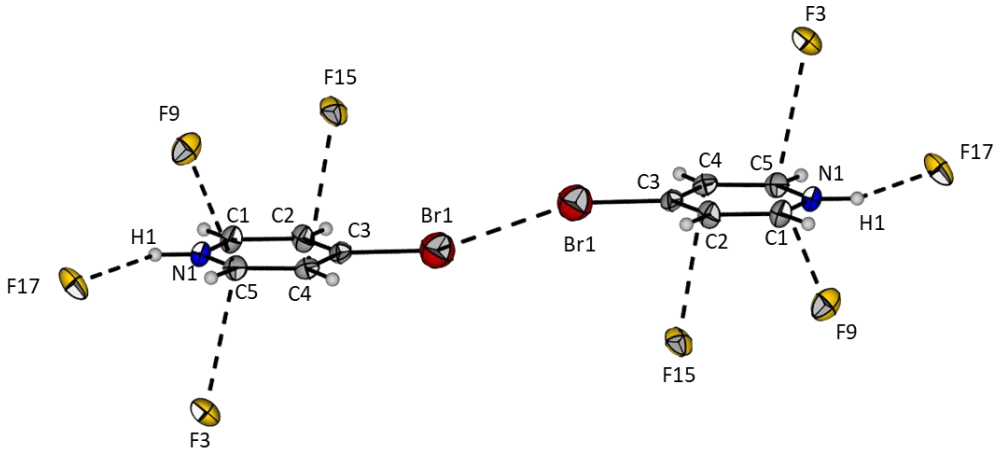

Figure 3.1.2.3. Short contacts of the $[C_5H_4BrN\text{-}H]^+$ cationic units in the solid state structure of $[C_5H_4BrN\text{-}H][Al(OTeF_5)_4]$ salt with thermal ellipsoids shown at the 50 % probability level. Anionic moieties are omitted for clarity. Selected bond length in pm and angles in °: F17-N1 310.27(174), F9-C5 303.02(132), F3-C5 297.60(145), F15-C4 316.85(132), Br1-Br1 358.98(20), F3-C1 362.57(180); C3-Br1-C3 136.92(39).

3.2 Selective C(sp^3)-F Activation in HFO-1234yf starting from Brønsted Superacids

Arenium complexes are the key intermediates in electrophilic aromatic substitution reactions.[125] They are formed in Friedel-Crafts alkylation reactions, when a Lewis acid like AlX_3, X = Cl, Br, I is used as a catalyst.[126] In 2017, *Braun et al*. used the Lewis superacid ACF for the selective C(sp^3)-F bond activation of the commercial refrigerant 2,3,3,3-tetrafluoropropene, also known as HFO-1234yf (Fig. 3.2.1).[127]

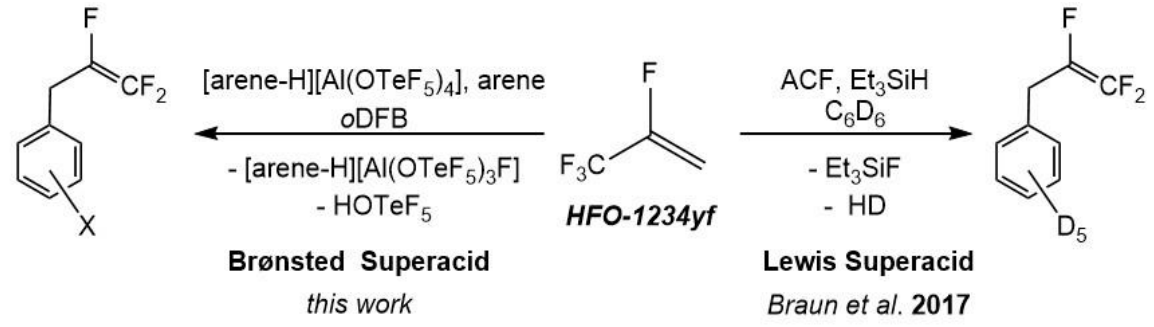

arene = C_6H_6, C_7H_8, *o*-$C_6F_2H_4$
X = H, CH_3, 2F

Figure 3.2.1. Selective C(sp^3)-F bond activation of HFO-1234yf starting from Brønsted superacids (this work) and Lewis superacid ACF.[127]

Lewis acids tend to form Lewis acid-base adducts. This behavior is in particular pronounced for Lewis superacids, such as the dimeric $[Al(OTeF_5)_3]_2$ – shown for instance in the formation of Lewis acid-base $Al(OTeF_5)_3 \rightarrow (RCN)_3$ adduct.[24] The neat Lewis superacid $Al(OTeF_5)_3$ have not be isolated so far and it is debatable whether it exists in its monomeric form in bulk. Therefore, for the HFO-1234yf activation, three different Brønsted superacids were used: $[arene\text{-}H][Al(OTeF_5)_4]_{(solv)}$, [arene-H] = [$C_6H_6$-H], [$C_7H_8$-H] and [*o*-$C_6F_2H_4$-H] (Fig. 3.2.2). These are also known as Wheland intermediates since they contain arenium ions. Their formation follows a color change of the reaction mixture to yellow, which is typical for protonated arenes. The condensation of about one equivalent of HFO-1234yf to the frozen yellow solution leads immediately after thawing while still below –30 °C to a red solution and a precipitation shortly after (Fig. 3.2.2).

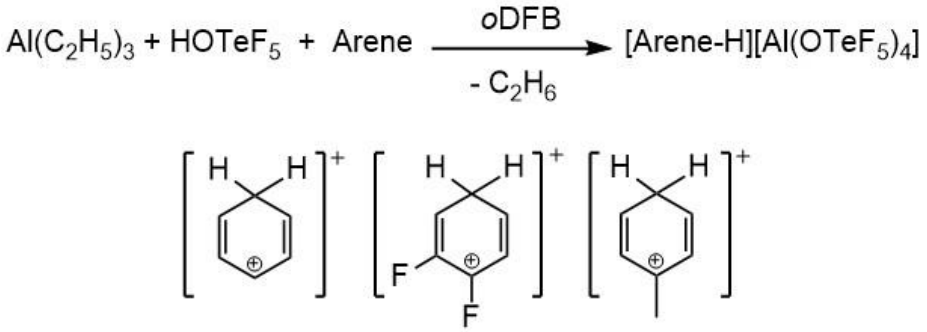

Figure 3.2.2. Brønsted superacids formation.

The organic (liquid) phase after the reaction contained the typical Friedel-Crafts-like activation products and was separated by condensation (Fig. 3.2.3).

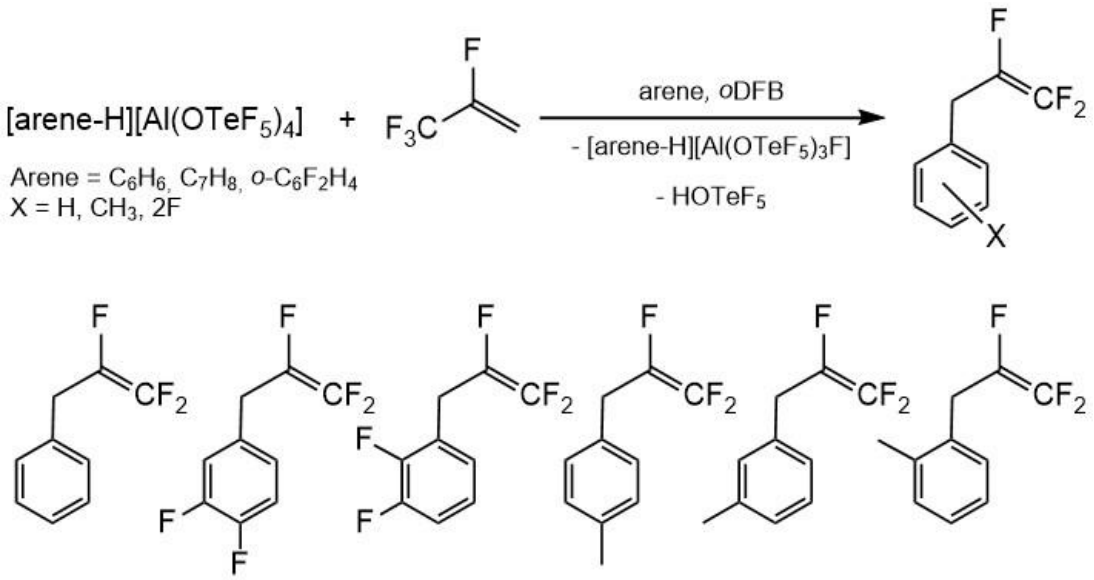

Figure 3.2.3. C-F bond activation in HFO-1234yf starting from arene-based Brønsted superacids in *o*DFB.

Separation of the products from the solvent was observed in GC-MS spectra (appendix). For the assignment of inorganic species after the activation reaction, a set of low-temperature NMR spectra of the reaction using between HFO-1234yf and deuterated toluene-based Brønsted superacid $[C_7D_8\text{-}H][Al(OTeF_5)_4]$ were recorded. The ^{27}Al NMR depicts a major sharp resonance at δ = 47.9 ppm assigned to the homoleptic $[Al(OTeF_5)_4]^-$ anion (appendix). This resonance is accompanied by a broad peak at δ = 50.7 ppm that can be attributed to the tetrahedrally coordinated $[Al(OTeF_5)_{4-x}F_x]^-$ unit, where one or several $OTeF_5$ moieties are substituted by a fluoride, formally subtracted from the CF_3-group of HFO-1234yf. The assignment of the ^{19}F NMR spectrum is complicated due to the presence of different AB_4 spin-splitting patterns of magnetically different $OTeF_5$ groups (appendix).

Aiming to crystalize an intermediate, *n*-pentane was added to a solution of the reaction mixture of the Brønsted superacid $[C_7H_8\text{-}H][Al(OTeF_5)_4]$ with HFO-1234yf. The yellow crystals of the Wheland intermediate $[C_7H_8\text{-}H][Al(OTeF_5)_3F]\cdot C_7H_8$ were grown by slowly cooling the mixture from –40 °C to –80 °C. The compound crystallized in the monoclinic space group *P2₁* (Fig. 3.2.4). The crystals decompose already while picking at –80 °C, resulting in colorless oil and fume. The shortest F-C contact in the solid state structure was found to be 307.7 pm, being below the sum of vdW radii of 317 pm, indicating weak interaction (Fig. 3.2.4). Due to the high number of formula

units per unit cell (Z = 8) in the solid state structure of $[C_7H_8\text{-}H][Al(OTeF_5)_3F]\cdot C_7H_8$, the Al-F distances were 180.5(14)-181.4(14) pm, ∠(O-Al-F) angles 99.7(7)-110.4(7) pm and ∠(O-Al-O) angles 109.0(7)-115.3(8) pm.

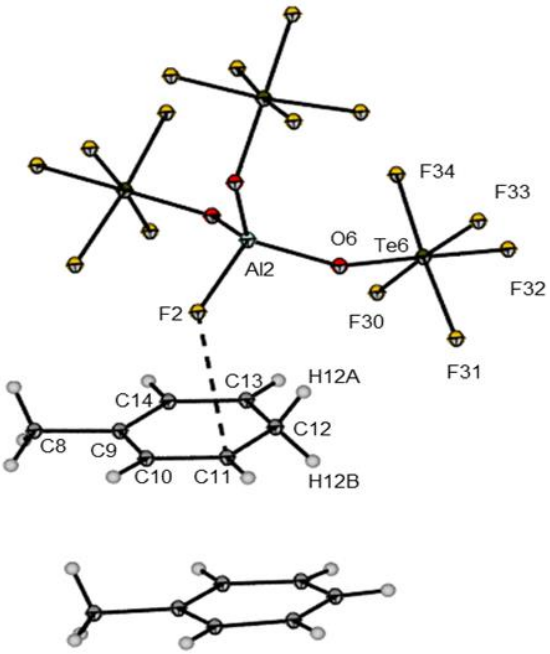

Figure 3.2.4. Molecular structure of $[C_7H_8\text{-}H][Al(OTeF_5)_3F]\cdot C_7H_8$ in the solid state with thermal ellipsoids shown at the 50 % probability level. A dashed line indicates the shortest C-F contact. Selected bond length, contacts [pm] and angle in°: C12-C13 134.0(3), C14-C9 137.0(3), C9-C8 153.0(3), C9-C10 138.0(3), C10-C11 144.0(3), C11-C12 140.0(3), Al2-F2 180.6(1), C11-F2 307.7(3), O-Al-F 104.8(7).

As previously discovered by our group, the addition of the strong electrophile Et_3SiH to a solution of the Brønsted superacid $[C_7H_8\text{-}H][Al(OTeF_5)_4]$ leads to the $-OTeF_5$ group abstraction and formation of the Lewis acid-base adduct $Al(OTeF_5)_3{\rightarrow}C_7H_8$ and $Et_3SiOTeF_5$.[24] Presumably, the weakly coordinating $[Al(OTeF_5)_4]^-$ anion, as a part of the Brønsted superacid $[C_7H_8\text{-}H][Al(OTeF_5)_4]$, undergoes thermodynamic equilibrium between the Lewis acid-base adduct $Al(OTeF_5)_3{\rightarrow}C_7H_8$ and teflic acid $HOTeF_5$ in solution. Similar adducts, namely $[C_5H_2F_3N\text{-}H][Al(OTeF_5)_4]$ salt and its Lewis acid-base adduct $Al(OTeF_5)_3{\rightarrow}C_5H_2F_3N$, were previously described in chapter 3.1.1. Potentially, upon the addition of HFO-1234yf, the Lewis acid-base adduct $Al(OTeF_5)_3{\rightarrow}C_7H_8$ is formed. Thereafter, the C-F bond in HFO-1234yf is most likely polarized, with further fluoride abstraction and formation of the weakly coordinating $[Al(OTeF_5)_3F]^-$ anion and trifluoroallyl $[CF_2CFCH_2]^+$ cation (Fig. 3.2.5). The calculated $Al(OTeF_5)_3{\rightarrow}CF_3CFCH_2$

adduct exhibit elongated F-C distance of 155.3 pm in the gas phase and considerably long F-C distance of 238.7 pm using CPCM model (Fig. 3.2.5) that can be contributed to the respective contact ion pair and solvent-separated ion pair, consisting of $[Al(OTeF_5)_3F]^-$ anion and the $[CF_2CFCH_2]^+$ cation.

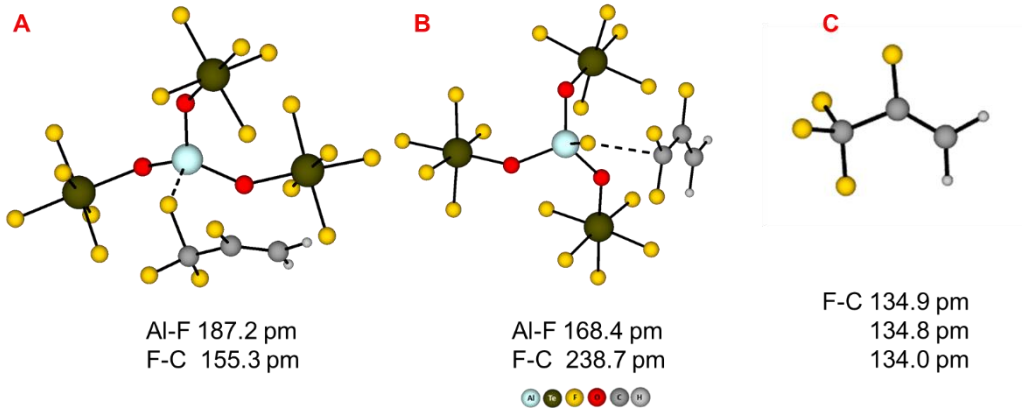

Figure 3.2.5. Calculated minimum structures of the $Al(OTeF_5)_3 \rightarrow CF_3CFCH_2$ adduct on the B3LYP-d3/def2-TZVPP level of theory (A) and B3LYP-d3/def2-TZVPP (CPCM, ε_R 14.26) (B, C) level of theory.

In the calculation using CPCM model (Fig. 3.2.5) and crystal structure data of the $[Al(OTeF_5)_3F]^-$ anion of $[C_7H_8\text{-}H][Al(OTeF_5)_3F]\cdot C_7H_8$ crystal (Fig. 3.2.4), the ∠(O-Al-O) and ∠(O-Al-F) ascend the comparable bond angles (Table 3.2.1). The Al-F distance in the $[Al(OTeF_5)_3F]^-$ anion is best described by the gas phase optimization, when compared to the crystal data of the $Al(OTeF_5)_3 \rightarrow CF_3CFCH_2$ adduct (Table 3.2.1).

Table 3.2.1. Selected bond distances and angles of calculated minimum structures of the $Al(OTeF_5)_3 \rightarrow CF_3CFCH_2$ adduct versus solid state structure data of $[C_7H_8\text{-}H][Al(OTeF_5)_3F]\cdot C_7H_8$.

Level of Theory / Crystal Data	Al-F, pm	F-C, pm	∠(O-Al-O),°	∠(O-Al-F),°
B3LYP-D3/def2-TZVPP	187.2	155.3	114.3	98.2
			114.9	103.1
			118.9	103.6
B3LYP-D3/def2-TZVPP	168.4	238.7	108.4	105.6
(CPCM, ε_R 14.26)			110.6	109.4
			112.0	110.8
$[C_7H_8\text{-}H][Al(OTeF_5)_3F]\cdot C_7H_8$	180.5	-	107.0	99.7
	180.6		108.7	103.5
	181.1		109.5	104.1
			110.4	104.7
			111.6	104.8
			112.7	105.1
			113.7	107.0
			114.0	109.6
			115.4	109.8
			115.6	110.4

IV Publications

4.1 Synthesis and Structural Characterization of Tetraalkylammonium Salts of the Weakly Coordinating Anion $[Al(OTeF_5)_4]^-$

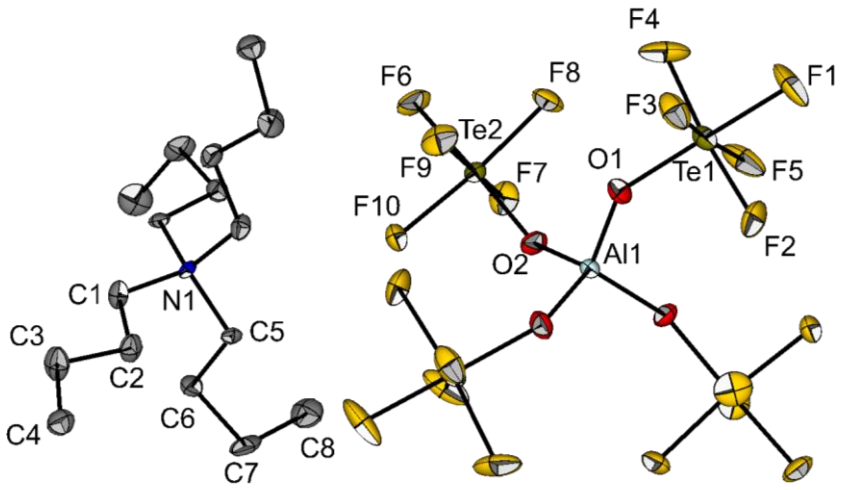

Figure 4.1.1. Graphical abstract. © 2020 The Authors. Published by Wiley-VCH Verlag GmbH & Co. KGaA, Weinheim.

Sofiya Kotsyuda, Anja Wiesner, Simon Steinhauer, Sebastian Riedel

Zeitschrift für Allgemeine und Anorganische Chemie **2020**, *23*, 13501 – 13509.

https://doi.org/10.1002/zaac.202000101

Author Contribution

Sofiya Kotsyuda performed experiments and product characterization and wrote the manuscript. Anja Wiesner conducted the crystallographic measurements of $[N(C_2H_5)_4][Al(OTeF_5)_4]$ and $[N(C_4H_9)_4][Al(OTeF_5)_4]$. Simon Steinhauer revised the manuscript. Sebastian Riedel managed the project and revised the manuscript.

The pages 30–33 contain the printed article.

https://doi.org/10.1002/zaac.202000101

The pages 34–42 contain the Supporting Information of the article, which is available under the same URL.

4.2 Noncovalent Interactions in Halogenated Pyridinium Salts of the Weakly Coordinating Anion $[Al(OTeF_5)_4]^-$

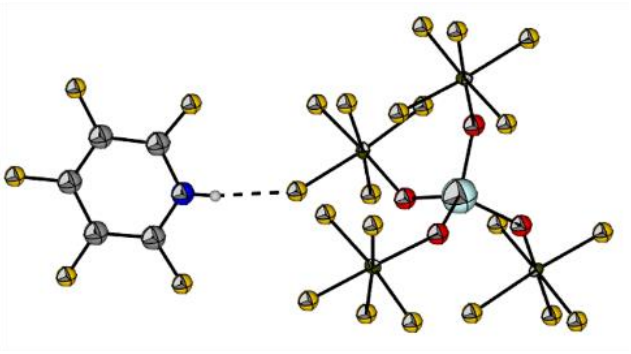

Figure 4.2.1. Graphical abstract. © 2022 The Authors. Chemistry – A European Journal. Published by Wiley-VCH GmbH.

Sofiya Kotsyuda, Ahmet N. Toraman, Patrik Voßnacker, Mathias A. Ellwanger, Simon Steinhauer, Carsten Müller, Sebastian Riedel

Chemistry – a European Journal **2022**, *e202202749.*

https://doi.org/10.1002/chem.202202749

Author Contribution

Sofiya Kotsyuda carried out experiments and characterization, density functional theory calculations and wrote the manuscript. Ahmet N. Toraman carried out some experiments during his research internship that was supervised by Sofiya Kotsyuda. Patrick Voßnacker performed crystallographic measurements and refinements of crystal structures. Mathias A. Ellwanger and Simon Steinhauer provided scientific guidelines and revised the manuscript. Carsten Müller performed atoms in molecules analysis calculations. Sebastian Riedel managed the project and revised the manuscript.

The pages 45–51 contain the printed article.

https://doi.org/10.1002/chem.202202749

The pages 52–73 contain the Supporting Information of the article, which is available under the same URL.

V Conclusions

Firstly, the Brønsted superacid [*o*-$C_6H_4F_2$-H][$Al(OTeF_5)_4$] was used for the synthesis and transfer of the weakly coordinating $[Al(OTeF_5)_4]^-$ anion (WCA) to the tetraalkylammonium salts. A clear transition from classical salts to ionic liquids was indicated by the decrease of melting points from 190° to 58°C in the row [$N(CH_3)_4$][WCA] < [$N(C_2H_5)_4$][WCA] < [$N(C_3H_7)_4$][WCA] < [$N((C_2H_5)_3CH_3)_4$][WCA] < < [$(C_4H_9)_4$][WCA]. In addition to their tunable melting points, these salts exhibit a high stability towards electrophiles that can be reached by variation of the alkyl chain length and by breaking the symmetry in the cation, like in case of [$N(C_2H_5)_3CH_3$][$Al(OTeF_5)_4$]. Secondly, the focus of the present work lies on extensive study of unprecedented halogenated pyridinium $[C_5F_5N\text{-}H]^+$, $[C_5F_4ClN\text{-}H]^+$ $[(C_5Cl_5N)_2H]^+$, $[(C_5F_5N)_2H]^+$, $[C_5H_4BrN\text{-}H]^+$ and $[C_5F_3H_2N\text{-}H]^+$ salts of the weakly coordinating $[Al(OTeF_5)_4]^-$ anion. The present WCA in these salts participates in fluorine-specific interactions as well as in hitherto undiscovered anion-π interactions. The surveyed ESP plots of halogenated pyridinium cations revealed the biggest depletion of electron density on the N-H moiety, illustrating the strongest interaction site with WCA via hydrogen bonding. Expectedly, no halogen bonding was found in fluorinated [$C_5F_3H_2N$-H][$Al(OTeF_5)_4$], [C_5F_5N-H][$Al(OTeF_5)_4$] and [$(C_5F_5N)_2H$][$Al(OTeF_5)_4$] salts. By contrast, *para*-halogen-substituted pyridinium cations, except for fluorine, exhibited σ-holes and participated in halogen bonding with the WCA. In addition, solid state structures revealed that the nature of the halogenated pyridinium cation dictates coplanar staggering of the $[(C_5F_5N)_2H]^+$ dimer versus orthogonal stacking in its higher $[(C_5Cl_5N)_2H]^+$ dimer homologue of the $[Al(OTeF_5)_4]^-$ salt. Finally, selective C(sp^3)-F activation in HFO-1234yf by arene-based Brønsted superacids [arene-H][$Al(OTeF_5)_4$], arene = *o*-$C_4H_4F_2$, C_6H_6, C_7H_8 led to the formation of known Friedel-Crafts-type products. This activation reaction induces plausible Lewis-acidic behavior of aforementioned Brønsted-acidic systems and opens new ways for its future applications. All in all, the weakly coordinating $[Al(OTeF_5)_4]^-$ is easily accessible from the Brønsted superacid [*o*-$C_6H_4F_2$-H][$Al(OTeF_5)_4$] and holds great promise for the design of supramolecular systems and comprehensive investigations of fluorine-specific interactions.

VI References

[1] N. F. Hall, J. B. Conant, *J. Am. Chem. Soc.* **1927**, *49*, 3047.
[2] G. A. Olah, J. Kaspi, J. Bukala, *J. Org. Chem.* **1977**, *42*, 4187.
[3] G. A. Olah, *Superacid chemistry*, Wiley, Hoboken, N.J., **2009**.
[4] G. A. Olah, M. B. Comisarow, C. A. Cupas, C. U. Pittman, *J. Am. Chem. Soc.* **1965**, *87*, 2997.
[5] G. A. Olah, *J. Org. Chem.* **2005**, *70*, 2413.
[6] S. Cummings, H. P. Hratchian, C. A. Reed, *Angew. Chem.* **2016**, *128*, 1404.
[7] E. Bernhardt, B. Bley, R. Wartchow, H. Willner, E. Bill, P. Kuhn, I. H. T. Sham, M. Bodenbinder, R. Bröchler, F. Aubke, *J. Am. Chem. Soc.* **1999**, *121*, 7188.
[8] C. Wang, B. Bley, G. Balzer-Jöllenbeck, A. R. Lewis, S. C. Siu, H. Willner, F. Aubke, *J. Chem. Soc., Chem. Commun.* **1995**, *31*, 2071.
[9] H. Willner, C. Bach, R. Wartchow, C. Wang, S. J. Rettig, J. Trotter, V. Jonas, W. Thiel, F. Aubke, *Inorg. Chem.* **2000**, *39*, 1933.
[10] G. Hwang, C. Wang, F. Aubke, H. Willner, M. Bodenbinder, *Can. J. Chem.* **1993**, *71*.
[11] M. Finze, E. Bernhardt, H. Willner, C. W. Lehmann, F. Aubke, *Inorg. Chem.* **2005**, *44*, 4206.
[12] C. A. Reed, K.-C. Kim, E. S. Stoyanov, D. Stasko, F. S. Tham, L. J. Mueller, P. D. W. Boyd, *J. Am. Chem. Soc.* **2003**, *125*, 1796.
[13] A. Wiesner, T. W. Gries, S. Steinhauer, H. Beckers, S. Riedel, *Angew. Chem. Int. Ed.* **2017**, *56*, 8263.
[14] C. A. Reed, Fackler, Nathanael L. P., K.-C. Kim, D. Stasko, D. R. Evans, P. D. W. Boyd, Rickard, Clifton E. F., *J. Am. Chem. Soc.* **1999**, *121*, 6314.
[15] Jack E. Baldwin, Andrew Au, Michael Christie, Stephen B. Haber, David Hesson, *J. Am. Chem. Soc.* **1975**, 5958.
[16] K. Züchner, T. J. Richardson, O. Glemser, N. Bartlett, *Angew. Chem.* **1980**, *92*, 956.
[17] A. Wiesner, S. Steinhauer, H. Beckers, C. Müller, S. Riedel, *Chem. Sci.* **2018**, *9*, 7169.
[18] C. Reed, *Chem. Comm.* **2005**, 1669.
[19] G. N. Lewis, *J. Frankl. Inst.* **1938**, *226*, 293.
[20] L. O. Müller, D. Himmel, J. Stauffer, G. Steinfeld, J. Slattery, G. Santiso-Quiñones, V. Brecht, I. Krossing, *Angew. Chem. Int. Ed.* **2008**, *47*, 7659.
[21] P. Erdmann, J. Leitner, J. Schwarz, L. Greb, *ChemPhysChem* **2020**, *21*, 987.
[22] L. Greb, *Chem. Eur. J.* **2018**, *24*, 17881.
[23] I. Krossing, I. Raabe, *Chem. Eur. J.* **2004**, *10*, 5017.
[24] K. F. Hoffmann, A. Wiesner, S. Steinhauer, S. Riedel, *Chem. Eur. J.* **2022**, e202201958.
[25] E. Breitmaier, G. Jung (Eds.) *Organische Chemie. Grundlagen, Stoffklassen, Reaktionen, Konzepte, Molekülstrukturen ; 129 Tabellen*, Thieme, Stuttgart, New York, **2005**.
[26] Lutz O. Müller, *Dissertation*, Albert-Ludwigs-Universität Freiburg, Freiburg (im Breisgau), **2008**.
[27] I. M. Riddlestone, S. Keller, F. Kirschenmann, M. Schorpp, I. Krossing, *Eur. J. Inorg. Chem.* **2019**, *2019*, 59.
[28] a) H. G. Mayfield, W. E. Bull, *J. Chem. Soc. A* **1971**, 2279; b) R. V. Honeychuck, W. H. Hersh, *Inorg. Chem.* **1986**, *28*, 2869.
[29] M. R. Rosenthal, *J. Chem. Educ.* **1973**, *50*, 331.
[30] I. Krossing, I. Raabe, *Angew. Chem. Int. Ed.* **2004**, *43*, 2066.
[31] S. H. Strauss, *Chem. Rev.* **1993**, *93*, 927.
[32] D. Stasko, C. A. Reed, *J. Am. Chem. Soc.* **2002**, *124*, 1148.
[33] E. S. Stoyanov, K.-C. Kim, C. A. Reed, *J. Am. Chem. Soc.* **2006**, *128*, 8500.
[34] I. Krossing, I. Raabe, *Angew. Chem.* **2004**, *116*, 2116.
[35] T. J. Marks, A. M. Seyam, *Inorg. Chem.* **1974**, *13*.

[36] E. Bernhardt, G. Henkel, H. Willner, G. Pawelke, H. Bürger, *Chem. Eur. J.* **2001**, *7*, 4696.
[37] a) H. Kobayashi, A. Sonoda, H. Iwamoto, N. Yoshimura, *Chem. Lett.* **1981**; b) H. Nishida, N. Takada, M. Yoshimura, T. Sonoda, H. Kobayashi, *Bull. Chem. Soc. Jpn.* **1984**, *57*, 2600.
[38] J. Zhou, S. J. Lancaster, D. A. Walker, S. Beck, M. Thornton-Pett, M. Bochmann, *J. Am. Chem. Soc.* **2001**, *123*, 223.
[39] T. H. Kim, H. M. Lee, H. S. Park, S. D. Kim, S. J. Kwon, A. Tahara, H. Nagashima, B. Y. Lee, *Appl. Organometal. Chem.* **2019**, *33*, e4829.
[40] T. S. M. Kaliner, *Tetrahedron Lett.* **2016**, *57*, 3453.
[41] K. Niedenzu, *Naturwissenschaften* **1969**, *56*, 305.
[42] C. A. Reed, *Acc. Chem. Res.* **1998**, *31*, 133.
[43] E. H.-H. M. Scholz, *Chemical Rev.* **2011**, *111*, 7035.
[44] S. Körbe, P. J. Schreiber, J. Michl, *Chemical Rev. 106*, 5208.
[45] W. Gu, B. J. McCulloch, J. H. Reibenspiesa, O. V. Ozerov, *Chem. Comm.* **2010**, *46*.
[46] S. V. Ivanov, J. J. Rockwell, O. G. Polyakov, C. M. Gaudinski, O. P. Anderson, K. A. Solntsev, S. H. Strauss, *J. Am. Chem. Soc.* **1998**, *120*, 4224.
[47] I. Krossing, *Chem. Eur. J.* **2001**, *7*, 490.
[48] T. Timofte, S. Pitula, A.-V. Mudring, *Inorg. Chem.* **2007**, *46*, 10938.
[49] M. Rohde, L. O. Müller, D. Himmel, H. Scherer, I. Krossing, *Chem. Eur. J.* **2014**, *20*, 1218.
[50] A. Martens, P. Weis, M. C. Krummer, M. Kreuzer, A. Meierhöfer, S. C. Meier, J. Bohnenberger, H. Scherer, I. Riddlestone, I. Krossing, *Chem. Sci.* **2018**, *9*, 7058.
[51] a) I. Krossing, A. Bihlmeier, I. Raabe, N. Trapp, *Angew. Chem. Int. Ed.* **2003**, *42*, 1531; b) I. Krossing, A. Bihlmeier, I. Raabe, N. Trapp, *Angew. Chem.* **2003**, *115*, 1569.
[52] P. J. Malinowski, T. Jaroń, M. Domańska, J. M. Slattery, M. Schmitt, I. Krossing, *Dalton Trans.* **2020**, *49*, 7766.
[53] K. Huse, C. Wölper, S. Schulz, *Organometallics* **2021**, *40*, 1907.
[54] T. A. Engesser, M. R. Lichtenthaler, M. Schleep, I. Krossing, *Chem. Soc. Rev.* **2016**, *45*, 789.
[55] A. Budanow, M. Bolte, M. Wagner, H.-W. Lerner, *Eur. J. Inorg. Chem.* **2015**, *2015*, 2524.
[56] A. Martens, M. Kreuzer, A. Ripp, M. Schneider, D. Himmel, H. Scherer, I. Krossing, *Chem. Sci.* **2019**, *55*, 2500.
[57] T. Birchall, R. D. Myers, H. d. Waard, G. J. Schrobilgen, *Inorg. Chem.* **1982**, *21*, 1068.
[58] K. Seppelt, *Angew. Chem. Int. Ed.* **1982**, *21*, 877.
[59] D. Lentz, K. Seppelt, *Z. Anorg. Allg. Chem.* **1980**, *460*, 5.
[60] F. Sladky, H. Kropshofer, *Inorg. Nucl. Chem. Lett.* **1972**, *8*, 195.
[61] P. Huppmann, H. Labischinski, D. Lentz, H. Pritzkow, K. Seppelt, *Z. Anorg. Allg. Chem.* **1982**, *487*, 7.
[62] A. Engelbrecht, F. Sladky, *Angew. Chem.* **1964**, *76*, 379.
[63] A. Engelbrecht, W. Loreck, W. Nehoda, *Z. Anorg. Allg. Chem.* **1968**, *360*, 88.
[64] K. Seppelt, D. Nothe, *Inorg. Chem.* **1973**, *12*, 2727.
[65] W. Tötsch, F. Sladky, *Chem. Ber.* **1982**, *115*, 1019.
[66] F. Sladky, H. Kropshofer, O. Leitzke, P. Peringer, *J. Inorg. Nucl. Chem.* **1976**, *28*, 69.
[67] M. A. Ellwanger, C. von Randow, S. Steinhauer, Y. Zhou, A. Wiesner, H. Beckers, T. Braun, S. Riedel, *Chem. Commun.* **2018**, *54*, 9301.
[68] P. Huppmann, H. Hartl, K. Seppelt, *Z. Anorg. Allg. Chem.* **1985**, *524*, 26.
[69] M. D. Noirot, O. P. Anderson, S. H. Strauss, *Inorg. Chem.* **1987**, *26*, 2216.
[70] M. Winter, N. Peshkur, M. A. Ellwanger, A. Pérez-Bitrián, P. Voßnacker, S. Steinhauer, S. Riedel, *Chem. Eur. J.* **2023**.
[71] G. D. Purvis, R. J. Bartlett, *J. Chem. Phys.* **1982**, *76*, 1910.
[72] D. Lentz, K. Seppelt, *Z. Anorg. Allg. Chem.* **1983**, *502*, 83.
[73] H. P. A. Mercier, J. C. P. Sanders, G. J. Schrobilgen, *J. Am. Chem. Soc.* **1994**, *116*, 2921.

[74] D. M. Van Seggen, P. K. Hurlburt, O. P. Anderson, S. H. Strauss, *Inorg. Chem.* **1995**, *34*, 3453.
[75] H. P. A. Mercier, M. D. Moran, J. C. P. Sanders, G. J. Schrobilgen, R. J. Suontamo, *Inorg. Chem.* **2005**, *44*, 49.
[76] T. S. Cameron, I. Dionne, I. Krossing, J. Passmore, *Solid State Sci.* **2002**, *4*, 1435.
[77] A. Pérez-Bitrián, K. F. Hoffmann, K. B. Krause, G. Thiele, C. Limberg, S. Riedel, *Chem. Eur. J.* **2022**, e202202016.
[78] a) M. R. Colsman, M. D. Noirot, M. M. Miller, O. P. Anderson, S. H. Strauss, *J. Am. Chem. Soc.* **1988**, *110*, 6886; b) M. R. Colsman, T. D. Newbound, L. J. Marshall, M. D. Noirot, M. M. Miller, G. P. Wulfsberg, J. S. Frye, O. P. Anderson, S. H. Strauss, *J. Am. Chem. Soc.* **1990**, *112*, 2349.
[79] P. K. Hurlburt, P. J. Kellett, O. P. Anderson, S. H. Strauss, *J. Chem. Soc., Chem. Commun.* **1990**, 576.
[80] D. M. Van Seggen, P. K. Hurlburt, M. D. Noirot, O. P. Anderson, S. H. Strauss, *Inorg. Chem.* **1992**, *31*, 1423.
[81] A. Wiesner, L. Fischer, S. Steinhauer, H. Beckers, S. Riedel, *Chem. Eur. J.* **2019**, *25*, 10441.
[82] J. R. DeBackere, H. P. A. Mercier, G. J. Schrobilgen, *Inorg. Chem.* **2015**, *54*, 1606.
[83] K. Schröder, F. Sladky, *Chem. Ber.* **1980**, *113*, 1414.
[84] S. H. Strauss, M. D. Noirot, O. P. Anderson, *Inorg. Chem.* **1986**, *25*, 3850.
[85] K. Koppe, V. Bilir, H.-J. Frohn, H. P. A. Mercier, G. J. Schrobilgen, *Inorg. Chem.* **2007**, *46*, 9425.
[86] H. Kropshofer, O. Leitzke, P. Peringer, F. Sladky, *Chem. Ber.* **1981**, *114*, 2644.
[87] P. K. Hurlburt, O. P. Anderson, S. H. Strauss, *J. Am. Chem. Soc.* **1991**, *113*, 6277.
[88] P. K. Hurlburt, J. J. Rack, S. F. Dec, O. P. Anderson, S. H. Strauss, *Inorg. Chem.* **1993**, *32*, 373.
[89] K. F. Hoffmann, A. Wiesner, N. Subat, S. Steinhauer, S. Riedel, *Z. Anorg. Allg. Chem.* **2018**, *644*, 1344.
[90] K. F. Hoffmann, D. Battke, P. Golz, S. M. Rupf, M. Malischewski, S. Hasenstab-Riedel, *Angew. Chem. Int. Ed.* **2022**, e202203777.
[91] M. Winter, N. Peshkur, M. A. Ellwanger, A. Pérez-Bitrián, P. Voßnacker, S. Steinhauer, S. Riedel, *In preparation*.
[92] a) J. Řezáč, P. Hobza, *Chem. Rev.* **2016**, *116*, 5038; b) A. S. Mahadevi, G. N. Sastry, *Chem. Rev.* **2016**, *116*, 2775.
[93] L. Barrientos, S. Miranda-Rojas, F. Mendizabal, *Int J Quantum Chem* **2019**, *119*, e25675.
[94] D. Braga, F. Grepioni, *Acc. Chem. Res.* **2000**, *33*, 601.
[95] a) Gautam R. Desiraju, *J. Chem. Sci.* **2010**, *122*, 667; b) I. K. Mati, S. L. Cockroft, *Chem. Soc. Rev.* **2010**, *39*, 4195; c) P. Pyykkö, *Chem. Soc. Rev.* **2008**, *37*, 1967; d) P. Pyykkö, *J. Chem. Res. Synop.* **1979**, 380; e) L. C. Gilday, S. W. Robinson, T. A. Barendt, M. J. Langton, B. R. Mullaney, P. D. Beer, *Chem. Rev.* **2015**, *115*, 7118.
[96] Y. Luo, M. T. B. Clabbers, J. Qiao, Z. Yuan, W. Yang, X. Zou, *J. Am. Chem. Soc.* **2022**, *144*, 10817.
[97] S. N. Johnson, T. L. Ellington, D. T. Ngo, J. L. Nevarez, N. Sparks, A. L. Rheingold, D. L. Watkins, G. S. Tschumper, *CrystEngComm* **2019**, *21*, 3151.
[98] a) A. J. Neel, M. J. Hilton, M. S. Sigman, F. D. Toste, *Nature* **2017**, *543*, 637; b) H. Takezawa, K. Shitozawa, M. Fujita, *Nature Chem.* **2020**, *12*, 574.
[99] J. Y. S. Lin, *Science* **2016**, *353*, 121.
[100] X. Ma, Y. Zhao, *Chem. Rev.* **2015**, *115*, 7794.
[101] L. Turunen, J. H. Hansen, M. Erdélyi, *Chemical Rec.* **2021**, *21*, 1252.
[102] J. H. O. Hassel, *Acta Chem. Scand.* **1954**, *8*, 873.
[103] R. G. Desiraju, P. Shing Ho, L. Kloo, C. A. Legon, R. Marquardt, P. Metrangolo, P. Politzer, G. Resnati, K. Rissanen, *Pure and App. Chem.* **2013**, *85*, 1711.
[104] T. Clark, M. Hennemann, J. S. Murray, P. Politzer, *J. Mol. Model.* **2007**, *13*, 291.
[105] P. Politzer, J.S. Murray, T. Clark, G. Resnati, *Phys. Chem. Chem. Phys.* **2017**, *19*, 32166.
[106] R. F. W. Bader, M. T. Carroll, J. R. Cheeseman, C. Chang, *J. Am. Chem. Soc.* **1987**, *109*, 7968.

[107] R. M. Kumar, M. Elango, V. Subramanian, *J. Phys. Chem. A* **2010**, *114*, 4313.
[108] V. G. Tsirelson, P. F. Zhou, T.-H. Tang, R. F. W. Bader, *Acta Cryst.A* **1995**, *51*, 143.
[109] A. Varadwaj, H. M. Marques, P. R. Varadwaj, *Molecules* **2019**, *24*.
[110] J. S. Murray, P. Lane, P. Politzer, *J. Mol. Model* **2009**, *15*, 723.
[111] D. A. Decato, E.A. John, O. B. Berryman, *Halogen Bonding: An Introduction*.
[112] K. Dongwook, P. Tarakeshwar, S. K. Kim., *J. Phys. Chem. A* **2004**, *108*, 1250.
[113] M. Albrecht, C. Wessel, M. de Groot, K. Rissanen, A. Lüchow, *J. Am. Chem. Soc.* **2008**, *130*, 4600.
[114] A. Bauzá, T. J. Mooibroek, A. Frontera, *CrystEngComm* **2016**, *18*, 10.
[115] M. R. Battaglia, A. D. Buckingham, J. H. Williams, *Chem. Phys. Lett.***1981**, *78*, 421.
[116] C. Garau, A. Frontera, D. Quiñonero, P. Ballester, A. Costa, P. M. Deyà, *ChemPhysChem* **2003**, *4*, 1344.
[117] a) M. Giese, M. Albrecht, K. Rissanen, *Chem. Rev.* **2015**, *115*, 8867; b) M. Giese, M. Albrecht, A. Valkonen, K. Rissanen, *Chem. Sci.* **2015**, *6*, 354; c) M. Giese, M. Albrecht, K. Rissanen, *Chem. Commun.* **2016**, *52*, 1778.
[118] B. L. Schottel, H. T. Chifotides, K. R. Dunbar, *Chem. Soc. Rev.* **2008**, *37*, 68.
[119] A. Frontera, P. Gamez, M. Mascal, T. J. Mooibroek, J. Reedijk, *Angew. Chem. Int. Ed. Engl.* **2011**, *50*, 9564.
[120] A. Bauzá, T. J. Mooibroek, A. Frontera, *CrystEngComm* **2016**, *18*, 10.
[121] K. Lekin, S. M. Winter, L. E. Downie, X. Bao, J. S. Tse, S. Desgreniers, R. A. Secco, P. A. Dube, R. T. Oakley, *J. Am. Chem. Soc.* **2010**, *132*, 16212.
[122] S. Kotsyuda, A. Wiesner, S. Steinhauer, S. Riedel, *Z. Anorg. Allg. Chem.* **2020**, *57*, 13982.
[123] a) S. Hämmerling, G. Thiele, S. Steinhauer, H. Beckers, C. Müller, S. Riedel, *Angew. Chem. Int. Ed.* **2019**, *58*, 9807; b) S. Hämmerling, P. Voßnacker, S. Steinhauer, H. Beckers, S. Riedel, *Chem. Eur. J.* **2020**.
[124] A. Bondi, *J. Phys. Chem.* **1964**, *68*, 441.
[125] C. Friedel, J. M. Crafts, *J. Chem. Soc.* **1877**, *32*, 725.
[126] C. Friedel, J. M. Crafts, *Compt. Rend.* **1877**, *84*, 1392.
[127] G. Meißner, K. Kretschmar, T. Braun, E. Kemnitz, *Angew. Chem.* **2017**, *129*, 16556.
[128] Adept Scientific, *gNMR V 5.0*, **2005**.
[129] O. V. Dolomanov, L. J. Bourhis, R. J. Gildea, J. A. K. Howard, H. Puschmann, *J. Appl. Cryst.* **2009**, *42*, 339.
[130] G. M. Sheldrick, *Acta Cryst. A* **2015**, *71*, 3.
[131] G. M. Sheldrick, *Acta Cryst. C* **2015**, *71*, 3.
[132] L. Bennett, B. Melchers, B. Proppe **2020**.
[133] M. J. Frisch, G. W. Trucks, H. B. Schlegel, G. E. Scuseria, M. A. Robb, J. R. Cheeseman, J. A. Montgomery, Jr., T. Vreven, K. N. Kudin, J. C. Burant et al., *Gaussian03 Revision C.02*, Gaussian, Inc, Wallingford CT, **2004**.
[134] S. Grimme, J. Antony, S. Ehrlich, H. Krieg, *J. Chem. Phys.* **2010**, *132*, 154104.
[135] F. Weigend, R. Ahlrichs, *Phys. Chem. Chem. Phys.* **2005**, *7*, 3297.
[136] K. Brandenburg, *Diamond*, Crystal Impact GbR, Bonn, **2009**.

VII Appendix

All reactions were carried out under inert conditions using standard Schlenk techniques. Glass vessels were greased with Triboflon III. All solid materials and triethylaluminium ($Al(C_2H_5)_3$, 93 %) were handled inside a glove box with an atmosphere of dry argon (O_2 <0.5 ppm, H_2O < 0.5 ppm). The pentafluoroorthotelluric acid was synthesized as reported in the literature.[64] All solvents were dried either with CaH_2 or with Sicapent® before use. IR spectra were collected on a Bruker ALPHA FTIR spectrometer equipped with a diamond ATR attachment in an argon-filled glove box. NMR spectra were recorded on either a JEOL 400 MHz ECS or ECZ-R spectrometer. Reported chemical shifts are referenced to the Ξ values given in IUPAC recommendations of 2008 using the ^2H signal of the deuterated solvent as internal reference. For external locking [D_6]-acetone was flame sealed in a glass capillary and the lock oscillator frequency was adjusted to give $\delta(^1H)$ = 7.26 ppm for a $CHCl_3$ sample locked on the capillary. Chemical shifts and coupling constants of strongly coupled spin systems are given as simulated in gNMR.[128] Crystal structures were obtained on a Bruker D_8 Venture diffractometer with a PHOTON 100 CMOS area detector using Mo–Kα radiation. Single crystals were coated with a perfluoroether oil at −25 °C and selected under nitrogen atmosphere. Using Olex2,[129] the structures were solved with the ShelXT[130] structure solution program by intrinsic phasing and refined with the ShelXL[131] refinement package using least-squares minimization. Crystal data for the $[C_5H_2F_3N\text{-}H][Al(OTeF_5)_4]$ CCDC number 2086774, $C_5F_3H_2N{\rightarrow}Al(OTeF_5)_3$ CCDC number 2074490, $[C_5H_5BrN\text{-}H][Al(OTeF_5)_4]$ CCDC number 209059, $[C_7H_8\text{-}H][Al(OTeF_5)_3F]{\cdot}C_7H_8$ CCDC number 2074485 can be obtained free of charge from the Cambridge Crystallographic Data Centre. GC-MS spectra were measured on a Saturn 2100 GC/MS system from Varian Inc. equipped with a "HP-5 ms Ultra Inert" (length 30 m) column, injection volume 1 µL, split 100. The following temperature program was used: ramp with 10 °C/min, constant helium gas flow of 280 l/min. Ionization voltage for EI (electron ionization): 80 eV. All calculations were performed using a general-purpose High-Performance Computer at ZEDAT (CURTA), provided by Freie Universität Berlin.[132] For density functional calculations the Gaussian 16[133] software was used with its implementation of B3LYP, and Grimme-D3[134] together with the basis set def2-TZVPP[135]. All structures were pre-optimized via SV(P) basis set. For *o*DFB ε_R = 14.26

was used at 20°C as near values. NBO analysis was performed with NBO 7.0 executed from Gaussian 16 as well as GIAO calculations. Calculated structures, as well as crystal structures, were visualized with Diamond.[136]

Reaction of the Brønsted superacid [*o*-$C_6F_2H_4$-H][$Al(OTeF_5)_4$] with 2,4,6-trifluoropyridine.

A sample of $Al(C_2H_5)_3$ (90 mg, 0.8 mmol, 1 eq.) was dissolved in 3 ml of 1,2-difluorobenzene. The solution was degassed and $HOTeF_5$ (600 mg, 2.6 mmol, 4 eq.) was condensed onto it at –196 °C. A bubbler was added and the reaction mixture was warmed up to –30 °C, giving rise to a yellow solution. Liquid $C_5F_3H_2N$ (1060 mg, 0.8 mmol, 1 eq.) was condensed into separate flask and dissolved in 3 ml of 1,2-difluorobenzene, added to the reaction mixture via a syringe, and the mixture was slowly warmed to room temperature. After stirring for 3 hours, the reaction mixture was placed in a –40 °C freezer. [$C_5F_3H_2N$-H][$Al(OTeF_5)_4$] and $C_5H_2F_3N{\rightarrow}Al(OTeF_5)_3$ were obtained as colorless crystals. **^{1}H NMR** (401 MHz, ext. [D_6]acetone, 22 °C): δ = 10.6 [s, H_A], 7.2 [ddd, $^1J(^1H_{BB'}, ^{19}F)$ = 6.2, $^1J(^1H, ^{19}F)$ = 1.4 $^1J(^1H, ^1H)$ = 1 Hz] ppm; **^{19}F NMR** (377 MHz, ext. [D_6]acetone, 22 °C): δ = −38.7 [m, $1F_A$, $^2J(^{19}F, ^{19}F)$ = 193 Hz, $^1J(^{19}F_A,^{125}Te)$ = 3363 Hz], −45.8 [m, $4F_B$, $^1J(^{125}Te,^{19}F_B)$ = 3414 Hz], −61.1 [s, F_Y], −112.7 [s, $2F_{XX'}$] ppm; **^{27}Al NMR** (104 MHz, ext. [D_6]acetone, 22 °C): δ = 50.1 [s, 75 % $[Al(OTeF_5)_4]^-$, d, 22.5 % $[Al(OTeF_5)_3(O^{125}TeF_5)]^-$, $^2J(^{27}Al,^{125}Te)$ = 73 Hz; t, 2.5 % $[Al(OTeF_5)_2(O^{125}TeF_5)_2]^-$, $^2J(^{27}Al, ^{125}Te)$ = 73.2 Hz], 53.5 [s] ppm.

Synthesis of [C_5H_5BrN-H][$Al(OTeF_5)_4$].

A sample of $Al(C_2H_5)_3$ (55 mg, 0.46 mmol, 1 eq.) was dissolved in 3 ml of 1,2-difluorobenzene. The solution was degassed and $HOTeF_5$ (450 mg, 1.88 mmol, 4 eq.) was condensed onto it at –196 °C. A bubbler was added and the reaction mixture was warmed up to –30 °C, giving rise to a yellow solution. Liquid $C_5H_4BrN{\cdot}HCl$ (91 mg, 0.47 mmol, 1 eq.) was condensed into a separate flask and dissolved in 3 ml of 1,2-difluorobenzene, added to the reaction mixture via a syringe, and the mixture was slowly warmed to room temperature. After stirring for 3 hours, the reaction mixture was placed in a –40 °C freezer. [C_5H_4BrN-H][$Al(OTeF_5)_4$] was obtained as colorless

crystals. **^{1}H NMR** (401 MHz, ext. [D$_6$]acetone, 22 °C): δ = 8.8 [s, H$_X$], 8.2 [t, H$_{BB'}$], 8.2 [t, H$_{AA'}$] ppm; **^{19}F NMR** (377 MHz, ext. [D$_6$]acetone, 22 °C): δ = −38.6 [m, 1F$_A$, ^{2}J(^{19}F, ^{19}F) = 191 Hz, ^{1}J(^{19}F$_A$,^{125}Te) = 3353 Hz], −45.8 [m, 4F$_B$, ^{1}J(^{125}Te,^{19}F$_B$) = 3410 Hz] ppm; **^{27}Al NMR** (104 MHz, ext. [D$_6$]acetone, 22 °C): δ = 50.0 [s] ppm.

Reaction of the Brønsted superacid [C$_6$H$_5$-H][Al(OTeF$_5$)$_4$] with 2,3,3,3-tetrafluoroporpene

In a typical experiment a sample of Al(C$_2$H$_5$)$_3$ (0.06 g, 0.053 mmol, 1 eq.) was dissolved in 3 ml 1,2-difluorobenzene and 0.1 ml of benzene. The solution was degassed and HOTeF$_5$ (0.5 g, 2.1 mmol, 4 eq.) was condensed on top at –196 °C. A bubbler was added and the reaction mixture was warmed up to –30 °C, giving rise to a yellow solution. Then, the HFO-1234yf (130 mbar, 1 eq) was condensed on top, giving rise to a red reaction mixture. After warming to ambient temperature, the volatile part of the reaction mixture was condensed into a separate vessel and distilled water (5 ml) was added to it. The organic phase was separated and filtered through a hydrophobic syringe filter (PTFE, 0.2 µm).

Reaction of the Brønsted superacid [*o*-C$_6$F$_2$H$_4$-H][Al(OTeF$_5$)$_4$] with 2,3,3,3-tetrafluoroporpene

The synthesis was similar to the typical experiment described above. As solvent only 3 ml of neat 1,2-difluorobenzene was used.

Reaction of the Brønsted superacid [C$_7$H$_8$-H][Al(OTeF$_5$)$_4$] with 2,3,3,3-tetrafluoroporpene

The synthesis was similar to the typical experiment described above. As solvent 3 ml 1,2-difluorobenzene and 0.1 ml of toluene was used.

Crystal Data and IR data for [C$_5$F$_3$H$_2$N-H][Al(OTeF$_5$)$_4$]. (M =1115.46 g/mol): monoclinic, space group P21/n (no. 14), a = 11.1920(6) Å, b = 17.6369(9) Å, c = 11.9454(6) Å, β = 104.433(2)°, V = 2283.5(2) Å^3, Z = 4, T = 100.0 K, μ(MoK$_\alpha$) = 5.301 mm^{-1}, D_{calc} = 3.245 g/cm^3, 63496 reflections measured

(4.21°≤ 2Θ ≤ 50.754°), 4196 unique (R_{int} = 0.0487, R_{sigma} = 0.0197) which were used in all calculations. The final R_1 value was 0.0533 (I > 2σ(I)) and wR_2 was 0.1297 (all data). **IR** (ATR, 22 °C): $\tilde{\nu}$ = 3291 (m), 3241 (m), 3122 (m), 1671 (w), 1687 (w), 1666 (s), 1629 (m), 1593 (w), 1544 (w), 1528 (w), 1478(m), 1389(vw), 1356(vw), 1344(vw), 1197(w), 1177(m), 1042(w), 1014 (m), 932 [vs, ν_{as}(Al−O)], 867(s), 757 (m), 679 [vs, ν_{as}(Te−F_4)], 622 [m, ν_{as}(O−Te−F)], 573 [m, ring, in-plane(Al_2O_2)], 533(m), 512 (s), 471 [w, ν(Te-O)] cm^{-1}.

Crystal Data and IR data for $C_5H_2F_3N{\rightarrow}Al(OTeF_5)_3$. ($M$ = 875.86 g/mol): monoclinic, space group *Cc* (no. 9), a = 16.7204(15) Å, b = 8.8361(8) Å, c= 14.171(2) Å, β = 119.280(3)°, V = 1826.2(4) $Å^3$, Z= 4, T= 100.0 K, μ(MoK_α) = 4.997 mm^{-1}, D_{calc} = 3.186 g/cm^3, 43227 reflections measured (5.39°≤ 2Θ ≤ 57.29), 4558 unique (R_{int} = 0.0649, R_{sigma} = 0.0418) which were used in all calculations. The final R_1 value was 0.0305 (I > 2σ(I)) and wR_2 was 0.0714 (all data). **IR** (ATR, 22 °C): $\tilde{\nu}$ = 3165 [vw, ν(C−N)], 1658(w), 1605(m), 1539 (s), 1503 (s), 1470 (w), 1381 (w), 1347(w), 1318(m), 1200(vw), 1158(vw), 1120(m), 1103(m), 1090(m), 984 (s), 938 [vs, ν_{as}(Al−O)], 854(w), 836(vw), 757 [s, ring, in-plane(Al_2O_2)], 698 [vs, ν_{as}(Te−F_4)], 639 [s, ring, in-plane(Al_2O_2)], 622 [m, ν_{as}(O−Te−F)], 563 [m, ν_s(Al−O)], 550 (m), 453 [w, ν(Te-O)], 415(w) cm^{-1}.

Crystal Data for $[C_5H_4BrN\text{-}H][Al(OTeF_5)_4]$. ($M$ = 1140.39 g/mol): triclinic, space group P $\bar{1}$ (no. 2), a = 9.9580(17) Å, b = 10.2325(18) Å, c = 12.850(2) Å, α = 80.728(6)°, β = 70.111(6)°, γ = 76.232(6)°, V = 1191.3(4) $Å^3$, Z = 2, T = 100(2) K, μ(MoK_α) = 6.734 mm^{-1}, D_{calc} = 3.179 g/cm^3, 14567 reflections measured (4.114° ≤ 2Θ ≤ 50.84°), 14567 unique (R_{sigma} = 0.0411) which were used in all calculations. The final R_1 value was 0.0503 (I > 2σ(I)) and wR_2 was 0.1285 (all data).

Crystal Data for $[C_7H_8\text{-}H][Al(OTeF_5)_4]\cdot C_7H_8$. ($M$ = 947.05 g/mol): monoclinic, space group $P2_1$, a = 18.7185(16) Å, b = 16.9001(14) Å, c = 18.8997(17) Å, α = 90.0°, β = 117.278(3)°, γ = 90.0°, V = 5313.9(8) $Å^3$, Z = 8, T = 100(2) K, μ(MoK_α) = 3.433 mm^{-1}, D_{calc} = 2.368 g/cm^3, 85032 reflections measured (4.81°≤ 2Θ ≤ 50.992°), 19506 unique (R_{sigma} = 0.0411) which were used in all calculations. The final R_1 value was 0.0420 I > 2σ(I)) and wR_2 was 0.0496 (all data).

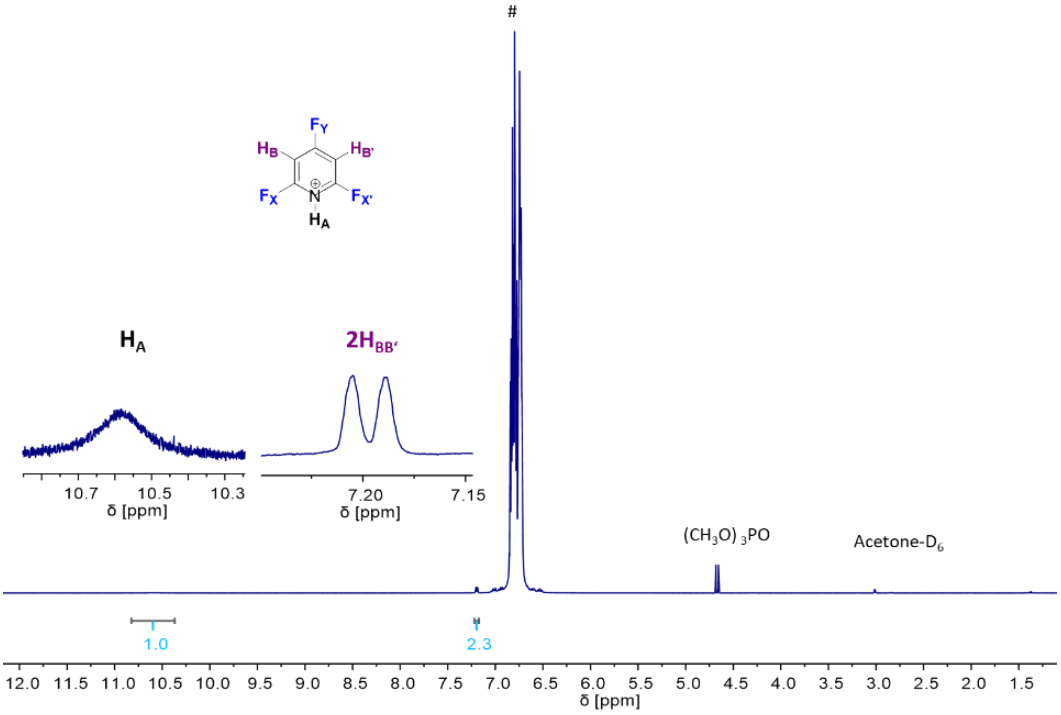

Figure. 7.1. ^{1}H NMR (ext. [D$_6$]acetone, 25 °C, 401 MHz). Spectrum of $[C_5F_3H_2N\text{-}H][Al(OTeF_5)_4]$ in *o*DFB (marked as #).

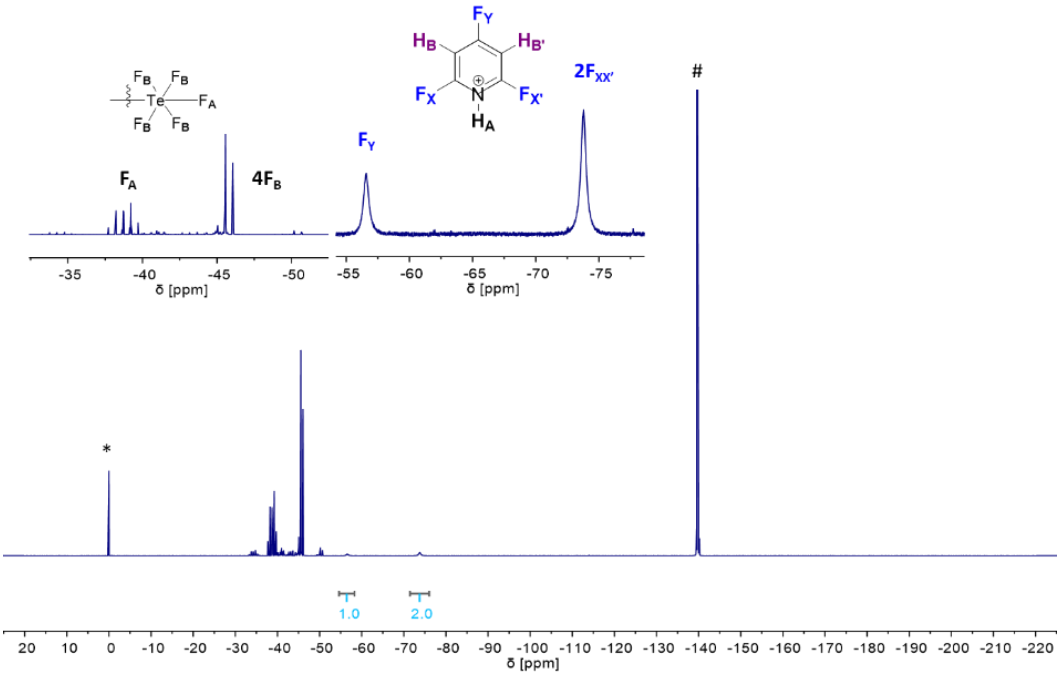

Figure. 7.2. ^{19}F NMR (ext. [D$_6$]acetone, 25 °C, 377 MHz). Spectrum of $[C_5F_3H_2N\text{-}H][Al(OTeF_5)_4]$ in 1,2-difluorobenzene. Corresponding resonances are labelled. * – ext. $CFCl_3$; # – *o*DFB

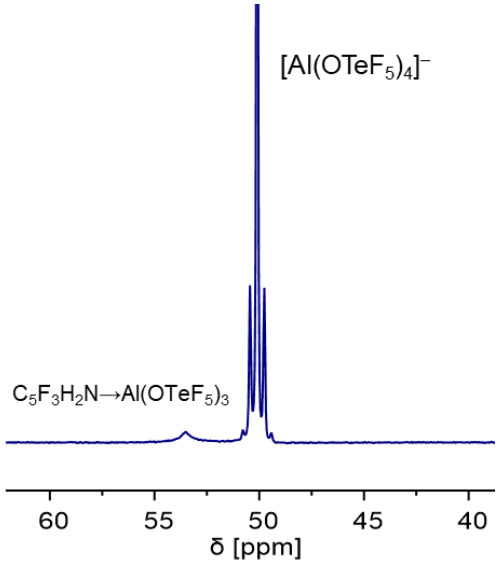

Figure 7.3. ^{27}Al NMR (ext. [D$_6$]acetone, 25 °C, 104 MHz). Spectrum of the solution of [C$_5$F$_3$H$_2$N-H][Al(OTeF$_5$)$_4$] in *o*DFB.

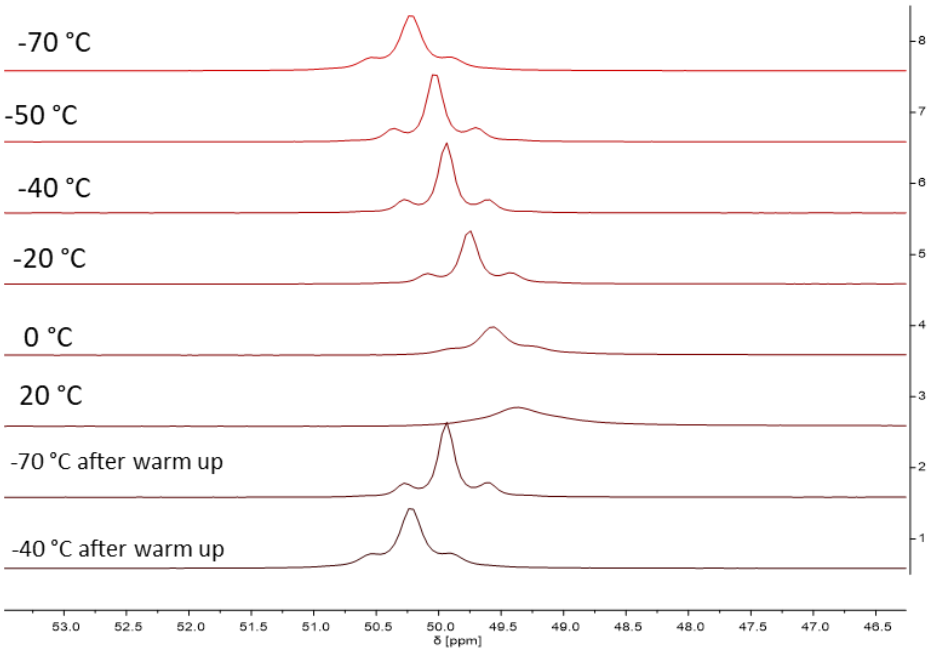

Figure 7.4. ^{27}Al NMR (CD_2Cl_2, −70-(+20)°C, 104 MHz). Spectra of the solution of [C$_5$H$_2$F$_3$N-H][Al(OTeF$_5$)$_4$] in CD_2Cl_2.

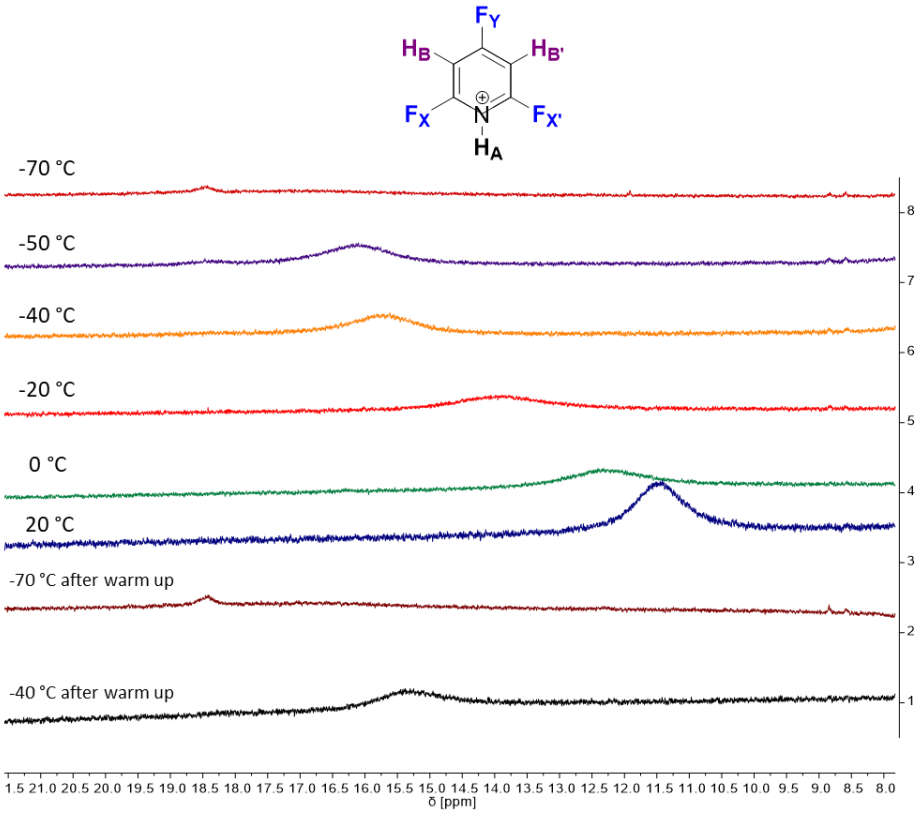

Figure 7.5. ^{1}H NMR (CD_2Cl_2, −70-(+20)°C, 401 MHz). Spectra of the solution of $[C_5F_3H_2N\text{-}H][Al(OTeF_5)_4]$ in CD_2Cl_2.

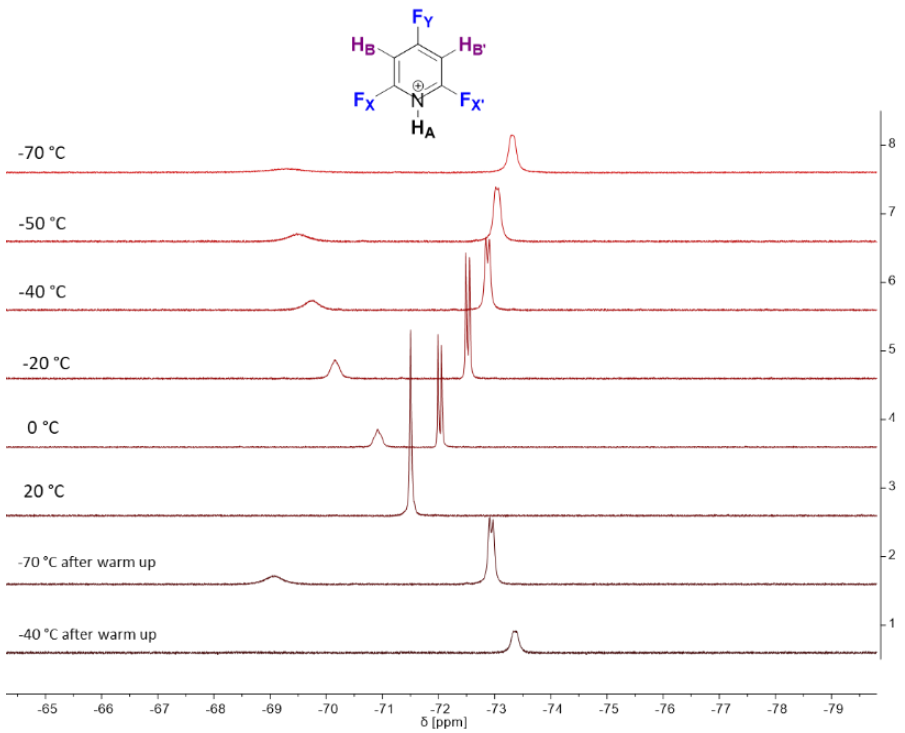

Figure 7.6. ^{19}F NMR (CD_2Cl_2, −70-(+20)°C, 377 MHz). Spectrum of the solution of $[C_5F_3H_2N\text{-}H][Al(OTeF_5)_4]$ in CD_2Cl_2

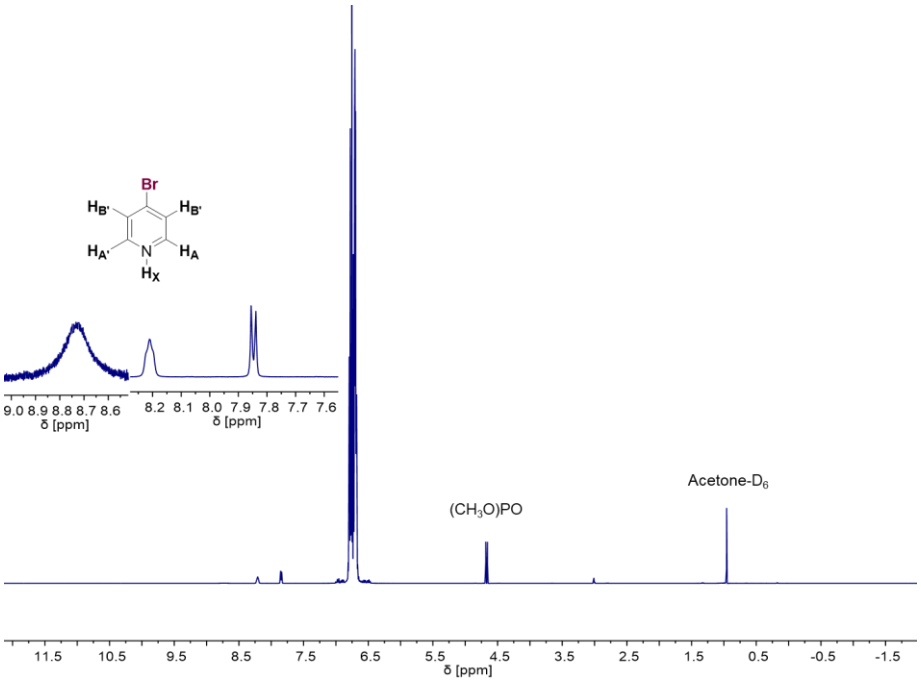

Figure 7.7. ^{1}H NMR (ext. [D$_6$]acetone, 25 °C, 401 MHz). Spectrum of [C$_5$H$_4$BrN-H][Al(OTeF$_5$)$_4$] in *o*DFB (marked as #).

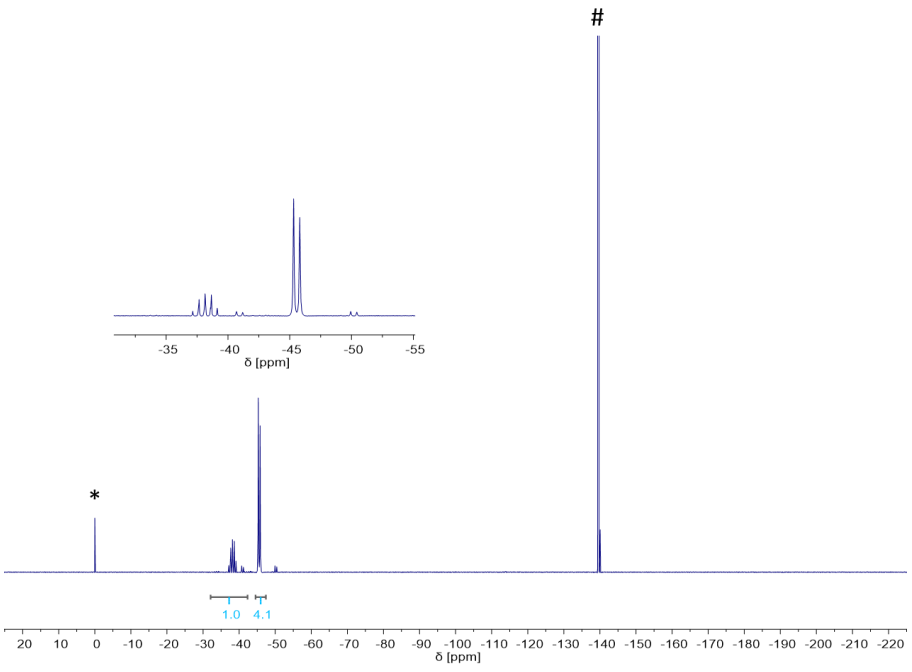

Figure 7.8. ^{19}F NMR (ext. [D$_6$]acetone, 25 °C, 377 MHz). Spectrum of [C$_5$H$_4$BrN-H][Al(OTeF$_5$)$_4$] in *o*DFB Corresponding resonances are labelled. * – ext. CFCl$_3$; # –*o*DFB.

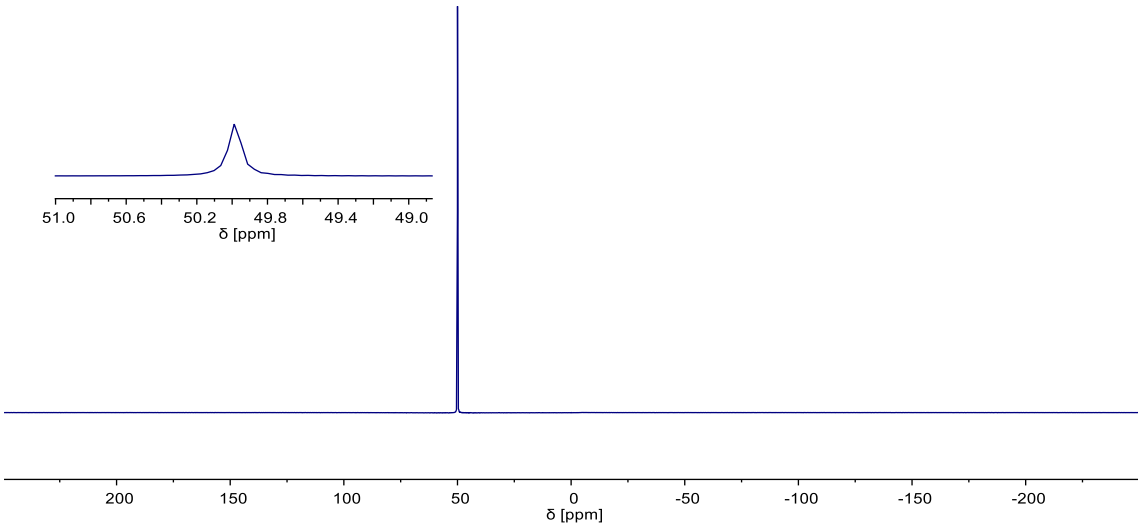

Figure 7.9. ^{27}Al NMR (ext. [D$_6$]acetone, 25 °C, 104 MHz). Spectrum of the solution of [C$_5$H$_4$BrN-H][Al(OTeF$_5$)$_4$] in *o*DFB.

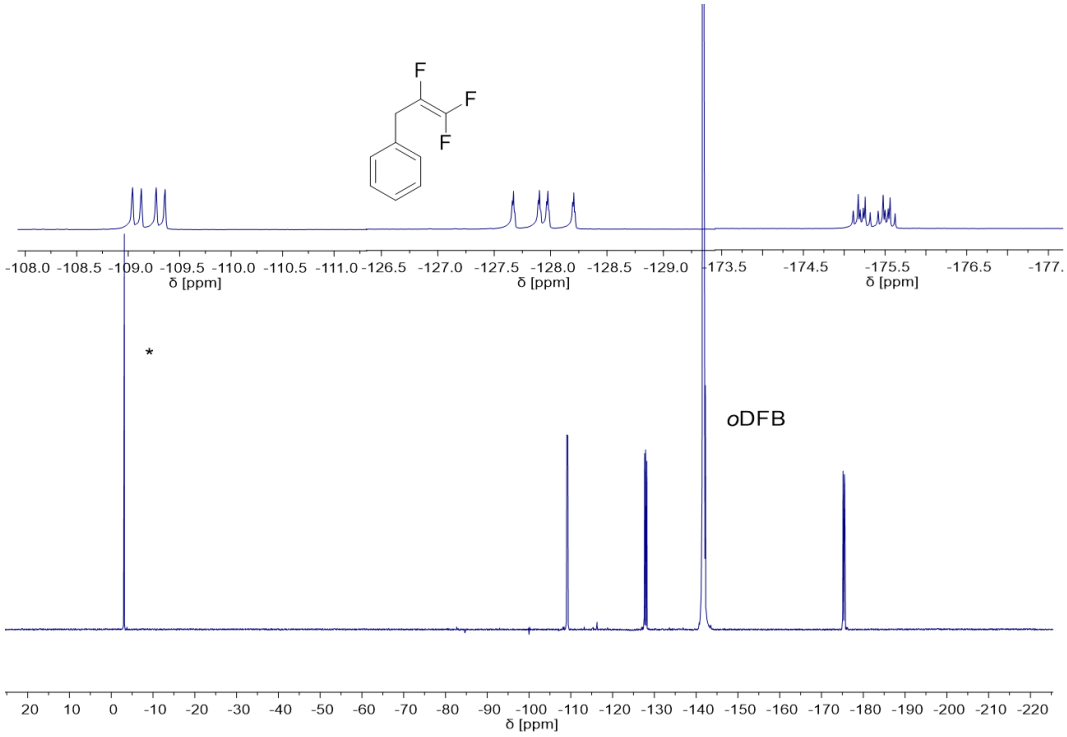

Figure 7.10. ^{19}F NMR (ext. [D$_6$]acetone, 25 °C, 377 MHz). Spectrum of purified product C$_6$D$_5$CH$_2$F$_3$ in *o*DFB (depicted as *o*DFB). Corresponding resonance is labeled. * – ext. CFCl$_3$.

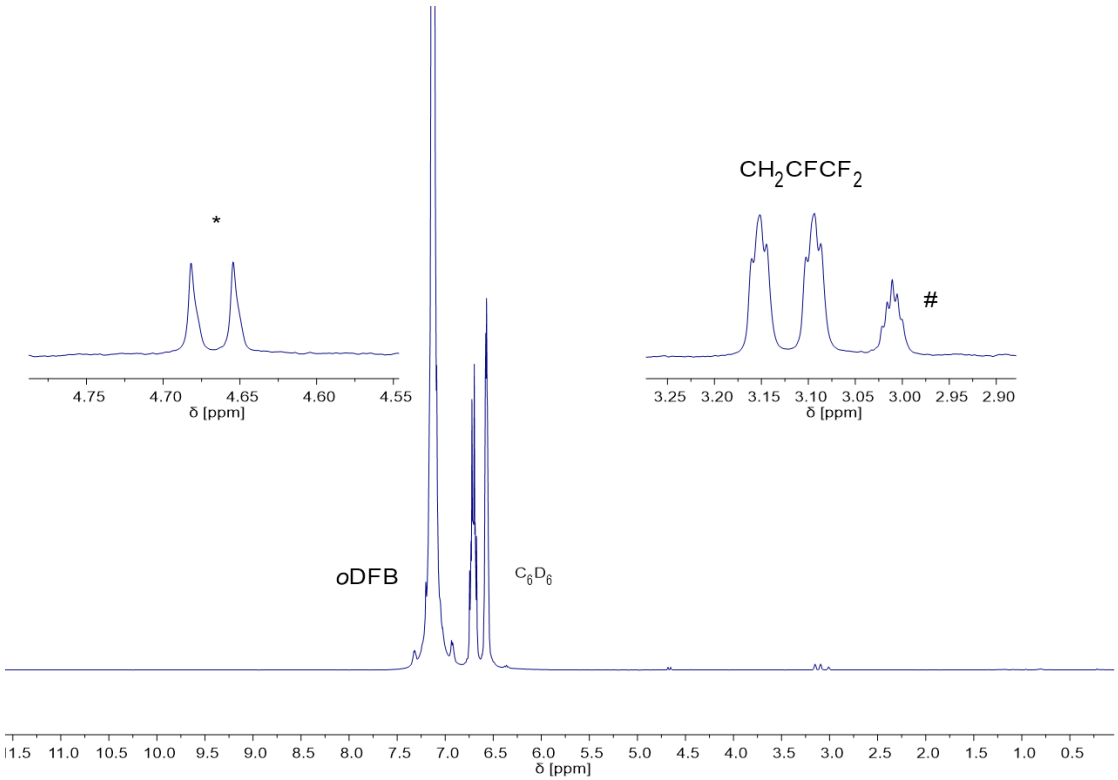

Figure 7.11. ^{1}H NMR (ext. [D_6]acetone, 25 °C, 401 MHz). Spectrum of purified product $C_6D_5CH_2F_3$ in *o*DFB (depicted as *o*DFB). * – ext. $(CH_3O)_3PO$, # – ext. [D_6]acetone.

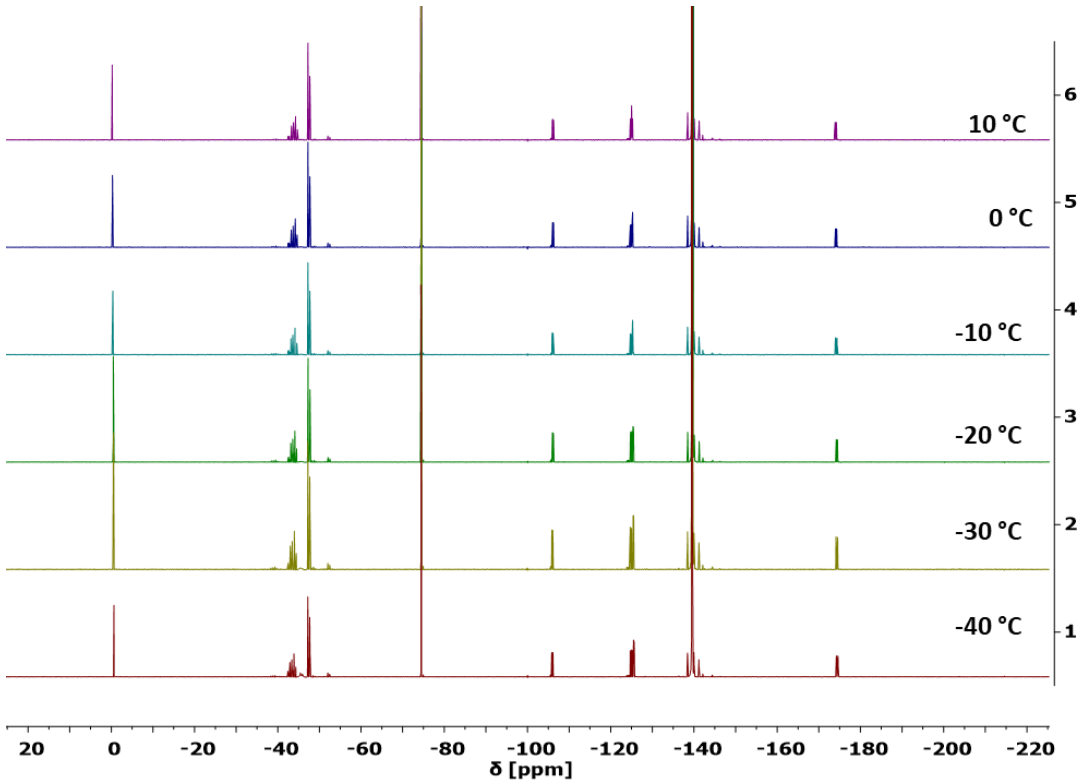

Figure 7.12. ^{19}F NMR (ext. [D_6]acetone, −40-(+10)°C, 377 MHz). Low-temperature spectra of reaction of $[C_6F_2H_4\text{-}H][Al(OTeF_5)_4]$ with HFO1234-yf in *o*DFB.

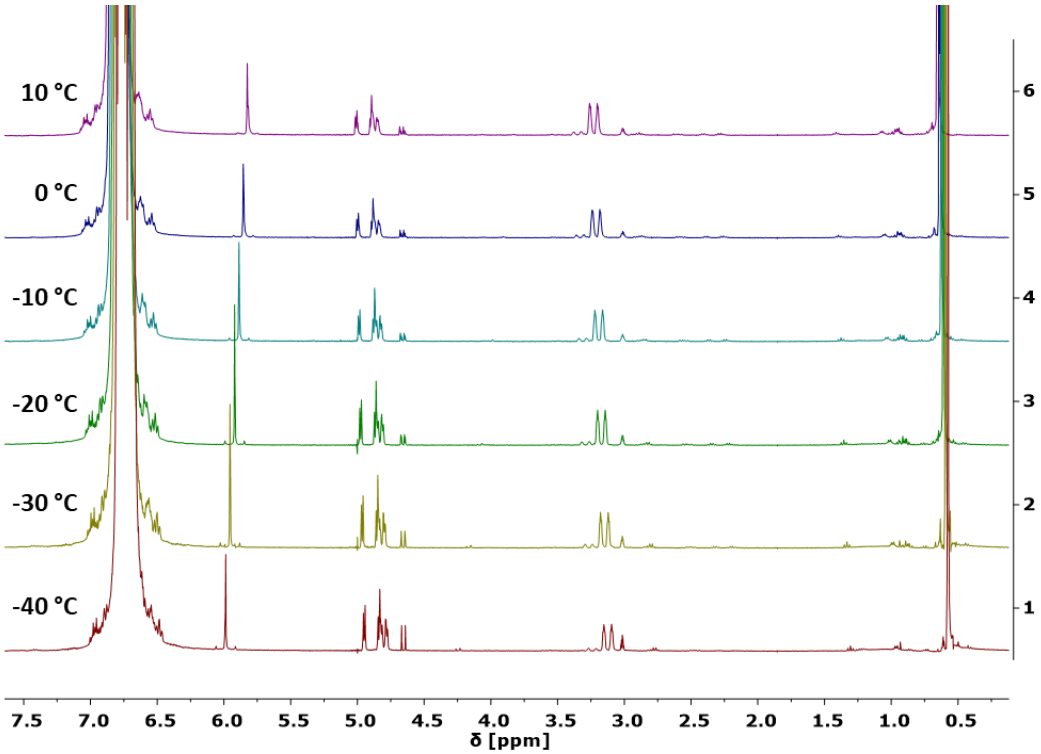

Figure 7.13. ^{1}H NMR (ext. [D$_6$]acetone, −40-(+10)°C, 401 MHz). Low-temperature spectra of reaction of [C$_6$F$_2$H$_4$-H][Al(OTeF$_5$)$_4$] with HFO1234-yf in *o*DFB.·

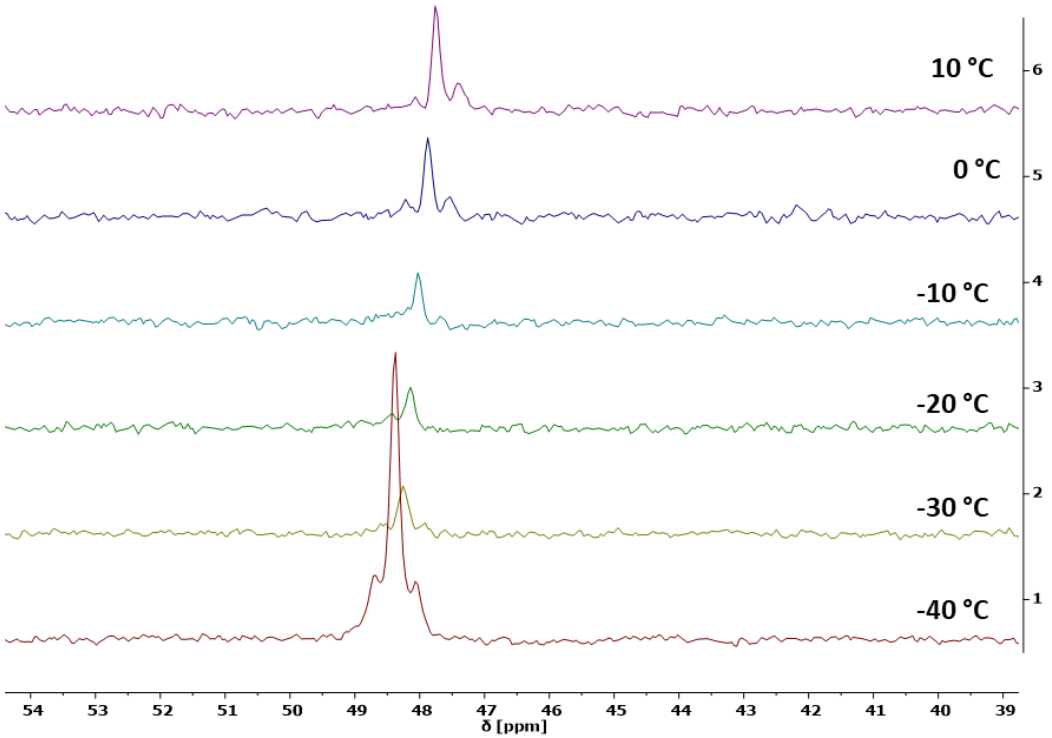

Figure 7.14. ^{27}Al NMR (ext. [D$_6$]acetone, −40-(+10)°C, 101 MHz). Low-temperature spectra of reaction of [C$_6$F$_2$H$_4$-H][Al(OTeF$_5$)$_4$] with HFO1234-yf in *o*DFB.

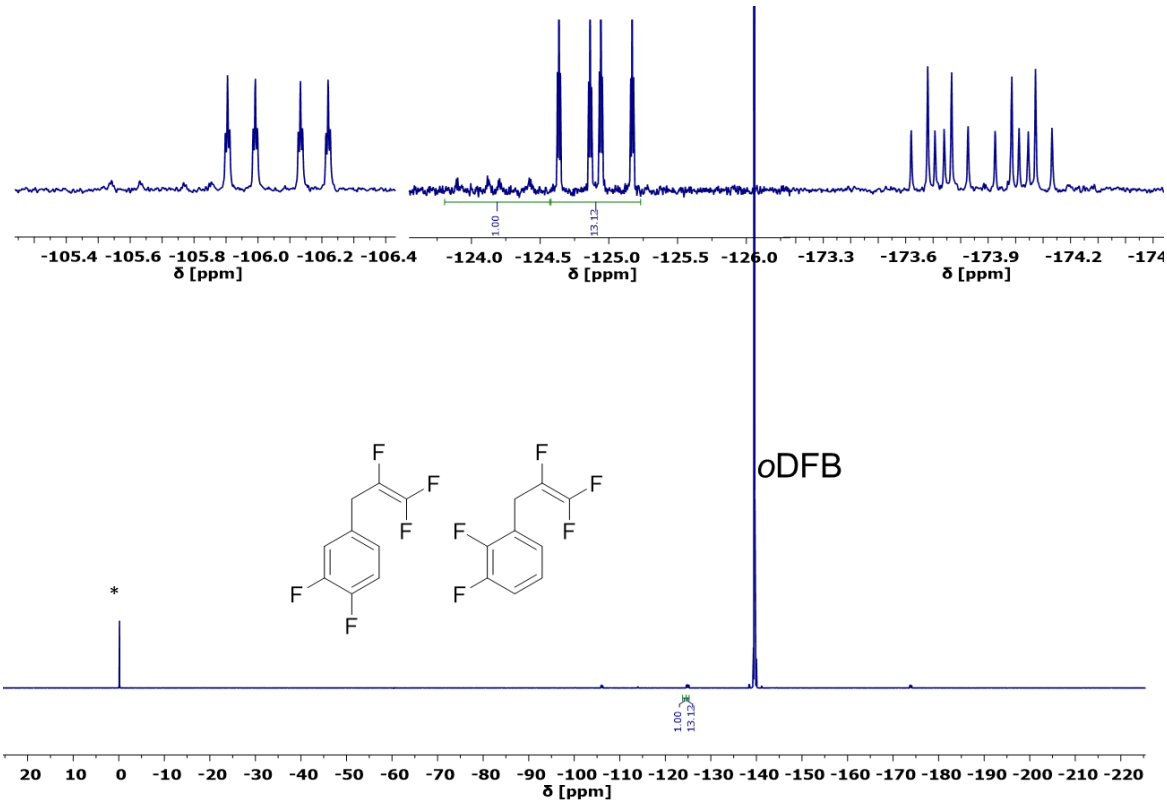

Figure 7.15. ^{19}F NMR (ext. [D_6]acetone, 25 °C, 377 MHz). Spectrum of isomer products $C_9H_5F_5$ in difluorobenzene (depicted as *o*DFB). Corresponding resonance is labeled. * – ext. $CFCl_3$.

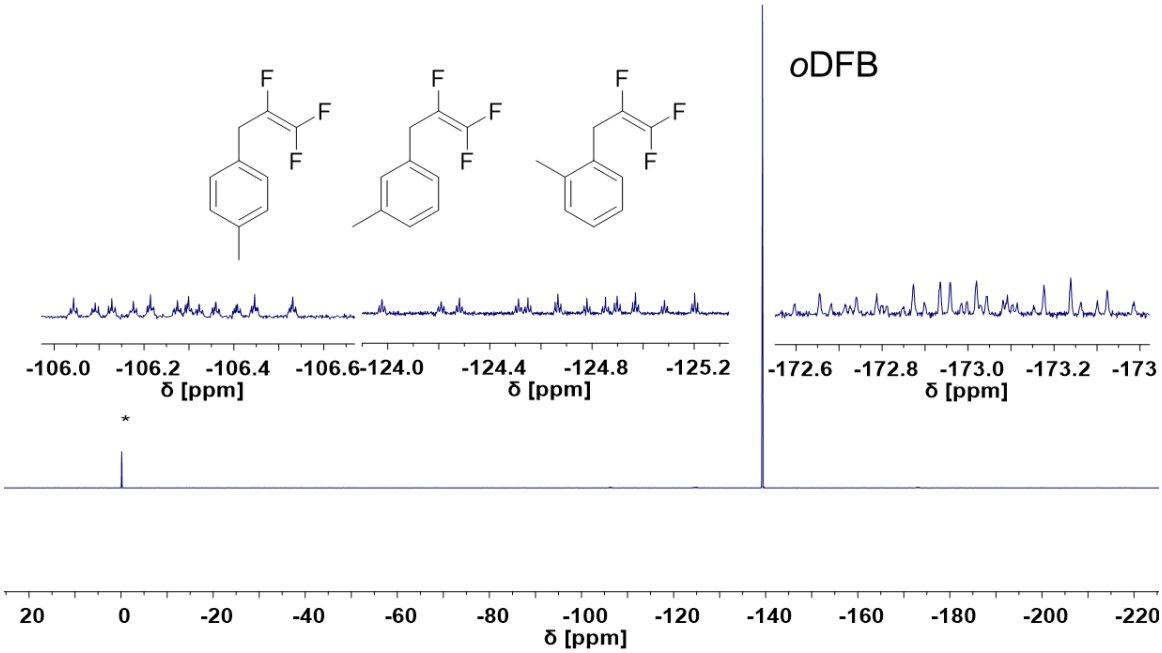

Figure 7.16. ^{19}F NMR (ext. [D_6]acetone, 25 °C, 377 MHz). Spectrum of isomer products $C_{10}H_9F_3$ in ratio 1:2 in *o*DFB (depicted as *o*DFB) after purification. Corresponding resonance is labeled. * – ext. $CFCl_3$.

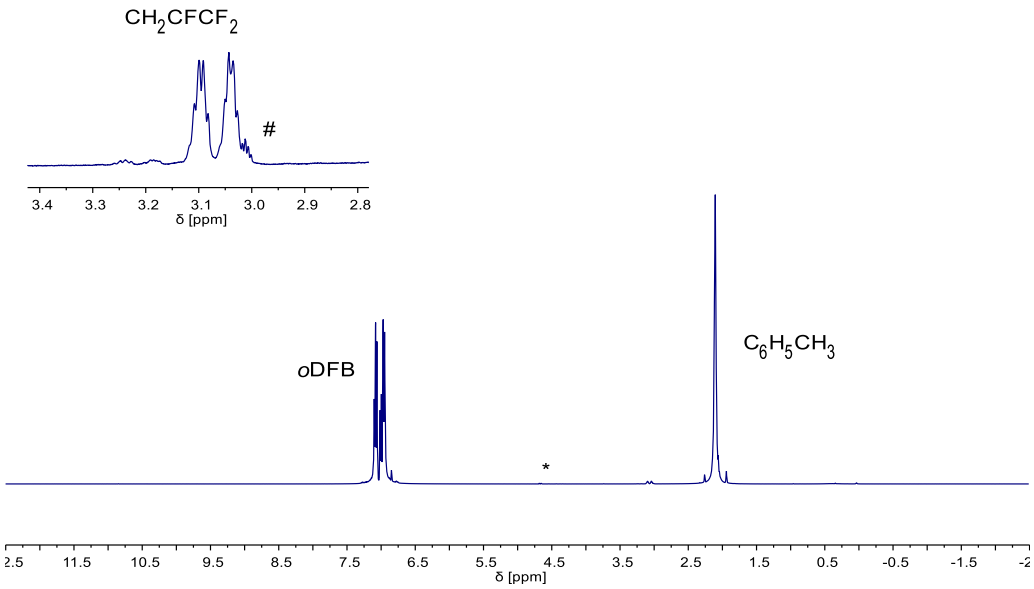

Figure 7.17. ^{1}H NMR (ext. [D$_6$]acetone, 25 °C, 401 MHz**).** Spectrum of isomer products $C_{10}H_9F_3$ in ratio 1:2 in 1,2-difluorobenzene (depicted as *o*DFB) after purification. Corresponding resonance is labeled. * – ext. $(CH_3O)_3PO$, # – ext. [D$_6$]acetone.

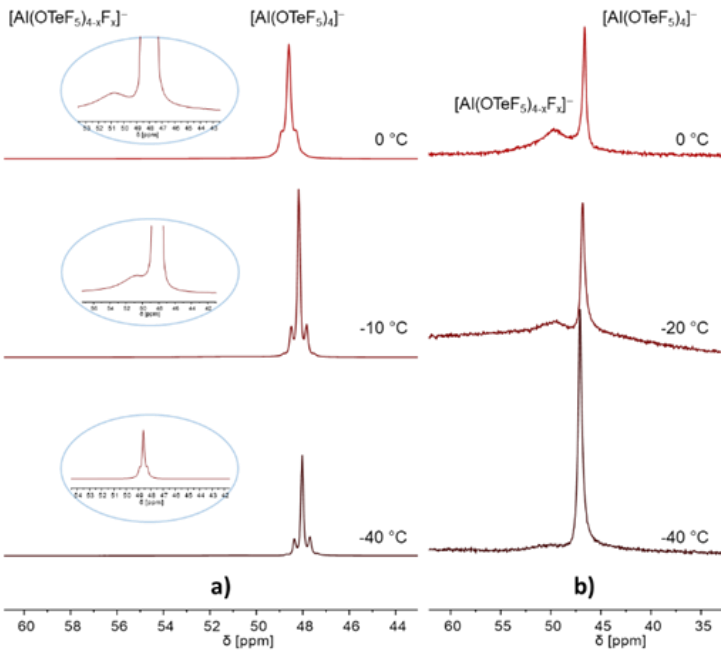

Figure 7.18. a) Low-temperature ^{27}Al NMR spectra (toluene-[D8]; 104 MHz) of the reaction between Brønsted superacid [C_7D_8-H][Al(OTeF$_5$)$_4$] and HFO-1234yf; b) low-temperature ^{27}Al NMR spectra (ext. [D$_6$]-acetone; 104 MHz) of the reaction between Brønsted superacid [*o*-$C_6F_2H_4$-H][Al(OTeF$_5$)$_4$] and HF.

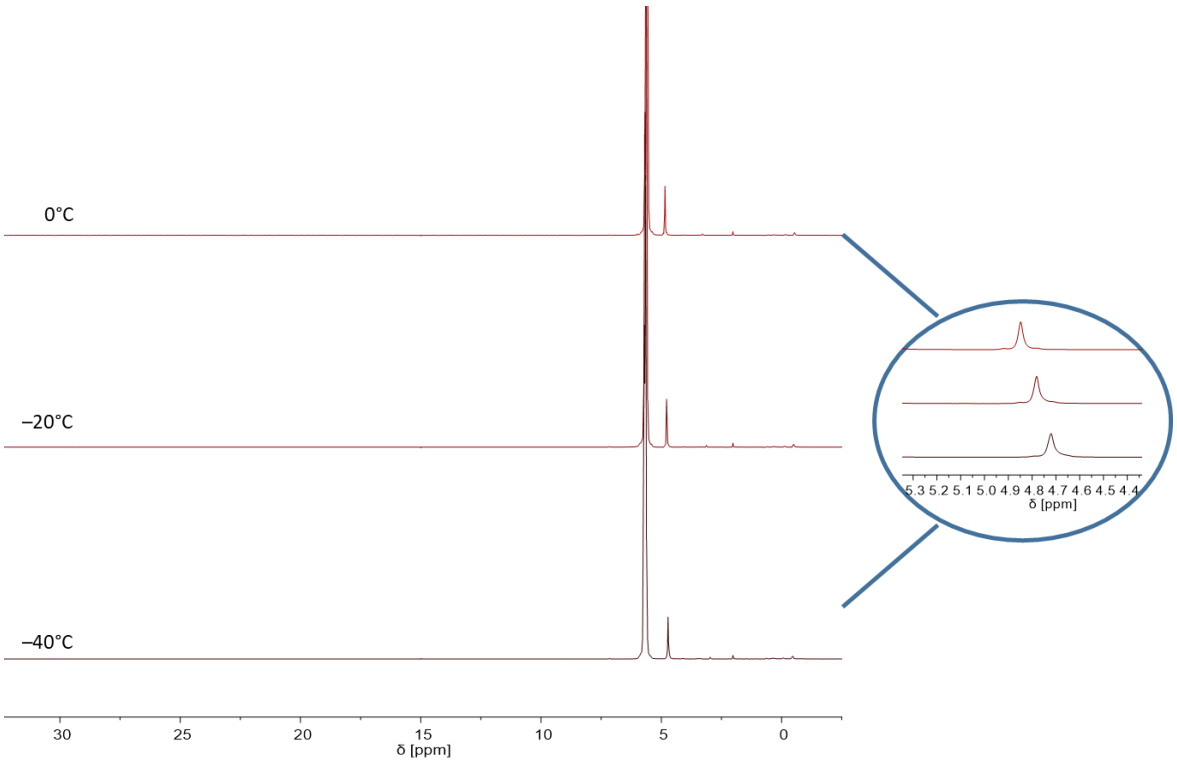

Figure 7.19. Low-temperature ^{1}H NMR (ext. Acetone-[D_6], 401 MHz). Spectra of the reaction of HF with the Brønsted Superacid [$C_6F_2H_9$][$Al(OTeF_5)_4$] in *o*DFB**.**

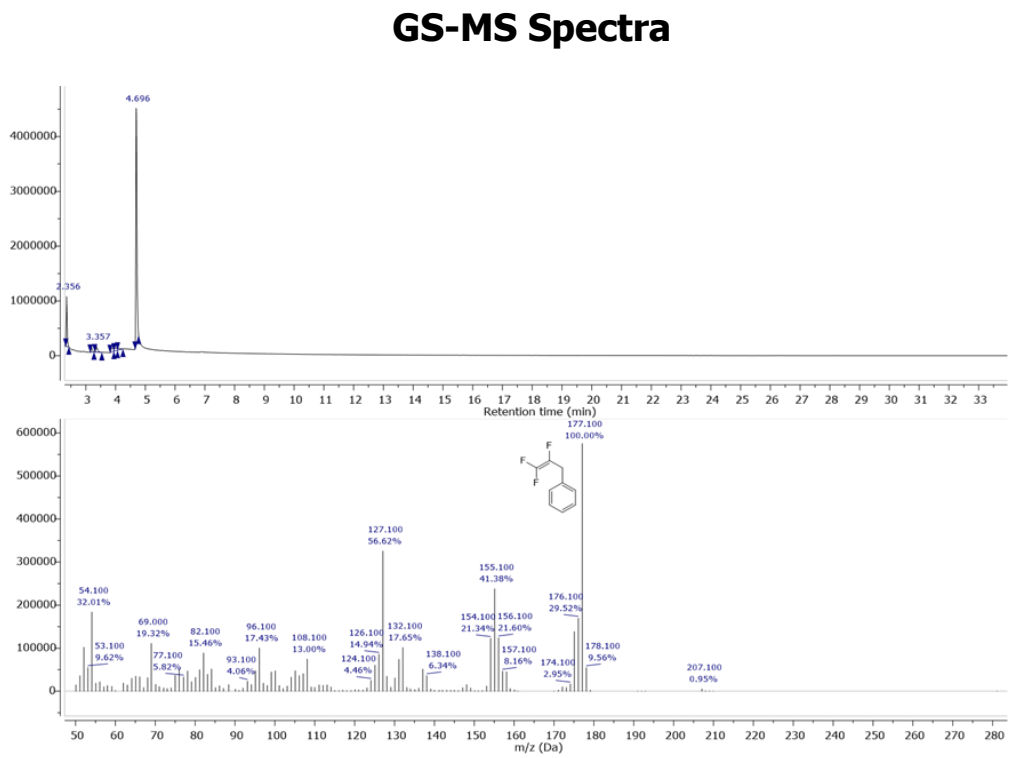

Figure 7.20. GC/MS TIC spectrum (above) and extracted mass spectrum (bottom) of reaction product, obtained from reaction of between Brønsted superacid [C_6H_5-H][$Al(OTeF_5)_4$] and HFO-1234yf.

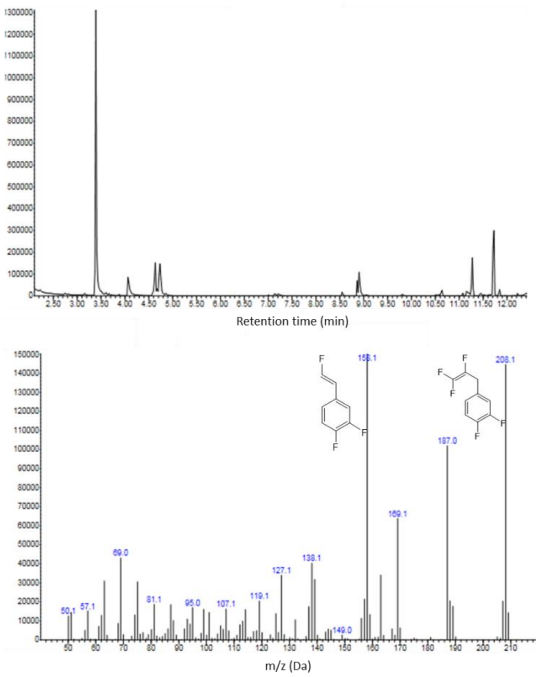

Figure 7.21. GC/MS TIC spectrum (above) and extracted mass spectrum (bottom) of reaction product, obtained from the reaction between Brønsted superacid [*o*-$C_6H_4F_2$-H][$Al(OTeF_5)_4$] and HFO-1234yf.

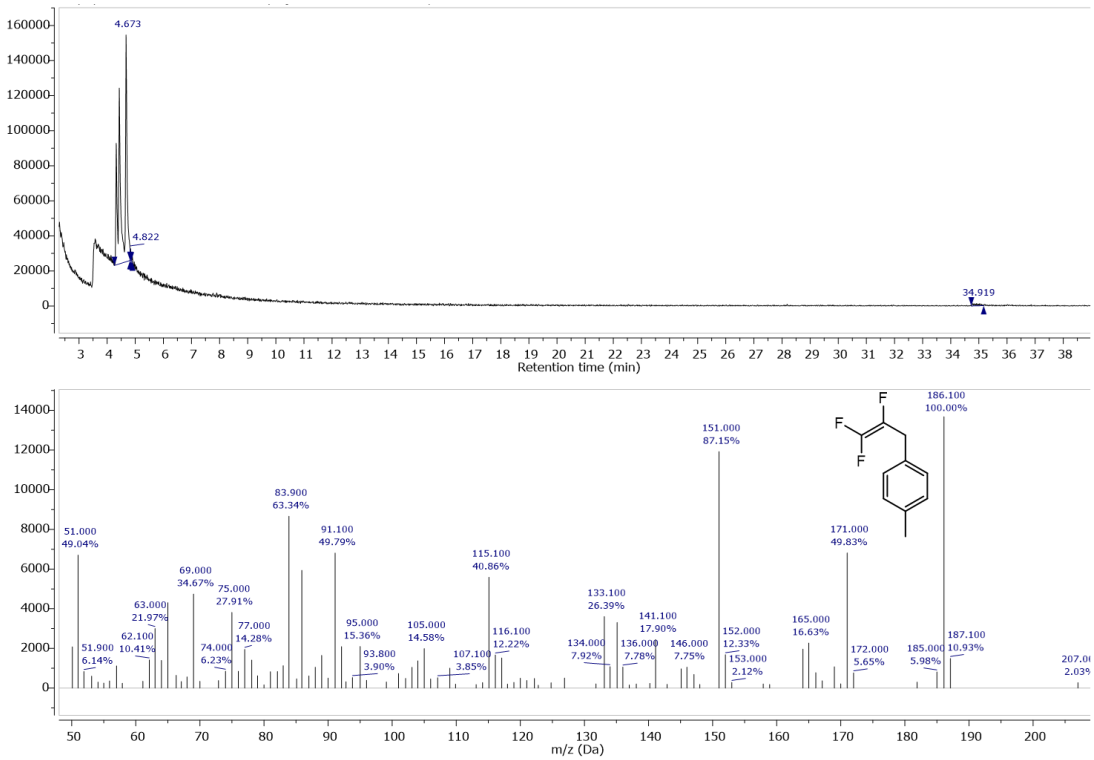

Figure 7.22. GC/MS TIC spectrum (above) and extracted mass spectrum (bottom) of reaction products, obtained from the reaction between Brønsted superacid [C_6H_8-H][$Al(OTeF_5)_4$] and HFO-1234yf.

Crystallographic Data

Table 7.1. Bond Angles for $[C_5F_3H_2N\text{-}H][Al(OTeF_5)_4]$.

Atom	Atom	Atom	Angle/°	Atom	Atom	Atom	Angle/°
F8	Te2	F7	90.4(3)	F17	Te4	F18	91.9(4)
O2	Te2	F8	94.2(3)	F18	Te4	F20	171.8(3)
O2	Te2	F9	93.0(3)	F18	Te4	F19	90.2(4)
O2	Te2	F7	93.0(3)	F18	Te4	F16	86.6(3)
O2	Te2	F6	178.5(3)	F1	Te1	F4	86.7(4)
O2	Te2	F10	91.7(3)	F1	Te1	F5	86.5(3)
F9	Te2	F8	90.4(3)	O1	Te1	F1	179.2(4)
F9	Te2	F7	173.8(3)	O1	Te1	F4	92.5(3)
F9	Te2	F10	89.1(3)	O1	Te1	F3	92.2(4)
F6	Te2	F8	87.2(3)	O1	Te1	F2	92.4(4)
F6	Te2	F9	86.8(3)	O1	Te1	F5	93.6(3)
F6	Te2	F7	87.1(3)	F3	Te1	F1	87.6(4)
F6	Te2	F10	86.9(3)	F3	Te1	F4	90.4(4)
F10	Te2	F8	174.1(3)	F3	Te1	F5	174.1(3)
F10	Te2	F7	89.5(3)	F2	Te1	F1	88.4(4)
F15	Te3	F13	172.8(3)	F2	Te1	F4	175.0(4)
F14	Te3	F15	90.7(3)	F2	Te1	F3	90.5(4)
F14	Te3	F12	171.6(3)	F2	Te1	F5	89.7(4)
F14	Te3	F13	90.2(3)	F5	Te1	F4	88.9(3)
F14	Te3	F11	86.2(3)	O2	Al1	O4	106.4(4)
F12	Te3	F15	89.0(3)	O1	Al1	O2	111.6(4)
F12	Te3	F13	89.1(3)	O1	Al1	O4	110.1(4)
F11	Te3	F15	86.9(3)	O1	Al1	O3	108.6(4)
F11	Te3	F12	85.4(3)	O3	Al1	O2	111.0(4)
F11	Te3	F13	86.0(3)	O3	Al1	O4	109.1(4)
O3	Te3	F15	93.0(3)	Al1	O2	Te2	146.5(4)
O3	Te3	F14	94.6(4)	Al1	O1	Te1	145.9(4)
O3	Te3	F12	93.8(4)	C1	N1	C5	118.5(8)
O3	Te3	F13	94.1(3)	Al1	O4	Te4	144.5(4)
O3	Te3	F11	179.2(4)	Al1	O3	Te3	141.3(4)
F19	Te4	F20	87.6(4)	F21	C5	N1	116.1(8)
O4	Te4	F20	94.0(3)	F21	C5	C4	121.3(9)
O4	Te4	F19	91.2(3)	N1	C5	C4	122.6(8)
O4	Te4	F16	179.0(3)	C1	C2	C3	117.3(8)
O4	Te4	F17	94.7(3)	F22	C1	N1	116.8(8)
O4	Te4	F18	93.9(4)	F22	C1	C2	121.0(8)
F16	Te4	F20	85.5(3)	C2	C1	N1	122.2(9)
F16	Te4	F19	87.9(4)	F23	C3	C2	116.9(8)
F17	Te4	F20	89.5(4)	F23	C3	C4	118.9(9)
F17	Te4	F19	173.6(3)	C2	C3	C4	124.2(8)
F17	Te4	F16	86.2(4)	C5	C4	C3	115.2(9)

Table 7.2. Bond Lengths for $[C_5F_3H_2N\text{-}H][Al(OTeF_5)_4]$.

Atom	Atom	Length/Å	Atom	Atom	Length/Å
Te2	F8	1.831(6)	Te1	O1	1.795(7)
Te2	O2	1.803(6)	Te1	F4	1.837(7)
Te2	F9	1.828(6)	Te1	F3	1.815(7)
Te2	F7	1.832(6)	Te1	F2	1.812(7)
Te2	F6	1.824(6)	Te1	F5	1.828(6)
Te2	F10	1.828(6)	Al1	O2	1.743(7)
Te3	F15	1.826(5)	Al1	O1	1.734(8)
Te3	F14	1.808(6)	Al1	O4	1.744(7)
Te3	F12	1.823(6)	Al1	O3	1.740(7)
Te3	F13	1.841(6)	F21	C5	1.299(10)
Te3	F11	1.822(6)	F23	C3	1.309(10)
Te3	O3	1.797(7)	F22	C1	1.311(11)
Te4	F20	1.824(6)	N1	C5	1.361(12)
Te4	F19	1.823(7)	N1	C1	1.352(12)
Te4	O4	1.786(6)	C5	C4	1.369(12)
Te4	F16	1.818(6)	C2	C1	1.346(13)
Te4	F17	1.802(7)	C2	C3	1.352(13)
Te4	F18	1.809(7)	C3	C4	1.374(12)
Te1	F1	1.825(7)			

Table 7.3. Bond Lengths for $C_5F_3H_2N{\rightarrow}Al(OTeF_5)_3$.

Atom	Atom	Length/Å	Atom	Atom	Length/Å
Te2	F12	1.827(6)	Te1	F6	1.810(6)
Te2	O2	1.797(7)	Te1	F7	1.818(5)
Te2	F13	1.824(6)	Al1	O1	1.726(6)
Te2	F11	1.813(6)	Al1	O2	1.712(7)
Te2	F10	1.830(5)	Al1	N1	1.960(7)
Te2	F9	1.824(6)	Al1	O3	1.717(7)
Te3	F18	1.826(7)	F2	C3	1.327(10)
Te3	F14	1.821(7)	F1	C1	1.304(10)
Te3	F15	1.821(6)	F3	C5	1.319(8)
Te3	F17	1.821(6)	C4	C5	1.341(13)
Te3	O3	1.801(6)	C4	C3	1.388(12)
Te3	F16	1.816(7)	N1	C1	1.335(11)
Te1	F5	1.829(6)	N1	C5	1.364(11)
Te1	F8	1.829(6)	C1	C2	1.390(12)
Te1	O1	1.815(6)	C2	C3	1.347(13)
Te1	F4	1.835(5)			

Table 7.4. Bond Angles for $C_5F_3H_2N \rightarrow Al(OTeF_5)_3$.

Atom	Atom	Atom	Angle/°	Atom	Atom	Atom	Angle/°
F12	Te2	F10	173.9(3)	O1	Te1	F8	93.2(3)
O2	Te2	F12	93.5(3)	O1	Te1	F4	179.5(3)
O2	Te2	F13	93.5(3)	O1	Te1	F7	92.4(3)
O2	Te2	F11	91.9(3)	F6	Te1	F5	90.3(3)
O2	Te2	F10	92.4(3)	F6	Te1	F8	174.6(3)
O2	Te2	F9	179.1(4)	F6	Te1	O1	92.2(3)
F13	Te2	F12	90.3(3)	F6	Te1	F4	87.9(3)
F13	Te2	F10	90.7(3)	F6	Te1	F7	89.3(3)
F11	Te2	F12	89.1(3)	F7	Te1	F5	174.4(3)
F11	Te2	F13	174.6(3)	F7	Te1	F8	90.2(3)
F11	Te2	F10	89.4(3)	F7	Te1	F4	88.1(3)
F11	Te2	F9	87.6(4)	O1	Al1	N1	110.4(3)
F9	Te2	F12	87.2(3)	O2	Al1	O1	108.9(3)
F9	Te2	F13	87.1(3)	O2	Al1	N1	103.8(3)
F9	Te2	F10	86.8(3)	O2	Al1	O3	118.0(3)
F14	Te3	F18	87.2(4)	O3	Al1	O1	112.6(3)
F14	Te3	F15	87.2(4)	O3	Al1	N1	102.6(3)
F14	Te3	F17	86.8(3)	Al1	O1	Te1	140.3(4)
F15	Te3	F18	90.2(3)	Al1	O2	Te2	154.7(5)
F17	Te3	F18	89.3(3)	C5	C4	C3	114.9(8)
F17	Te3	F15	174.1(4)	C1	N1	Al1	126.8(6)
O3	Te3	F18	91.9(4)	C1	N1	C5	115.8(7)
O3	Te3	F14	179.0(4)	C5	N1	Al1	117.3(5)
O3	Te3	F15	92.8(3)	F1	C1	N1	115.0(7)
O3	Te3	F17	93.1(3)	F1	C1	C2	121.4(7)
O3	Te3	F16	93.1(4)	N1	C1	C2	123.7(8)
F16	Te3	F18	175.0(5)	Al1	O3	Te3	152.1(4)
F16	Te3	F14	87.9(4)	C3	C2	C1	116.3(7)
F16	Te3	F15	90.4(3)	F3	C5	C4	121.3(8)
F16	Te3	F17	89.7(3)	F3	C5	N1	113.0(7)
F5	Te1	F4	86.3(3)	C4	C5	N1	125.7(7)
F8	Te1	F5	89.7(3)	F2	C3	C4	118.3(7)
F8	Te1	F4	86.7(3)	F2	C3	C2	118.1(8)
O1	Te1	F5	93.2(3)	C2	C3	C4	123.5(8)

Table 7.5. Bond Lengths for $[C_5H_4BrN\text{-}H][Al(OTeF_5)_4]$.

Atom	Atom	Length/Å	Atom	Atom	Length/Å
Te3	O3	1.820(8)	Te4	F19	1.818(8)
Te3	F11	1.831(7)	Te4	O4	1.823(8)
Te3	F13	1.831(8)	Te4	F18	1.827(8)
Te3	F12	1.832(8)	Te4	F16	1.829(8)
Te3	F15	1.841(8)	Te4	F20	1.830(8)
Te3	F14	1.846(7)	Te4	F17	1.834(8)
Te1	O1	1.809(9)	Br1	C3	1.871(13)
Te1	F3	1.829(8)	Al1	O1	1.728(9)
Te1	F5	1.830(8)	Al1	O2	1.734(9)
Te1	F2	1.830(8)	Al1	O3	1.742(9)
Te1	F1	1.832(8)	Al1	O4	1.768(9)
Te1	F4	1.837(8)	N1	C5	1.318(17)
Te2	O2	1.821(8)	N1	C1	1.332(17)
Te2	F9	1.827(8)	C5	C4	1.380(18)
Te2	F8	1.828(7)	C4	C3	1.392(18)
Te2	F6	1.829(8)	C1	C2	1.387(18)
Te2	F10	1.836(8)	C2	C3	1.394(19)
Te2	F7	1.837(8)			

Table 7.6. Bond angles for $[C_5H_4BrN\text{-}H][Al(OTeF_5)_4]$.

Atom	Atom	Atom	Angle/°	Atom	Atom	Atom	Angle/°
O3	Te3	F11	178.4(4)	F6	Te2	F10	87.6(4)
O3	Te3	F13	92.6(4)	O2	Te2	F7	92.7(4)
F11	Te3	F13	86.0(4)	F9	Te2	F7	175.4(4)
O3	Te3	F12	92.6(4)	F8	Te2	F7	89.5(4)
F11	Te3	F12	88.3(3)	F6	Te2	F7	88.0(4)
F13	Te3	F12	89.7(4)	F10	Te2	F7	89.3(4)
O3	Te3	F15	93.7(4)	F19	Te4	O4	93.1(4)
F11	Te3	F15	87.7(4)	F19	Te4	F18	90.1(5)
F13	Te3	F15	173.6(4)	O4	Te4	F18	90.8(4)
F12	Te3	F15	89.2(4)	F19	Te4	F16	87.9(4)
O3	Te3	F14	92.2(4)	O4	Te4	F16	178.5(4)
F11	Te3	F14	86.9(3)	F18	Te4	F16	88.1(4)
F13	Te3	F14	90.9(3)	F19	Te4	F20	91.0(5)
F12	Te3	F14	175.1(3)	O4	Te4	F20	92.6(4)
F15	Te3	F14	89.6(3)	F18	Te4	F20	176.4(4)
O1	Te1	F3	92.1(4)	F16	Te4	F20	88.5(4)
O1	Te1	F5	93.6(4)	F19	Te4	F17	174.4(4)
F3	Te1	F5	174.4(4)	O4	Te4	F17	92.5(4)
O1	Te1	F2	94.4(4)	F18	Te4	F17	89.4(4)
F3	Te1	F2	90.2(4)	F16	Te4	F17	86.5(4)
F5	Te1	F2	89.6(4)	F20	Te4	F17	89.2(4)
O1	Te1	F1	178.2(4)	O1	Al1	O2	112.9(5)
F3	Te1	F1	87.0(4)	O1	Al1	O3	109.7(5)
F5	Te1	F1	87.4(4)	O2	Al1	O3	112.5(5)
F2	Te1	F1	87.2(4)	O1	Al1	O4	109.4(5)
O1	Te1	F4	91.2(4)	O2	Al1	O4	99.4(4)
F3	Te1	F4	89.5(5)	O3	Al1	O4	112.6(4)
F5	Te1	F4	90.2(4)	Al1	O2	Te2	138.4(5)
F2	Te1	F4	174.4(4)	Al1	O4	Te4	133.2(5)
F1	Te1	F4	87.2(4)	Al1	O3	Te3	134.4(5)
O2	Te2	F9	91.9(4)	Al1	O1	Te1	145.5(6)
O2	Te2	F8	92.8(4)	C5	N1	C1	122.9(11)
F9	Te2	F8	90.6(4)	N1	C5	C4	120.7(12)
O2	Te2	F6	179.1(4)	C5	C4	C3	117.5(12)
F9	Te2	F6	87.4(4)	N1	C1	C2	120.7(12)
F8	Te2	F6	86.6(4)	C1	C2	C3	116.8(11)
O2	Te2	F10	93.0(4)	C4	C3	C2	121.4(12)
F9	Te2	F10	90.1(4)	C4	C3	Br1	119.2(10)
F8	Te2	F10	174.1(4)	C2	C3	Br1	119.4(10)

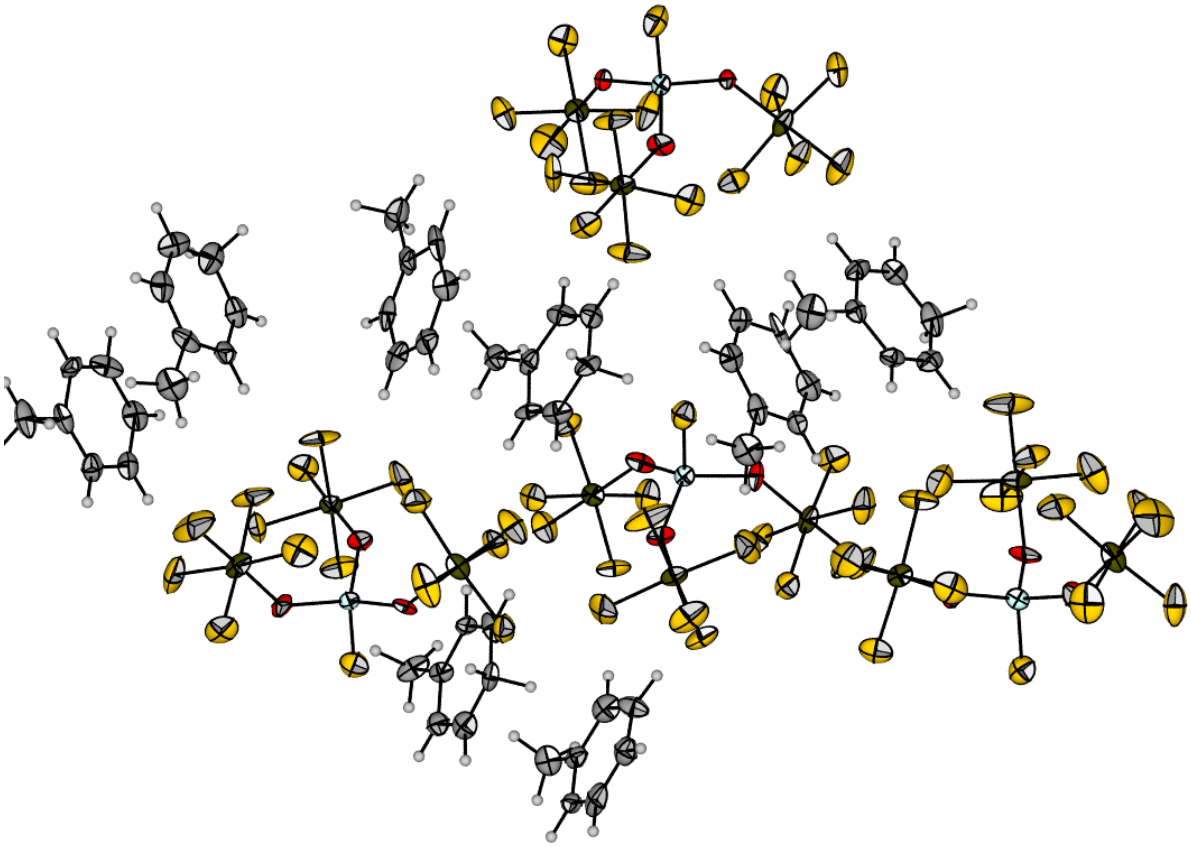

Figure 7.23. Molecular structure of $[C_7H_8\text{-}H][Al(OTeF_5)_3F]\cdot C_7H_8$ in the solid state with thermal ellipsoids shown at the 50% probability level.

Table 7.7. Bond Lengths for the $[C_7H_8\text{-}H][Al(OTeF_5)_3F]\cdot C_7H_8$

Atom	Atom	Length/Å	Atom	Atom	Length/Å	Atom	Atom	Length/Å
Te5	F27	1.830(11)	Al1	F1	1.814(14)	C2	C03S	1.40(3)
Te5	F28	1.816(11)	Al1	O1	1.737(15)	Te11	F58	1.807(13)
Te5	F29	1.822(12)	Al1	O2	1.720(14)	Te11	F59	1.836(12)
Te5	O5	1.810(13)	Al1	O3	1.675(15)	Te11	F56	1.847(12)
Te5	F25	1.824(11)	Al2	O6	1.724(14)	Te11	F57	1.824(13)
Te5	F26	1.831(11)	Al2	F2	1.806(14)	Te11	F55	1.833(14)
Te1	F9	1.822(13)	Al2	O5	1.732(14)	Te8	O8	1.814(13)
Te1	F8	1.842(13)	Al2	O4	1.728(14)	Te8	F40	1.828(13)
Te1	F5	1.818(13)	Al4	O12	1.730(13)	Te8	F44	1.839(12)
Te1	F7	1.804(13)	Al4	O11	1.735(13)	Te8	F42	1.825(12)
Te1	O3	1.811(14)	Al4	F4	1.805(14)	Te8	F43	1.837(13)
Te1	F6	1.829(13)	Al4	O10	1.710(13)	Te8	F41	1.827(12)
Te12	F62	1.838(12)	Al3	O8	1.723(13)	Te3	F15	1.845(13)
Te12	F63	1.830(13)	Al3	O7	1.720(14)	Te3	F18	1.831(12)
Te12	O10	1.817(12)	Al3	F60	1.810(14)	Te3	O2	1.796(13)
Te12	F64	1.828(12)	Al3	O9	1.725(13)	Te3	F16	1.837(15)
Te12	F61	1.825(12)	C52	C53	1.40(3)	Te3	F19	1.830(16)
Te12	F3	1.832(12)	C52	C51	1.39(3)	Te3	F17	1.824(14)
Te9	O7	1.806(13)	C55	C54	1.37(3)	Te4	F21	1.821(12)
Te9	F47	1.845(11)	C55	C56	1.41(3)	Te4	O4	1.801(12)
Te9	F45	1.824(12)	C10	C9	1.38(3)	Te4	F24	1.820(15)
Te9	F46	1.826(11)	C10	C11	1.44(3)	Te4	F23	1.836(12)
Te9	F49	1.829(11)	C6	C5	1.37(3)	Te4	F20	1.846(15)
Te9	F48	1.823(11)	C6	C7	1.40(3)	Te4	F22	1.815(13)
Te7	F38	1.827(13)	C9	C14	1.37(3)	C2	C7	1.40(3)
Te7	F35	1.811(12)	C9	C8	1.53(3)	C2	C1	1.50(3)
Te7	O9	1.812(12)	C54	C53	1.42(3)	C39	C40	1.38(3)
Te7	F36	1.846(13)	C17	C18	1.38(3)	C39	C38	1.39(3)
Te7	F39	1.825(13)	C17	C16	1.38(3)	C033	C25	1.39(4)
Te7	F37	1.841(12)	C47	C48	1.41(3)	C033	C24	1.39(3)
Te6	O6	1.807(13)	C47	C46	1.39(3)	C37	C38	1.42(3)
Te6	F34	1.813(13)	C14	C13	1.39(3)	C37	C36	1.51(3)
Te6	F31	1.803(12)	C27	C26	1.38(3)	C37	C42	1.36(3)
Te6	F33	1.836(11)	C27	C23	1.35(3)	C33	C32	1.37(3)
Te6	F30	1.844(12)	C12	C11	1.40(3)	C50	C51	1.52(3)
Te6	F32	1.828(13)	C12	C13	1.34(3)	C30	C35	1.41(3)
Te2	F10	1.802(14)	C20	C19	1.41(3)	C30	C31	1.38(3)
Te2	F14	1.794(13)	C20	C21	1.39(3)	C30	C29	1.54(3)
Te2	F13	1.826(15)	C26	C25	1.38(3)	C21	C16	1.35(3)
Te2	F12	1.829(14)	C4	C5	1.38(3)	C40	C41	1.38(3)
Te2	O1	1.775(15)	C4	C03S	1.40(3)	C44	C45	1.40(3)
Te2	F11	1.821(13)	C48	C49	1.41(3)	C44	C49	1.34(3)
Te10	O11	1.792(12)	C19	C18	1.36(3)	C44	C43	1.56(3)
Te10	F53	1.817(13)	C34	C33	1.39(3)	C31	C32	1.38(3)
Te10	F54	1.826(13)	C34	C35	1.37(3)	C51	C56	1.39(3)
Te10	F51	1.819(13)	C46	C45	1.42(3)	C23	C24	1.42(3)
Te10	F50	1.815(14)	C2	C03S	1.40(3)	C23	C22	1.51(3)
Te10	F52	1.838(13)	C2	C7	1.40(3)	C16	C15	1.51(3)
C41	C42	1.40(3)						

Table 7.8. Bond Angles for the $[C_7H_8\text{-}H][Al(OTeF_5)_3F\ C_7H_8$

Atom	Atom	Atom	Angle/°	Atom	Atom	Atom	Angle/°	Atom	Atom	Atom	Angle/°
F27	Te5	F26	87.8(6)	F45	Te9	F47	89.9(6)	O2	Al1	F1	103.5(7)
F28	Te5	F27	86.8(6)	F45	Te9	F46	173.8(6)	O2	Al1	O1	113.7(8)
F28	Te5	F29	89.5(7)	F45	Te9	F49	89.3(6)	O3	Al1	F1	107.0(7)
F28	Te5	F25	174.7(6)	F46	Te9	F47	90.0(6)	O3	Al1	O1	115.3(8)
F28	Te5	F26	88.9(7)	F46	Te9	F49	90.2(5)	O3	Al1	O2	111.6(8)
F29	Te5	F27	86.7(6)	F49	Te9	F47	174.6(5)	O6	Al2	F2	104.8(7)
F29	Te5	F25	90.6(8)	F40	Te8	F44	90.6(6)	O6	Al2	O5	109.5(7)
F29	Te5	F26	174.4(6)	F40	Te8	F43	173.4(6)	O6	Al2	O4	114.2(7)
O5	Te5	F27	178.7(6)	F42	Te8	F40	86.6(6)	O5	Al2	F2	110.1(7)
O5	Te5	F28	93.2(6)	F42	Te8	F44	87.0(6)	O4	Al2	F2	103.1(7)
O5	Te5	F29	92.0(6)	F42	Te8	F43	86.8(6)	O4	Al2	O5	114.6(7)
O5	Te5	F25	92.0(6)	F42	Te8	F41	87.1(6)	O12	Al4	O11	114.0(6)
O5	Te5	F26	93.5(6)	F43	Te8	F44	88.5(6)	O12	Al4	F4	105.1(7)
F25	Te5	F27	88.0(6)	F41	Te8	F40	90.1(6)	O11	Al4	F4	104.1(6)
F25	Te5	F26	90.5(7)	F41	Te8	F44	174.1(6)	O10	Al4	O12	108.7(7)
F9	Te1	F8	90.2(6)	F41	Te8	F43	90.1(7)	F48	Te9	F47	87.3(6)
F9	Te1	F6	174.9(6)	F18	Te3	F15	174.5(6)	F48	Te9	F45	87.6(6)
F5	Te1	F9	89.7(7)	F18	Te3	F16	90.7(7)	F48	Te9	F46	86.2(6)
F5	Te1	F8	174.9(6)	O2	Te3	F15	92.8(6)	F48	Te9	F49	87.3(6)
F5	Te1	F6	90.5(7)	O2	Te3	F18	92.7(7)	F38	Te7	F36	88.8(8)
F7	Te1	F9	87.0(7)	O2	Te3	F16	92.3(7)	F38	Te7	F37	88.2(6)
F7	Te1	F8	86.9(6)	O2	Te3	F19	91.7(8)	F35	Te7	F38	174.2(6)
F7	Te1	F5	88.0(7)	O2	Te3	F17	178.0(7)	F35	Te7	O9	93.4(6)
F7	Te1	O3	178.7(8)	F16	Te3	F15	89.2(7)	F35	Te7	F36	90.5(7)
F7	Te1	F6	88.0(7)	F19	Te3	F15	89.6(7)	F35	Te7	F39	88.4(7)
O3	Te1	F9	93.3(7)	F19	Te3	F18	90.2(8)	F35	Te7	F37	86.1(6)
O3	Te1	F8	91.8(7)	F19	Te3	F16	175.9(8)	O9	Te7	F38	92.3(6)
O3	Te1	F5	93.2(7)	F17	Te3	F15	85.3(6)	O9	Te7	F36	92.4(6)
O3	Te1	F6	91.8(6)	F17	Te3	F18	89.3(7)	O9	Te7	F39	92.1(6)
F6	Te1	F8	89.2(6)	F17	Te3	F16	88.0(9)	O9	Te7	F37	179.2(7)
F63	Te12	F62	89.7(7)	F17	Te3	F19	88.0(9)	F39	Te7	F38	91.7(8)
F63	Te12	F3	176.0(6)	F21	Te4	F23	175.0(6)	F39	Te7	F36	175.4(6)
O10	Te12	F62	91.5(6)	F21	Te4	F20	90.1(7)	F39	Te7	F37	88.6(7)
O10	Te12	F63	91.3(6)	O4	Te4	F21	91.8(6)	F37	Te7	F36	86.9(7)
O10	Te12	F64	178.6(7)	O4	Te4	F24	92.7(7)	O6	Te6	F34	93.0(6)
O10	Te12	F61	93.4(6)	O4	Te4	F23	93.2(6)	O6	Te6	F33	93.0(6)
O10	Te12	F3	92.8(6)	O4	Te4	F20	93.3(6)	O6	Te6	F30	92.9(6)
F64	Te12	F62	87.8(6)	O4	Te4	F22	178.6(7)	O6	Te6	F32	179.0(7)
F64	Te12	F63	87.5(6)	F24	Te4	F21	90.6(7)	F34	Te6	F33	90.8(7)
F64	Te12	F3	88.4(6)	F24	Te4	F23	89.9(8)	F34	Te6	F30	89.3(6)
F61	Te12	F62	175.1(6)	F24	Te4	F20	173.9(7)	F34	Te6	F32	87.8(7)
F61	Te12	F63	90.5(7)	F23	Te4	F20	88.9(7)	F31	Te6	O6	91.6(6)
F61	Te12	F64	87.3(6)	F22	Te4	F21	87.0(7)	F31	Te6	F34	175.3(6)
F61	Te12	F3	89.6(8)	F22	Te4	F24	86.6(9)	F31	Te6	F33	89.6(7)
F3	Te12	F62	89.8(7)	F22	Te4	F23	88.1(7)	F31	Te6	F30	89.9(6)
O7	Te9	F47	93.1(6)	F22	Te4	F20	87.4(8)	F31	Te6	F32	87.6(6)
O7	Te9	F45	93.4(6)	O1	Al1	F1	104.4(7)	F33	Te6	F30	174.1(6)

Table 7.9. Bond Angles for the $[C_7H_8\text{-}H][Al(OTeF_5)_3F]\cdot C_7H_8$ continue.

Atom	Atom	Atom	Angle/°	Atom	Atom	Atom	Angle/°	Atom	Atom	Atom	Angle/°
F32	Te6	F33	87.5(6)	C10	C9	C8	117.7(18)	O12	Te11	F55	92.8(6)
F32	Te6	F30	86.6(6)	C14	C9	C10	120.5(18)	F58	Te11	F59	89.7(7)
F10	Te2	F13	175.1(6)	C14	C9	C8	121.7(17)	F58	Te11	F56	89.9(7)
F10	Te2	F12	86.2(8)	C55	C54	C53	119.8(18)	F58	Te11	F57	87.2(7)
F10	Te2	F11	90.3(7)	C16	C17	C18	120.9(19)	F58	Te11	F55	174.5(6)
F14	Te2	F10	90.7(8)	Al1	O1	Te2	149.4(10)	F59	Te11	F56	173.5(6)
F14	Te2	F13	89.1(8)	C46	C47	C48	119(2)	F57	Te11	F59	87.3(6)
F14	Te2	F12	87.5(9)	C9	C14	C13	122.7(18)	F57	Te11	F56	86.2(6)
F14	Te2	F11	174.7(7)	C23	C27	C26	123(2)	F57	Te11	F55	87.3(7)
F13	Te2	F12	89.0(8)	C13	C12	C11	119(2)	F55	Te11	F59	89.8(6)
O1	Te2	F10	93.6(7)	C21	C20	C19	117.7(19)	F55	Te11	F56	90.0(6)
O1	Te2	F14	92.6(8)	C27	C26	C25	119(2)	O8	Te8	F40	92.6(6)
O1	Te2	F13	91.2(7)	C5	C4	C03S	120(2)	O8	Te8	F44	93.4(6)
O1	Te2	F12	179.8(9)	Al1	O2	Te3	139.2(9)	O8	Te8	F42	179.1(7)
O1	Te2	F11	92.6(7)	C49	C48	C47	119(2)	O8	Te8	F43	94.0(6)
F11	Te2	F13	89.5(7)	C18	C19	C20	119(2)	O8	Te8	F41	92.4(6)
F11	Te2	F12	87.3(8)	C19	C18	C17	121(2)	C16	C21	C20	123.2(19)
O11	Te10	F53	92.0(6)	C35	C34	C33	120.0(19)	C34	C35	C30	120.0(19)
O11	Te10	F54	92.6(6)	Al1	O3	Te1	156.9(10)	C41	C40	C39	120(2)
O11	Te10	F51	92.6(6)	C47	C46	C45	121(2)	C45	C44	C43	117(2)
O11	Te10	F50	92.9(6)	C03S	C2	C7	118.3(19)	C49	C44	C45	123(2)
O11	Te10	F52	179.6(7)	C03S	C2	C1	120.2(19)	C49	C44	C43	120(2)
F53	Te10	F54	89.6(6)	C7	C2	C1	121.5(18)	C32	C31	C30	120(2)
F53	Te10	F51	90.3(6)	C40	C39	C38	121(2)	C39	C38	C37	119(2)
F53	Te10	F52	87.9(7)	C52	C53	C54	118.8(19)	C52	C51	C50	118.6(19)
F54	Te10	F52	87.7(7)	C24	C033	C25	118(2)	C52	C51	C56	119.8(19)
O10	Al4	O11	114.0(7)	C38	C37	C36	121(2)	C56	C51	C50	121.7(19)
O10	Al4	F4	110.4(7)	C42	C37	C38	117.4(19)	C33	C32	C31	120(2)
O8	Al3	F60	99.7(7)	C42	C37	C36	122(2)	C44	C45	C46	117(2)
O8	Al3	O9	115.6(7)	C32	C33	C34	120(2)	C27	C23	C24	117(2)
O7	Al3	O8	112.7(7)	C26	C25	C033	121(2)	C27	C23	C22	122(2)
O7	Al3	F60	109.8(7)	C12	C11	C10	122(2)	C24	C23	C22	121(2)
O7	Al3	O9	109.0(7)	C12	C13	C14	120(2)	C51	C56	C55	119.5(19)
O9	Al3	F60	109.6(7)	C35	C30	C29	120(2)	C4	C03S	C2	120(2)
Al4	O12	Te11	141.3(8)	C31	C30	C35	119.2(19)	C033	C24	C23	122(2)
Al4	O11	Te10	140.7(8)	C31	C30	C29	121(2)	C17	C16	C15	119(2)
Al2	O6	Te6	143.8(8)	C6	C5	C4	120(2)	C21	C16	C17	117.8(19)
Al3	O8	Te8	140.6(9)	F51	Te10	F54	174.8(6)	C21	C16	C15	123(2)
Al3	O7	Te9	144.7(8)	F51	Te10	F52	87.1(7)	C40	C41	C42	118(2)
Al4	O10	Te12	146.0(9)	F50	Te10	F53	175.0(6)	C44	C49	C48	121(2)
C51	C52	C53	121(2)	F50	Te10	F54	89.1(7)	C6	C7	C2	120(2)
Al2	O5	Te5	141.1(9)	F50	Te10	F51	90.5(7)	C37	C42	C41	124(2)
Al3	O9	Te7	140.1(8)	F50	Te10	F52	87.3(7)				
C54	C55	C56	121.1(19)	O12	Te11	F58	92.7(6)				
Al2	O4	Te4	137.3(9)	O12	Te11	F59	93.4(6)				
C9	C10	C11	116(2)	O12	Te11	F56	93.0(6)				
C5	C6	C7	120(2)	O12	Te11	F57	179.2(7)				

IR Spectra

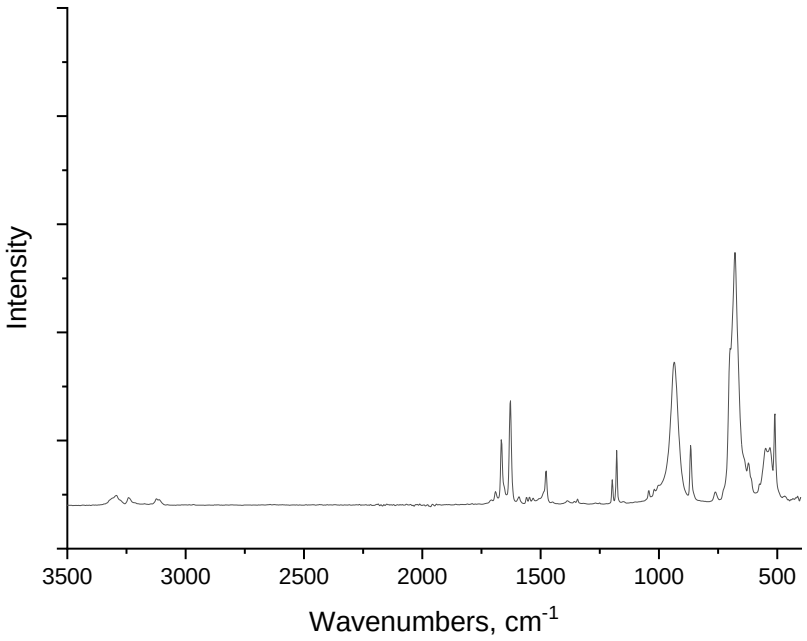

Figure 7.24. Experimental IR spectrum of crystals $[C_5H_2F_3N\text{-}H][Al(OTeF_5)_4]$.

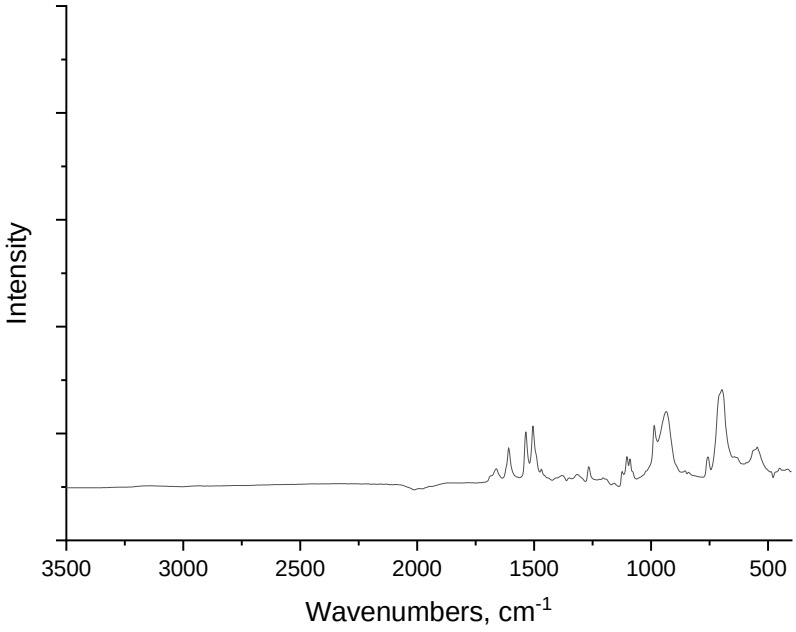

Figure 7.25. Experimental IR spectrum of crystals $C_5F_3H_2N{\rightarrow}Al(OTeF_5)_3$.

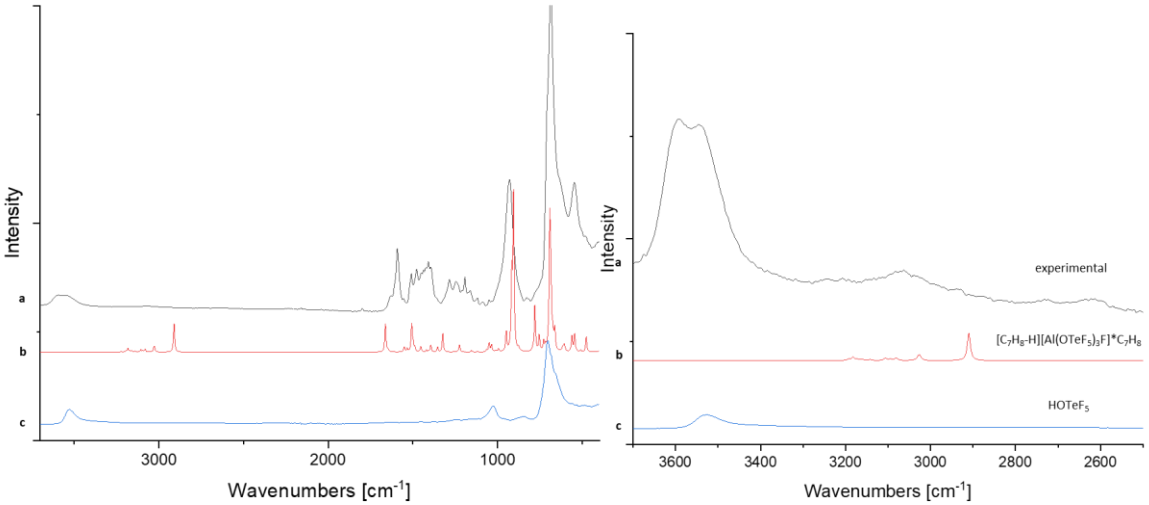

Figure 7.26. Experimental IR spectrum of $[C_7H_8\text{-}H][Al(OTeF_5)_3F]\cdot C_7H_8$ crystals and calculated (B3-LYP-D3/def2-TZVPP) IR spectra.

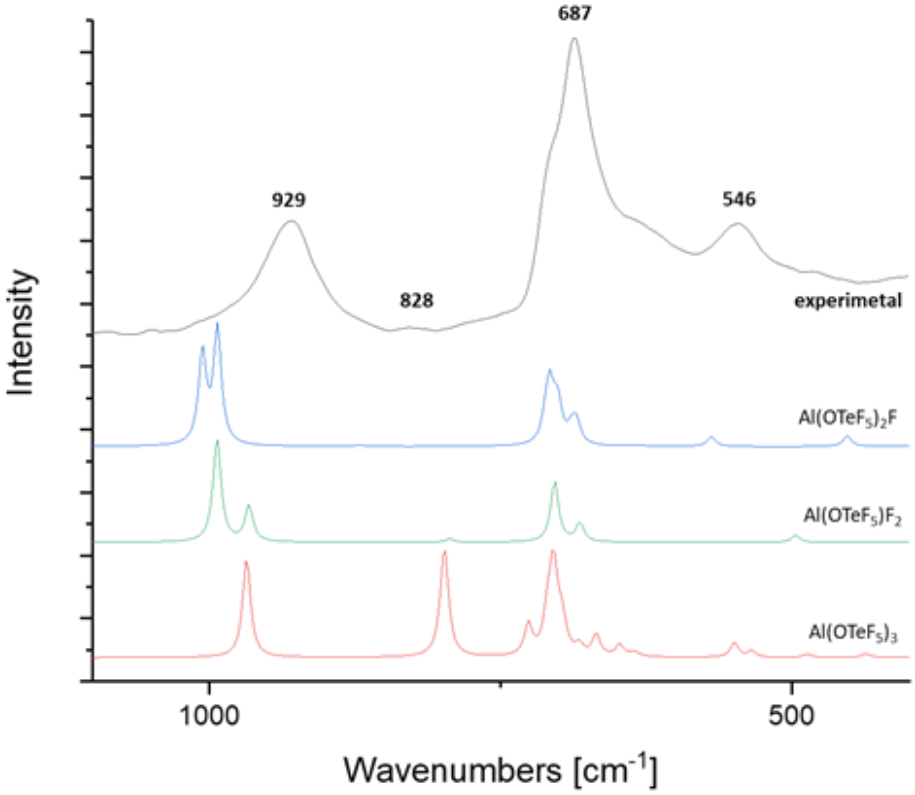

Figure 7.27. Zoomed experimental IR spectrum of $[C_7H_8\text{-}H][Al(OTeF_5)_3F]\cdot C_7H_8$ crystals and calculated (B3-LYP-D3/def2-TZVPP) IR spectra.

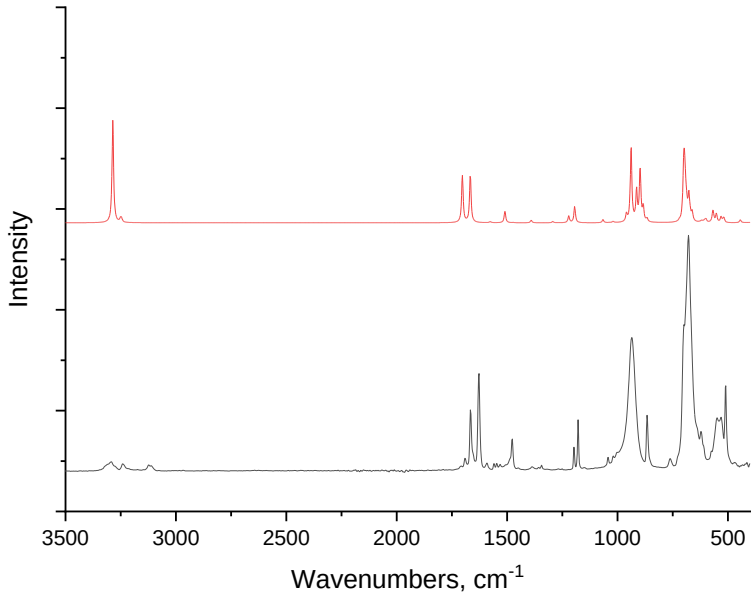

Figure 7.28. Calculated (red, top) on the B3-LYP-D3/def2-TZVPP level of theory and experimental (black, bottom) IR spectrum of $[C_5H_2F_3N\text{-}H][Al(OTeF_5)_4]$.

DFT Calculation Data

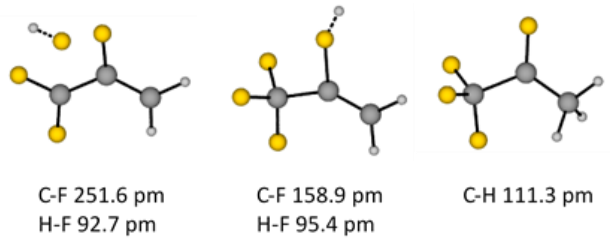

Figure 7.29. Calculated minimum structures of protonated HFO-1234yf on B3LYP-D3/def2-TZVPP (CPCM, ε_R 14.26) level of theory.

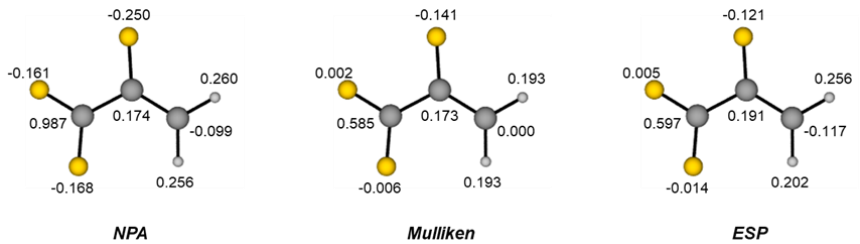

Figure 7.30. Calculated partial charges of trifluoroallyl cation on B3LYP-D3/def2-TZVPP (CPCM, ε_R 14.26) level of theory.

VIII Publications and Conference Contributions

Publication List

[1] **S. Kotsyuda**, A. N. Toraman, M.A. Ellwanger, S. Steinhauer, C. Müller, S. Riedel, *Chemistry – a European Journal* **2022**, *e202202749.*

[2] **S. Kotsyuda**, S. Steinhauer, A. Wiesner, S. Riedel, *Zeitschrift für Anorganische und Allgemeine Chemie* **2020**, *23*, 13501–13509.

[3] V.V. Tomina, I.M. Furtat, A.P. Lebed, **S. Kotsyuda,** H. Kolev, M. Kanuchova, D.M., Behunova, M. Vaclavikova, I.V. Melnyk, *ACS Omega* **2020**, *25*, 15290–15300.

[4] **S. Kotsyuda,** V.V. Tomina, Yu.L. Zub, I.M. Furtat, A.P. Lebed, M. Vaclavikova, I.V. Melnyk *Applied Surface Science* **2017**, *420*, 782–791.

Conference Contributions

08/2019 19th European Symposium on Fluorine Chemistry
Warsaw, Poland

09/2018 18. Deutscher Fluortag
Berlin, Germany

09/2017 GDCh-Wissenschaftsforum Chemie 2017
Berlin, Germany

07/2017 5. Tag der Anorganische Chemie
Berlin, Germany